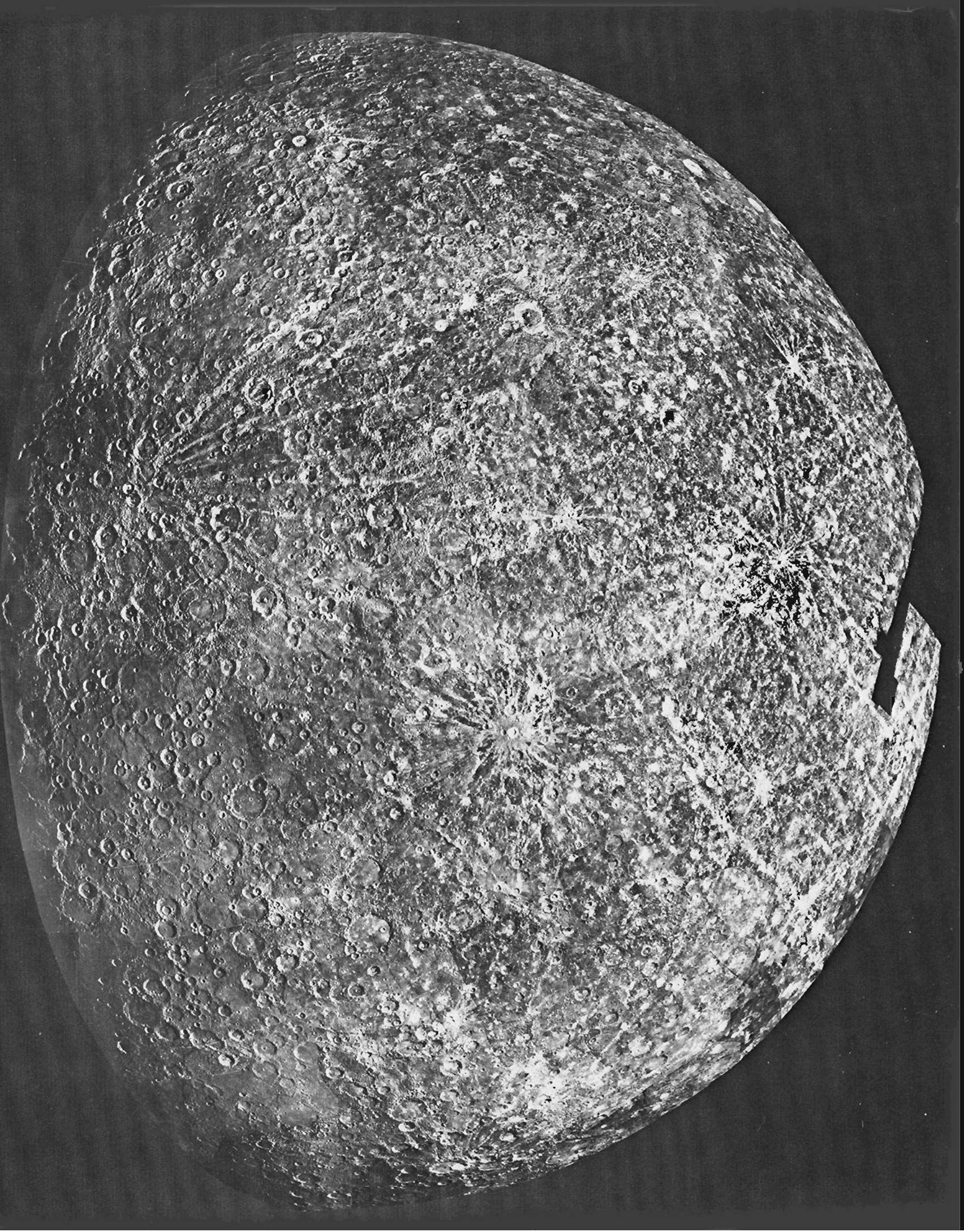

3
MERCURY

Robert G. Strom

INTRODUCTION

Prior to the flight of Mariner 10 very little was known about the smallest and innermost terrestrial planet, Mercury. At maximum elongation Mercury is no more than 28 degrees from the Sun as viewed from Earth, and therefore telescopic observations must be made during daytime or at twilight through a long path-length of the Earth's atmosphere. As a consequence of this, and because of Mercury's small size and large distance from Earth, telescopic observations provide only scanty data. However, Earth-based observations did determine three major facts about Mercury which were subsequently confirmed by Mariner 10: (1) Mercury has a very high mean density (5.44 g/cm^3) comparable to that of Venus (5.25) and Earth (5.52), and much larger than that of the Moon (3.34) and Mars (3.94); (2) Mercury's surface reflects electromagnetic radiation at all wavelengths in a similar, but not exact, manner as the Moon, when differences in their solar distances are taken into account; and (3) Mercury's rotation period is in 3:2 resonance with its orbital period. Table 3.1 lists the best current values for the more important orbital and physical properties of Mercury.

On March 29, 1974 the Mariner 10 spacecraft flew by Mercury for the first time and provided a wealth of new information about this poorly understood planet. On the first encounter, pictures were obtained of Mercury's surface at about quarter-phase illumination during its incoming and outgoing passages. Two subsequent flybys on September 21, 1974 and March 16, 1975 extended the coverage to the south polar region and provided high resolution pictures of selected areas of interest seen at lower resolutions on the first encounter. The second encounter coverage of the south polar region established a cartographic and geologic link between the incoming and outgoing sides photographed on the first encounter (Strom et al., 1975a). In addition, photographs taken during the second encounter were at significantly different viewing angles from those taken on the first encounter and so provided stereoscopic coverage of large areas of the southern hemisphere.

Over 2700 useful pictures were taken by Mariner 10 during its three encounters. The combined coverage of these pictures is about 45 percent of the surface at resolutions varying from about 4 km to 100 meters. This is approximately equivalent to Earth-based telescopic coverage and resolution of the Moon. Because of constraints imposed by Mercury's rotation period and the orbital periods of the spacecraft and Mercury, all three encounters took place when the terminator was in the same position. Consequently much of the coverage was obtained at high solar elevation angles, which made discrimination of surface morphology and topography difficult. This was somewhat offset by the stereoscopic coverage in the southern hemisphere, but in practice only about half the explored area was viewed under favorable illumination conditions. About 70 percent of Mercury is viewed under poor lighting conditions or is not visible at all, imposing difficulties in interpreting surface processes on a global scale. As a consequence, several major questions concerning the origin of certain terrains and the history of Mercury must remain open. Nevertheless, the wealth of new information from Mariner 10 has elevated Mercury from a poorly known planet to one as familiar to us as the Moon was before the era of space exploration. [An excellent

Table 3.1. Orbital and Physical Data for Mercury

Orbital data	
Semimajor axis	0.3871 AU (5.79×10^7)
Perihelion distance	0.3075 AU (4.60×10^7 km)
Aphelion distance	0.4667 AU (6.98×10^7 km)
Sidereal period	87.97 days
Synodic period	115.88 days
Orbital eccentricity	0.20563
Inclination of orbit to ecliptic	7.004 deg
Mean orbital velocity	47.87 km/s
Rotational period	58.646 days
Physical data	
Radius	2439 km
Surface area	7.475×10^7 km^2
Volume	6.077×10^{10} km^3
Mass	3.302×10^{26} g
Mean density	5.44 g/cm^3
Surface gravity	370 cm/s^2
Escape velocity	4.25 km/s
Surface temperature extremes	~90 to 740 K (- 183 to 467° C)
Normal albedo (5° phase angle)	0.125
Magnetic dipole moment	$4.9 (\pm 0.2) \times 10^{22}$ gauss cm^3

presentation of much of the imagery, cartography and nomenclature is contained in the Atlas of Mercury (Davies et al., 1978).]

In addition to the imaging experiment, Mariner 10 carried a complement of other scientific instruments that obtained information on Mercury's mass and size, atmospheric composition and density, charged-particle environment, infrared thermal radiation, and magnetic field.

Orbit

Except for Pluto, Mercury's orbit has the largest eccentricity ($e = 0.206$) and inclination to the ecliptic ($i = 7.0°$) of any planet in the solar system. These high values of e and i may be chance occurrences; or the Mercurian inclination may have a primordial link to the solar equatorial plane, which is inclined 6 degrees to the invariable plane (the plane fixed with respect to orbital precessions). Kaula (1976) has suggested that the large eccentricity is the result of very high velocity collisions between proto-Mercury and planetesimals perturbed into the inner solar system by Jupiter. An alternative explanation for Mercury's large e and i has been offered by Ward, Colombo and Franklin (1976). They suggest that Mercury's e and i have been pumped up by Venus during secular resonances between the precession rates of the lines of apsides of Mercury and Venus when, and if, the Sun had an oblateness $j_2 \sim 10^{-3}$, corresponding to a rotation rate of about five hours. This same j_2 would produce another resonance between the precession rates of the line of nodes of the two planets. For this mechanism to produce the observed e and i, the time scale for decay of the solar rotation must be about 10^6 years. By analogy with T-Tauri and other young stars, such an early rapid solar rotation and decay does not seem implausible.

Rotation

For nearly a century Mercury's rotation period was thought to be synchronous with its orbital period of 88 days. In 1965 Pettengill and Dyce (1965) measured a rotation period of 59 ± 5 days from radar observations. This period was subsequently refined by Goldstein (1971) to 58.65 ± 0.25 days from additional radar data. From shadow positions measured on consecutive Mariner 10 encounters Klaasen (1975, 1976) further refined the rotation period to 58.646 ± 0.005 days. This period corresponds to a 3:2 commensurability between the axial and orbital periods. Klaasen's (1976)

analysis of Mariner 10 pictures also determined that Mercury's rotation axis is almost perpendicular to the orbital plane (obliquity = 2° with an error ellipse of 2.6° × 6.5°).

Mercury's rotation period was probably much faster in the past (possibly as much as 8 hours), but subsequently was slowed by solar tides (Burns, 1976). For a tidal dissipation factor Q = 30, the characteristic decay time to despin Mercury to its present rate would be about 10^9 years. As a consequence of this despinning the interior temperature would have increased by 100 K, and surface stresses would have caused strains above the fracture limits (Melosh, 1977). Such stresses may have been partly responsible for some of the tectonic features seen on Mariner 10 imagery. Goldreich and Peale (1968) showed that the 3:2 resonant rotation is stable as long as the solar torque exerted on the asymmetric equatorial shape is always larger than the time-averaged tidal torque. The value of $j_2 \sim 10^{-4}$ derived from Mariner 10 data indicates that the stability criterion is satisfied. Furthermore, the capture probability of Mercury into a 3:2 resonance is much greater than into higher-order resonances for the most common tidal models. Peale (1974, 1976) also finds from obliquity histories for all realistic initial conditions that the spin axis lies near the normal to the orbit in the final state.

Internal Structure

Although Mercury superficially resembles the Moon, its internal constitution must be very different. Mercury's very high mean density of 5.44 g/cm³ is exceeded only by that of the Earth (5.52 g/cm³). However, Mercury is only about one-third the size of Earth, and its uncompressed density (5.3 g/cm³) is considerably greater than that of the Earth's (4.0 g/cm³). This indicates that Mercury's composition is 60 to 70 percent by weight of metal phases (probably iron), and only about 30 percent by weight of silicate phases. Therefore, Mercury contains proportionately twice as much iron as any other planet in the solar system. If most of this iron is concentrated in a core, then the core radius is about 75 percent (1830 km) of the planet radius and the core volume is about 42 percent of the total volume, and somewhat larger than the volume of the Moon (fig. 3.1). Virtually nothing is known about the structure of the relatively thin (610 km) outer silicate layer. If Mercury was entirely or largely molten in the past, as thermal history models suggest, then the silicate layer may be differentiated into a mantle and crust.

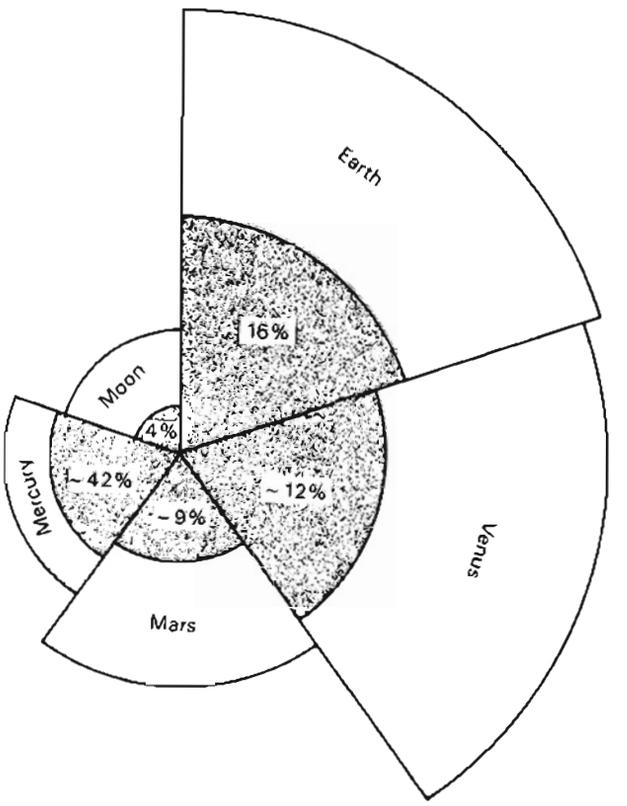

Figure 3.1. Comparison of terrestrial planet size and core radii. The percent of the total planetary volume of the core is also shown.

Magnetic Field

One of the most important discoveries made by Mariner 10 was the presence of a permanent magnetic field probably associated with Mercury's large iron core (Ness et al., 1974, 1975, 1976). Although the field is much weaker than Earth's, it is strong enough (~350 gammas) to form a magnetosheath and magnetosphere. The near-planet field is well represented by a dipole (with moment 5×10^{22} G cm³) inclined about 11° to the rotation axis, and with the same polarity as Earth's field. Although Mariner 10 did not explore this region, there are indications that the magnetosphere is elongated in the antisolar direction and may form a long magnetotail with an embedded neutral sheet. Also like Earth, there is evidence that the magnetosphere undergoes complex transient distortions (substorms) caused by interaction with the solar wind (Siscoe et al., 1975). Mercury encompasses much more of its magnetosphere than Earth. The average distance from the center of the planet to the solar wind stagnation point at the magnetopause is only 1.45 planetary radii. For Earth, the distance is about 11 Earth radii. Therefore, Mercury's magneto-

sphere is a factor of 7.5 smaller than Earth's when normalized to the planet radius. Consequently, charged particles reach Mercury much more easily than they reach Earth and no trapped radiation regions similar to the Van Allen belts occur. The solar wind may be strong enough during rare periods to actually compress the field to the surface (Siscoe and Christopher, 1975). A comparison of Earth's and Mercury's magnetic field is shown in figure 3.2.

The source of Mercury's magnetic field is not well established. By analogy with Earth and Jupiter, the favored hypothesis is an active magnetohydrodynamic dynamo within the planet (Ness, 1978). This implies a presently molten core of high electrical conductivity such as iron. Mercury is a slow rotator (58.6 days), and although rotation has been cited as a necessary condition for astrophysical dynamos, the amount necessary may be small. Gubbins (1977) has shown that for a planetary-sized dynamo of low viscosity only a slight angular velocity is required for the Coriolis force to dominate the momentum balance, a characteristic of "rapid rotation."

Another possible source of the Mercurian field is a remanent magnetization of iron-bearing rocks in the outer layers of the planet (Stevenson, 1974). Such a field can be acquired by rocks cooling through the Curie temperature in the presence of an ambient field. If Mercury once had a dipolar field caused by a dynamo which subsequently died out (possibly due to solidification of the core upon cooling) then a remanent dipolar field would be frozen in the crust. The level of magnetization necessary to support this hypothesis is comparable to that measured by Mariner 10 (Stevenson, 1976). However, this explanation requires about 5 percent free iron in the several hundred kilometer thick mantle, and whether the mantle would retain this much free iron (which is many times the typical values found in lunar basalts) is uncertain. Furthermore, estimates of the amount of contraction derived from the study of compressional surface features are not compatible with a complete or even extensive solidification of a once molten core (Solomon, 1977).

A presently active magnetohydrodynamic dynamo requires that at least the outer portion of the core is presently molten. The main problem with this explanation is the need for a concentration of heat sources in the core in order to maintain a fluid state over geologic time; a heat source density equivalent to about 2 ppb of uranium is required (Toksöz et al., 1978). Several explanations, although flawed, have been offered to account for a presently fluid core, such as the presence of K or S in the core (Toksöz and Johnston, 1977; Stevenson, 1980), a density and conductivity discontinuity at the core-mantle boundary which forms an insulating layer (Fricker et al., 1976; Gubbins, 1977), or late or extended core formation (Solomon, 1977). In any event, both explanations for Mercury's magnetic field (remanence or a magnetohydrodynamic dynamo) require that the interior is differentiated into a core and mantle, that the core was molten in the past, and very likely that it is at least partly molten at present.

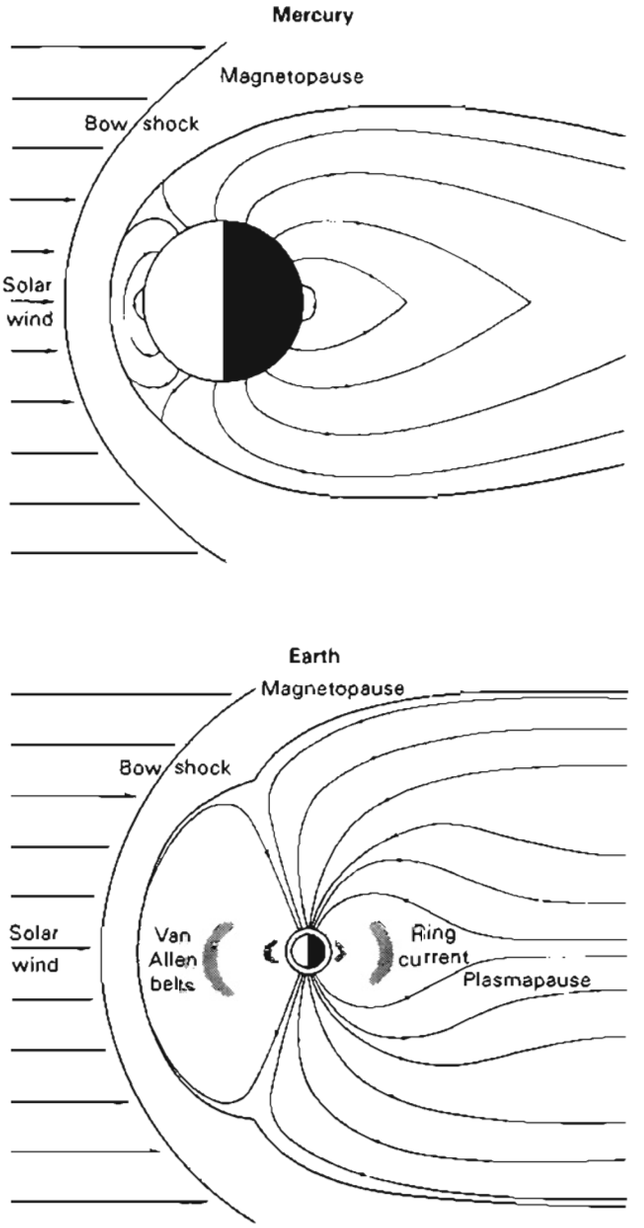

Figure 3.2. Comparison of the magnetic fields of Mercury and Earth.

Atmosphere

The ultraviolet spectrometer aboard Mariner 10 established upper limits on the atmospheric surface pressure and its composition (Broadfoot et al., 1974, 1976; Broadfoot, 1976a). The atmosphere is extremely tenuous with a surface pressure at the subsolar point less than a few times 10^{-10} mb. Consequently the gases are probably collisionless at the surface and the atmosphere essentially exospheric. Helium and atomic hydrogen have been identified in the ultraviolet spectrograms and upper limits placed on other possible constituents (H_2, O_2, Ne, Ar, O, CO_2, H_2O, and N_2). Furthermore, the Mariner 10 radio occultation experiment set an upper limit to the electron density of 10^3 cm^{-3} (Fjeldbo et al., 1976). This very tenuous atmosphere is probably derived largely from the solar wind.

Infrared Thermal Emission

The Mariner 10 infrared radiometer measured the thermal emission from Mercury at a spatial resolution as small as 40 km (Chase et al., 1974). In the equatorial regions just before dawn the minimum temperature is 90 K (at the subsolar point near perihelion the temperature is about 740 K). The temperatures thus have a range of at least 650 K (1170° F), greater than for any other planet or satellite in the solar system. The cooling curve of the surface during the night indicates the surface is composed of a homogeneous, porous material with a thermal inertia of 0.0017 cal $cm^{-2}sec^{-½}$ K^{-1}, which is similar to the value for the surface of the Moon. However, from near midnight until dawn the temperature fluctuated over a range of about 10 K, indicating regions with thermal inertias as high as 0.003 cal $cm^{-2}sec^{-½}$ K^{-1}. These observations are consistent with the presence of a layer of insulating silicate dust similar to the lunar regolith. The layer may be a few to tens of meters thick and was probably generated by impacts. The spatial variations in the thermo-physical properties of the layer indicate large-scale regions of enhanced thermal conductivity. These regions may be either areas of more compacted soil or regions where rock outcrops or boulders are not blanketed by dust.

GENERAL SURFACE CHARACTERISTICS

Although Mercury's internal constitution must be totally different from that of the Moon, its surface is remarkably similar (fig. 3.3a, b, and c). The dominant surface features are craters ranging in size from basin dimensions (1300 km) down to the smallest resolvable on Mariner 10 imagery (100 m). The craters are in various states of preservation: sharp-rimmed with extensive ray systems to highly degraded ones with very low or discontinuous rims. Antipodal to the Caloris basin is a peculiar hilly and lineated terrain that disrupts pre-existing landforms and may have been the result of focused seismic waves from the Caloris impact. Large tracts of lightly cratered smooth plains occupy low areas principally within and surrounding the Caloris basin and in the north polar regions. The larger expanses of these plains contain ridges somewhat similar to lunar wrinkle ridges. The relatively low crater densities on these plains indicate they are among the youngest surface units on the planet. Both morphologically and temporally they are very similar to the lunar maria. Unlike the Moon, Mercury has extensive intercrater areas with gently rolling planar surfaces and high densities of craters <15 km diameter. These intercrater plains appear to span a range of ages coincident with the period of heavy bombardment. They are among the oldest surface units on Mercury. Sinuous cliffs traverse the surface for hundreds of kilometers and are probably fault scarps.

Although the surface of Mercury superficially resembles the Moon, two major differences are: (1) the very great areal extent of old intercrater plains in the Mercurian highlands, and (2) the widespread distribution of lobate scarps which probably represent a period of global compression relatively late in Mercurian history. Furthermore, Mercurian crater ejecta characteristics are somewhat different from those of lunar craters, probably as a result of Mercury's greater surface gravity.

Photometry and Color

The integral optical, thermal and radar-reflecting properties of the Moon and Mercury are very similar (Hapke, 1977). These similarities indicate that Mercury is covered with a fragmental layer similar in depth and grain-size distribution to the lunar regolith. Photometric limb profiles measured from Mariner 10 data imply that small-scale slopes in the centimeter to meter size-range are about half those on the Moon, possibly caused by the influence of the stronger gravitational field of Mercury on the angle of repose of a cohesive soil (Hapke, 1977). In spite of the presence of a dipolar magnetic field, which would concentrate the solar wind

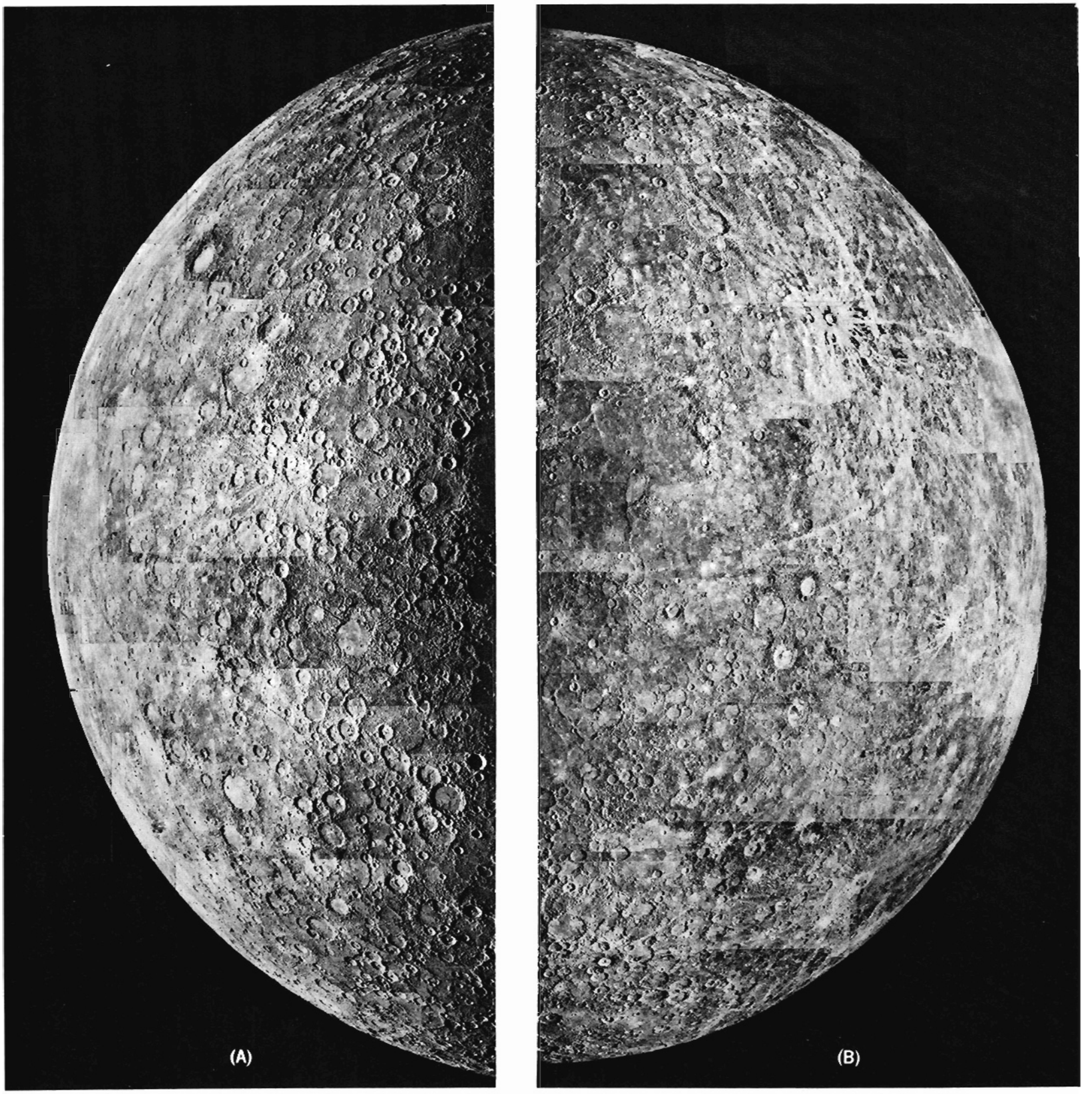

in the polar regions, Mercury displays no systematically lower albedo with increasing latitude. This implies that the dominant soil-darkening process is not dependent on the solar wind, but probably caused by processes resulting from meteoritic impact, e.g., redeposition of vaporized material.

Normal albedos were measured for various locations on Mercury using calibrated Mariner 10 images (Hapke et al., 1975). These albedos were determined for a phase angle of 5 degrees at a wavelength of 554 nm using a lunar photometric function. However, Mercury's photometric function differs enough from

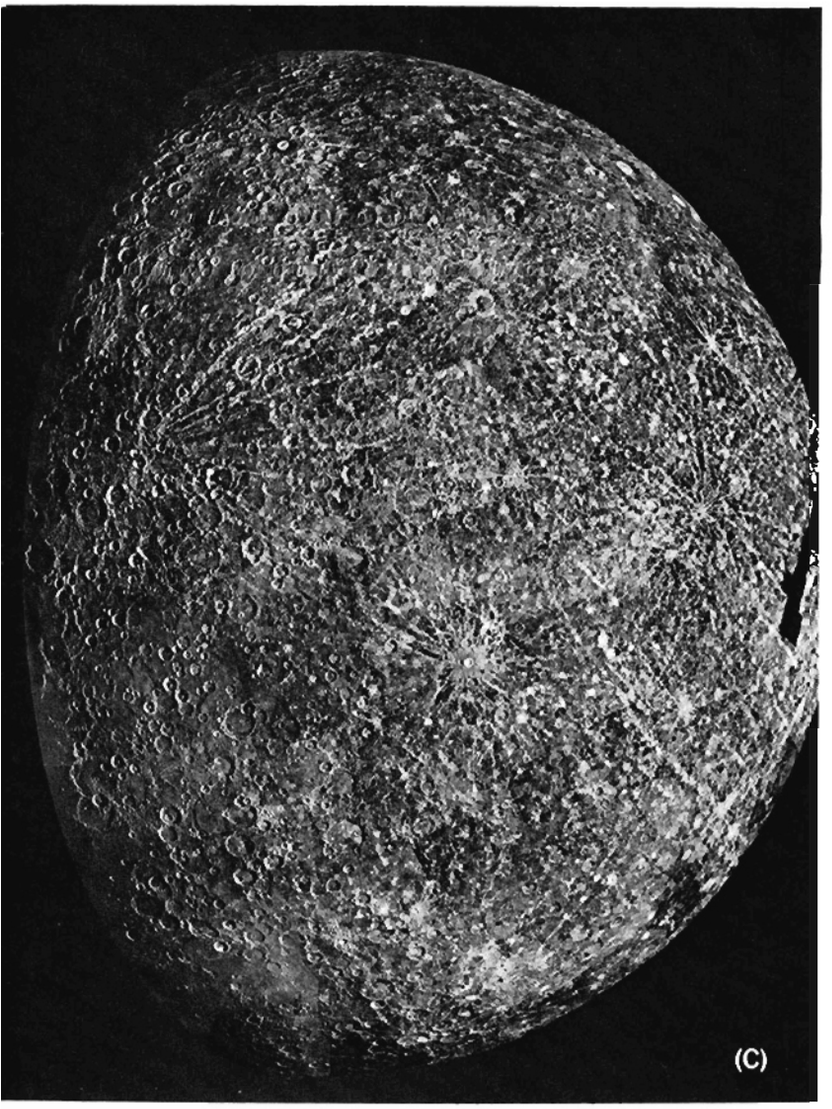

Figure 3.3. Photomosaics taken by Mariner 10 of (A) the incoming side of Mercury viewed by Mariner 10, (B) the outgoing side, and (C) the southern hemisphere.

the Moon's (Danjon, 1949) so that the Mercury values should be reduced by a factor of 0.92. The normal albedos quoted here have been so corrected. Hapke (personal communication) estimates that the absolute values are accurate to within 10 percent. The Mercury values vary from about 0.08 for an area on the rim of Tolstoj basin to about 0.41 for the brightest craters. The average of 52 points is about 0.13, which is in good agreement with the integral albedo of 0.125 determined by Dollfus and Auriere (1974) from Earth-based polarimetric measurements at a similar wavelength and phase angle. Earlier Earth-based albedo measurements from photometric observations of Mercury must be systematically too low because they violate the albedo versus maximum polarization criterion (Dollfus and Auriere, 1974).

On average the Mercurian highlands, which primarily consist of intercrater plains, have albedos of about 0.16 to 0.18. There appear to be two types of smooth plains: darker smooth plains in and around the Caloris basin with albedos of about 0.12 to 0.13, and brighter smooth plains primarily on the incoming side with albedos of about 0.18. The Caloris smooth plains are therefore about 26 percent darker than the Mercurian highlands. The brighter rayed craters have albedos ranging from 0.36 to 0.41.

Normal albedos on the Moon have been determined by Pohn and Wildey (1970) and Wildey (1977) at a similar wavelength and adjusted to 0° phase angle. When these values are corrected to a 5° phase angle then the lunar maria have average albedos of about 0.06 to 0.07, but in limited areas they are as high as 0.08. The lunar highlands average about 0.10 to 0.11 while the brighter rayed craters have average values of about 0.15 to 0.16. A comparison of lunar and Mercurian albedos is listed in table 3.2.

Mercury appears to have systematically higher albedos than comparable terrains on the Moon. The Caloris smooth plains are about 90 percent brighter than the lunar maria and have an albedo about 20 percent higher than the lunar highlands. The Mercurian highlands are about 26 percent brighter than the lunar highlands, and Mercury's bright rayed craters are over 100 percent brighter than those on the Moon. At shorter wavelengths in the extreme ultraviolet from 58 to 166 nm Mercury has a significantly lower albedo (⅔) than the Moon (Wu and Broadfoot, 1977).

Color-ratio studies by Hapke et al. (1980) using Mariner 10 images taken through the orange filter (effective wavelength 578 nm) and the ultraviolet filter (355 nm) showed that color differences occur on Mercury but are smaller (25 percent) than on the Moon (40 percent). This suggests that the surface of Mercury has a more homogeneous distribution of elements

Table 3.2. Comparison of Normal Albedos on the Moon and Mercury

Terrain	Normal albedo (554 nm wavelength; 5° phase angle)
Lunar maria	0.06–0.07
Mercury Caloris smooth plains	0.12–0.13
Lunar highlands	0.10–0.11
Mercury highlands (intercrater plains)	0.16–0.18
Lunar bright rayed craters	0.15–0.16
Mercury bright rayed craters	0.36–0.41

affecting color (e.g., titanium) than does the Moon. The color difference map (fig. 3.4) compiled by Hapke et al. (1980) shows that the side of Mercury viewed by Mariner 10 on its incoming trajectory, and dominated by cratered terrain and intercrater plains, is more homogeneous than the outgoing side which has large areas of smooth plains. Except in a few instances there is little correspondence between color boundaries and geologic boundaries.

Surface Composition

Data on the composition of the Mercurian surface are extremely limited. Spectra of Mercury show a continuous increase in reflectance with increasing wavelength from the visible to the infrared (McCord and Adams, 1972; Vilas and McCord, 1976; McCord and Clark, 1979). Spectra of lunar highlands regolith also display a similar rise in the continuum with wave-

Figure 3.4. Color difference maps of Mercury. The side of Mercury viewed by the approaching Mariner 10 is shown in (A) and should be compared with fig. 3.3a. The side viewed by the departing spacecraft is shown in (B) and should be compared with fig. 3.3b. The maps were compiled from the ratio of brightness at 578 nm (orange) to the brightness at 355 nm (UV). Areas with the highest spectral ratio are light orange, while those with the lowest ratio are black. Areas with the average ratio are medium brown. (From Hapke et al., 1980; with modifications.)

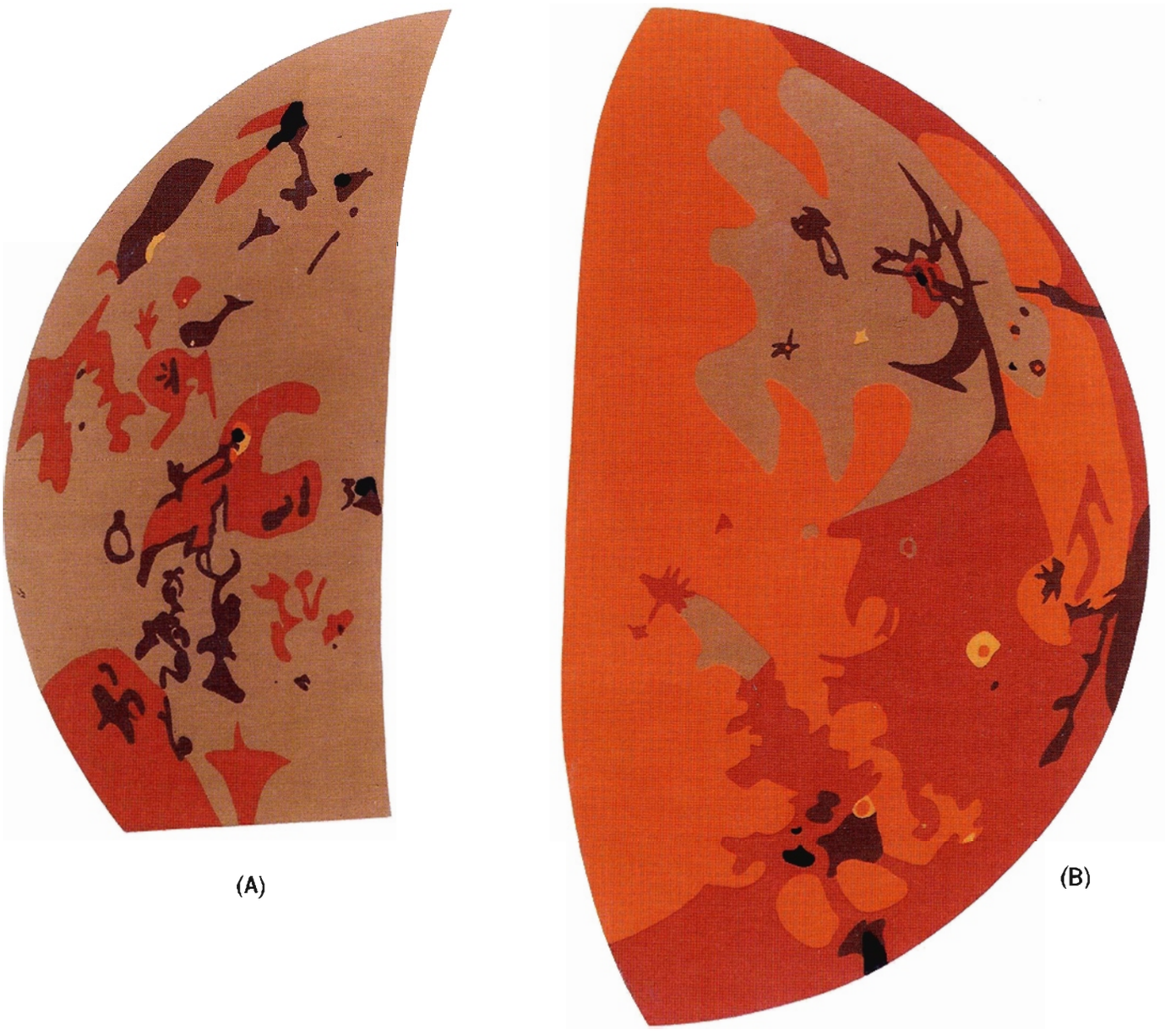

length. No other solar system objects yet observed have similar spectra. McCord and Clark (1979) reported a weak absorption feature between 0.75 and 0.95 μm, centered at 0.89 μm, which they attribute to Fe^{2+} ions in a pyroxene. A close comparison of this feature with an absorption band in lunar highlands regolith (Apollo 16 site) implies that both soils have the same amount of Fe^{2+}, suggesting an upper limit of about 5.5 percent FeO in average Mercurian regolith. Currently there is no evidence on Mercury for a 1.05 μm absorption band where Fe^{2+} absorbs in olivine.

The color ratio of Mariner 10 images discussed above show that, unlike the Moon, all Mercurian ray systems are blue relative to average (Hapke et al., 1975). Hapke et al. (1975) found that as the FeO abundance and Ti^{4+} abundance in Fe^{2+}-bearing materials increases, the spectrum reddens and the albedo decreases. Also, a relatively small amount of ilmenite ($FeTiO_3$) powder will cause the spectrum to become bluer and the albedo to drop significantly. Because all Mercurian ray systems possess the unique combination of bluish color and high albedo while those on the Moon are mostly red, Hapke et al. (1975) concluded that Mercury's surface is low in Ti, Fe^{3+}, and metallic Fe relative to the Moon's. This is also consistent with Mercury's lower ultraviolet reflectivity mentioned earlier. More recent studies by Hapke (1977) indicated that vapor-phase deposition accompanying micrometeorite impacts is an important darkening process on both Mercury and the Moon, and requires at least 3 percent FeO in the target material. Because comparisons of lunar and Mercurian reflection spectra indicate an average FeO content in the Mercurian soil of less than 6 percent, Hapke (1977) concluded that the average FeO content on the surface of Mercury is between 3 and 6 percent. These data suggest that on average at least the outer layers of Mercury are depleted in iron and titanium relative to the Moon. This also appears to be consistent with the albedo, color variations, and thermal history models.

CRATERS AND BASINS

The general morphology of Mercurian craters and basins is similar to that of their lunar counterparts (fig. 3.5). The craters range in size from as small as 100 m (highest resolution obtained by Mariner 10) up to basins over 1000 km in diameter. Small craters are bowl-shaped, but with increasing size they develop central peaks, terraces on their inner walls, and ejecta deposits with hummocky radial facies and swarms of secondary impact craters. Many fresh craters larger than about 100 km in diameter display interior concentric rings. As on the Moon, the craters and basins unquestionably represent the products of impacts by the complete size-range of meteoritic material. Similarly, crater morphologies become less sharp with increasing age until most of the crater elements are barely discernible. The dominant degradational process is apparently erosion and ballistic sedimentation by meteoritic bombardment, although in at least some cases the emplacement of plains units, viscous relaxation and possibly isostatic adjustments have contributed. Craters can be classified according to the degree of degradation of morphological components such as rays, secondary craters, various ejecta facies,

Figure 3.5. Comparison of a lunar (A), Mercurian (B), and Martian (C) crater. The width of the Mercurian continuous ejecta blanket (B) is less than that of the Moon (A) due to the reduced ballistic range. The Martian ejecta blanket (C) has a lobate form indicating flowage across the surface possibly due to impact in a subsurface permafrost layer. (Lunar crater is Copernicus, 93 km; Mercurian crater is Brahms, 75 km; Martian crater is Cerulli, 115 km.)

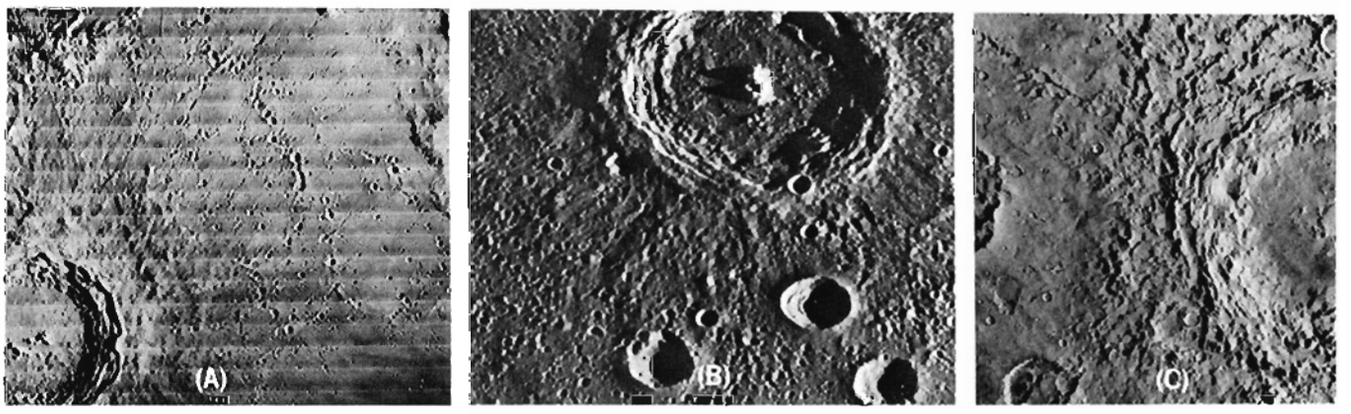

rim sharpness, and the state of interior terraces. Craters of similar size and state of preservation are considered to be about the same relative age.

In the 1960s, the Lunar and Planetary Laboratory (University of Arizona) developed a five-fold classification scheme for lunar craters (Arthur et al., 1963). The LPL classification designates Class 1 craters as the freshest and Class 5 craters as the most degraded. The U.S. Geological Survey has developed a somewhat similar five-fold classification designating the degradational state of craters as C_5 through C_1; C_5 being the freshest crater and C_1 being the most degraded (the reverse of the LPL scheme). Fortunately, the classification used by both organizations is based on somewhat similar criteria and therefore the crater classes are fairly interchangeable. However, investigators have used one or the other classification in various papers leading to extreme confusion for those unfamiliar with the two schemes. Because the LPL classification is found more frequently in the literature, it will be used here.

The freshest craters have well-developed and extensive ray systems; many extend hundreds of kilometers and some over 1000 km (fig. 3.3). Surrounding some craters are dark halos resembling those associated with such lunar craters as Tycho and Aristarchus. Other fresh-appearing craters have lost their ray systems and dark halos. Several relatively fresh craters have very bright patches on their floors. Unlike the Moon, color ratios from Mariner 10 images (Hapke et al., 1975) show that Mercurian ray systems and bright halos are bluer than their surroundings, and that the bright patches on the crater floors are redder than their surroundings.

Ejecta Deposits

One of the main differences between lunar and Mercurian craters is the character of their ejecta deposits (Gault et al., 1975). Lunar craters have outer rims of hummocky terrain grading outward into a radially ridged facies. These two facies comprise the continuous ejecta blanket. The continuous ejecta blanket, in turn, grades outward into discontinuous ejecta deposits where secondary impact craters form crater clusters and chains. For a given rim diameter the radial extent of Mercurian continuous ejecta blankets is uniformly smaller than that for the Moon (fig. 3.5) by a factor of about 0.65 (Gault et al., 1975). This reduced width is the result of the greater gravitational field on Mercury (370 cm/sec^2) which reduces the ballistic range of ejecta.

The distribution and characteristics of secondary impact craters of the discontinuous ejecta deposits also differ from their lunar counterparts (fig. 3.6). On Mercury the maximum areal density of secondary craters occurs closer to the primary crater's rim than for similar-sized lunar craters. The maximum density occurs at about 1.5 crater radii from the rim of Mercurian primaries, while on the Moon the maximum density occurs at about 2–2.5 crater radii. Furthermore, the maximum density of secondaries is over twice that of lunar craters of comparable size, but beyond two crater diameters the areal densities are about the same. The restricted distribution and enhanced areal density of Mercurian secondaries relative to those on the Moon can also be explained by the smaller ballistic range. This tends to reduce the dispersion between individual ejected fragments and concentrate them in a smaller area surrounding the crater (Gault et al., 1975). Long linear crateriform grooves near the rims of many Mercurian craters are probably the result of this reduced dispersion for larger ejected fragments. In a lower gravity field the secondaries would not overlap as much and would tend to form chains of more discrete craters as observed on the Moon.

Scott (1977) has noted that Mercurian secondaries are larger, deeper, and better preserved than those for primary craters on the Moon of similar size and degradation. He suggests that the difference is caused by greater secondary impact velocities on Mercury. For equivalent ranges, ejection velocities and therefore impact velocities are about 1.5 times greater on Mercury. These higher velocities may produce larger secondary craters which degrade more slowly than on the Moon.

Figure 3.7 illustrates the different ballistic ranges (R) for fragments launched at various ejection angles and velocities on the Moon and Mercury. The curves were derived from the ballistic equation for airless bodies and take into account the change in gravity with height and the radius of curvature of the surface. Because only gravitational forces modify the trajectories, an ejected fragment returns to the surface along a segment of an elliptical orbit. The apoapse of this orbit corresponds to the maximum height of the fragment while, in general, the periapse is within the body of the planet (Wright et al., 1963). Consequently,

$$R = 2r \tan^{-1}\left(\frac{V \sin\theta \cos\theta}{1 - V\cos^2\theta}\right)$$

where $0 \leq \theta \leq \pi/2$

and $V = V_c^2/rg$

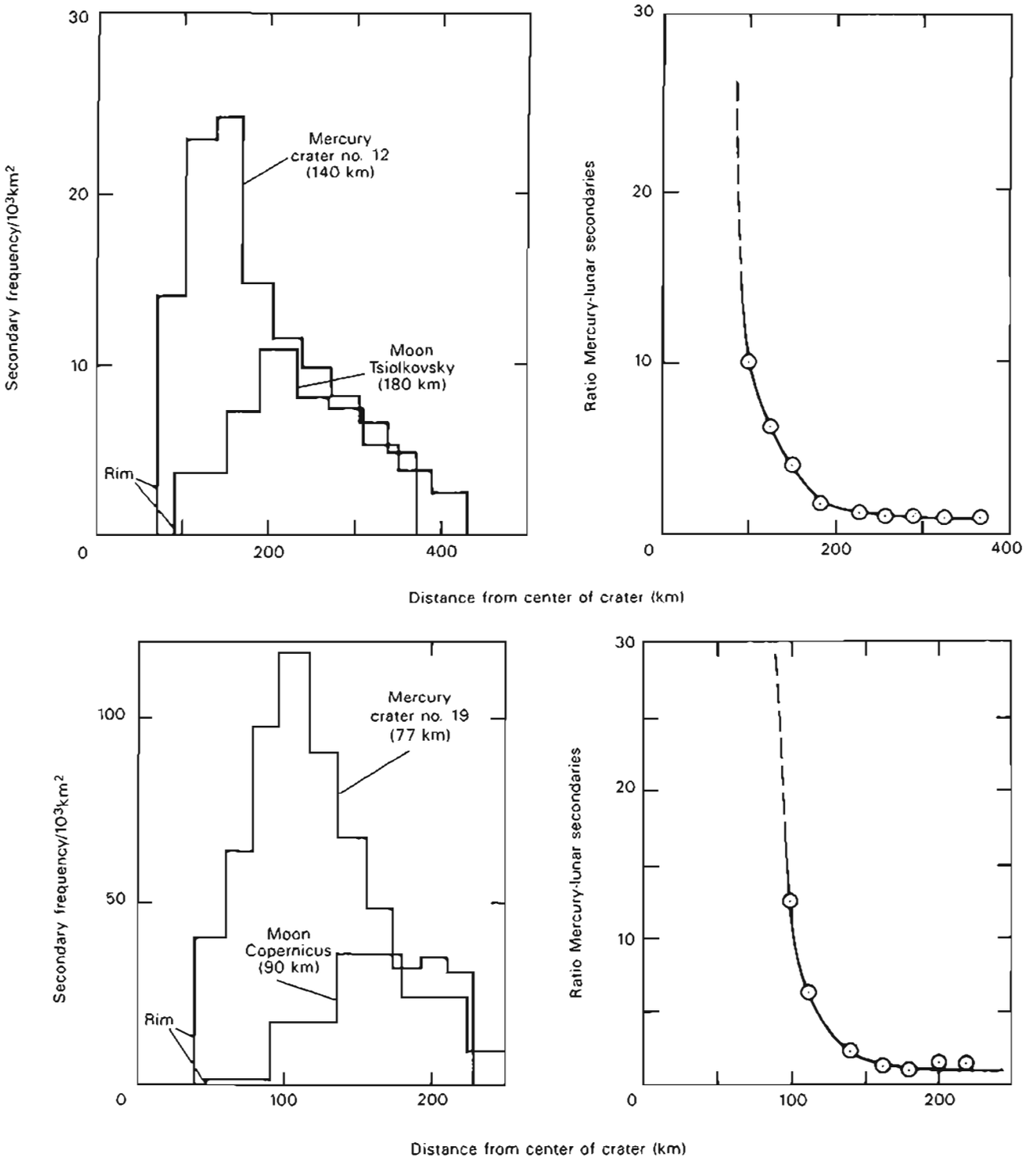

Figure 3.6. Radial variations in the areal density of secondary craters and the ratios of Mercurian to lunar secondary craters for Mercurian craters 12 (Verdi) and 19 (March) and for lunar craters Copernicus and Tsiolkovsky. (From Gault et al., 1975.)

V_c is the ejection velocity, g is gravitational acceleration (Moon = 162 cm/sec²; Mercury = 370 cm/sec²), r is the planet radius (Moon = 1738 km; Mercury = 2439 km), and θ is the ejection angle from the horizontal.

Experimental hypervelocity impacts (Gault et al., 1968) indicate that most material is ejected at angles between 30° and 45° from the horizontal. The curves in figure 3.7 show that for a given range at these ejection angles the ejection velocity is constrained within

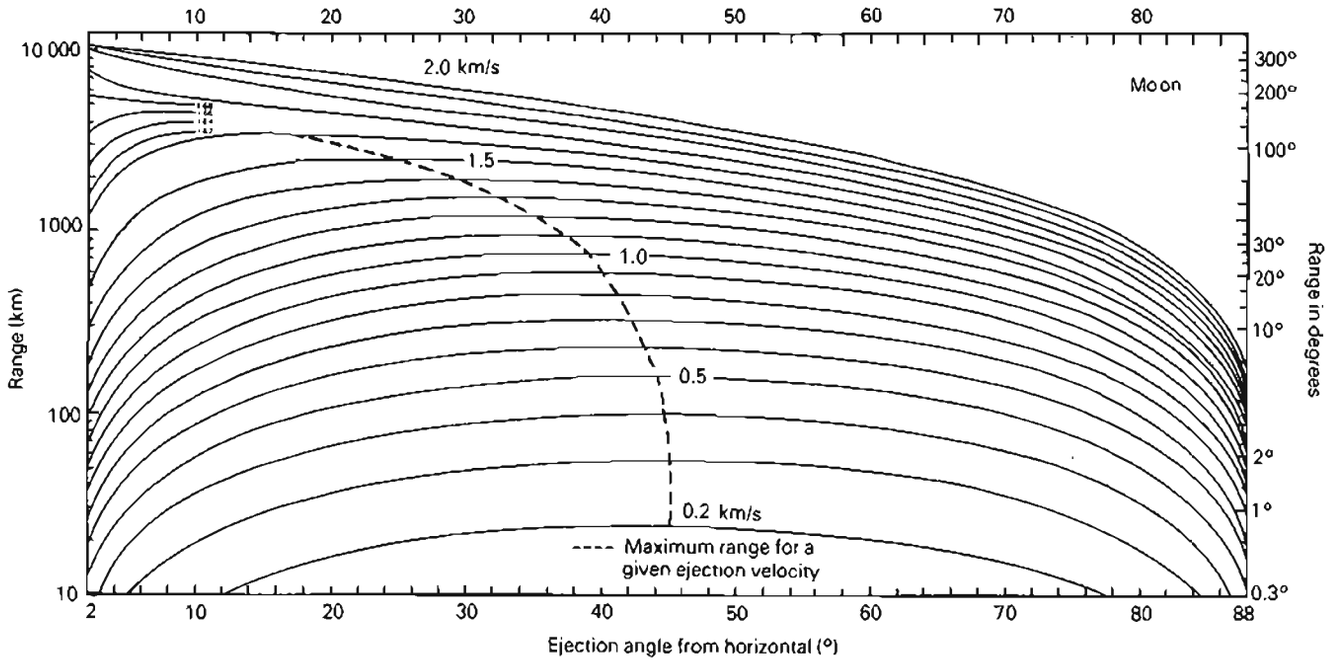

Figure 3.7. Plot of the range versus ejection angles from the horizontal for various ejection velocities for the Moon and Mercury.

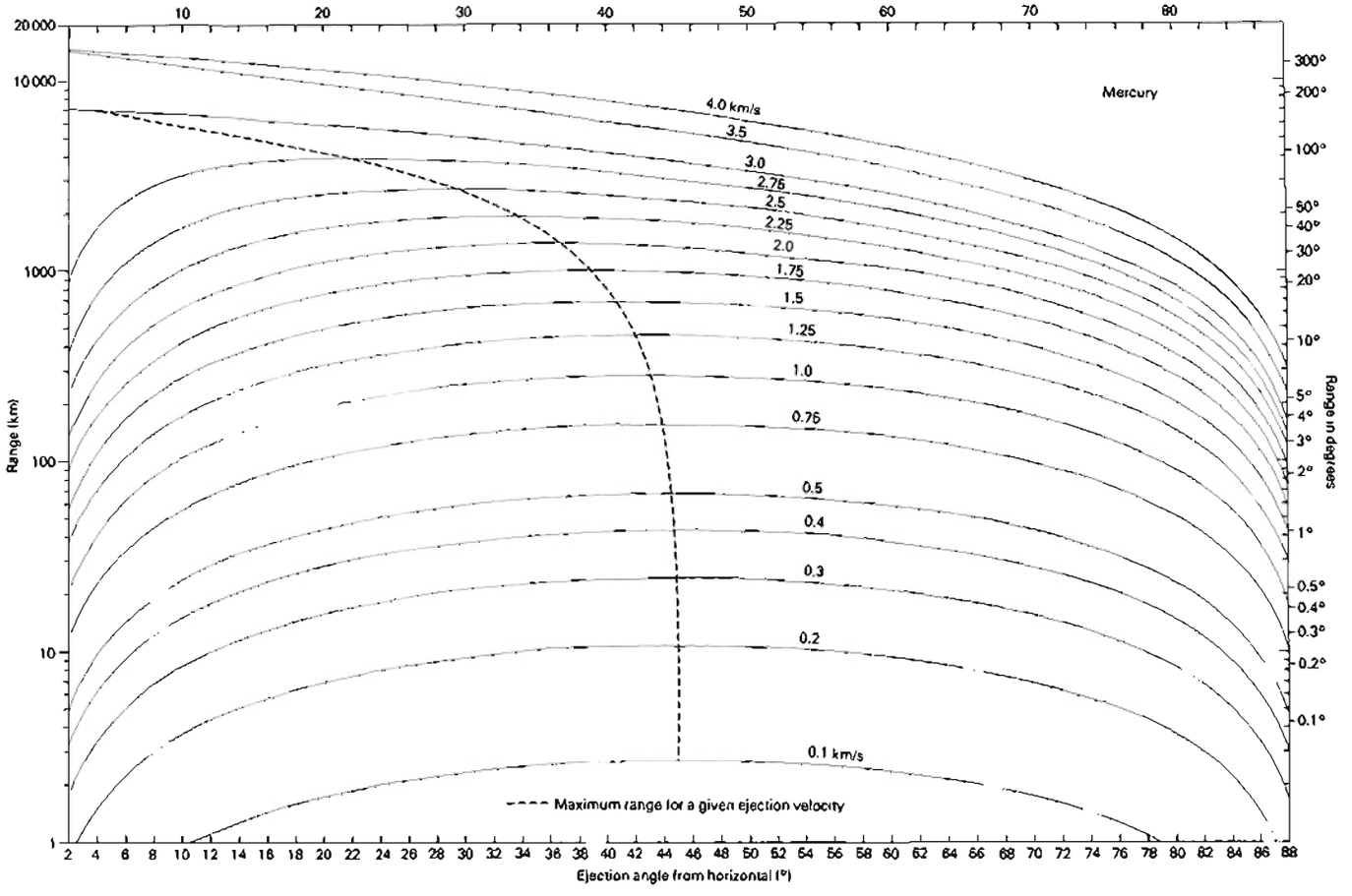

narrow limits. Even between ejection angles of 20–70° the ejection velocities are rather tightly constrained. Furthermore, with increasing ejection velocities above about 0.4 km/sec the maximum range occurs for progressively smaller ejection angles (less than 45°). Gault's studies indicate that the maximum secondary crater density occurs at about 1.5 crater radii on Mercury and about 2.0–2.5 crater radii on the Moon. Therefore, for both lunar and Mercurian craters in the diameter range 20–200 km, most of the larger fragments appear to have been ejected at velocities between 0.2–0.6 km/sec. For a given range, however, the ejection velocities are about 1.5 times greater on Mercury.

Interior Structure

The interior structure of Mercurian craters (terraces, central peaks, and rings) is similar to that of lunar craters (fig. 3.5) but the frequency of occurrence of some morphological features appears to be different. Fresh simple bowl-shaped craters have a depth/diameter ratio (1:5) similar to that for both lunar and Martian craters (Pike, 1980). The transition from simple bowl-shaped craters to complex craters (terraces and central peaks) occurs at about the same diameter on the Moon and Mercury (16–19 km), but at a much smaller diameter on Mars (6 km). Many other morphological and statistical differences occur between Martian craters and lunar and Mercurian craters. The most notable difference is the peculiar lobate ejecta blankets associated with Martian craters over a wide range of diameters and terrain types (fig. 3.5). These ejecta blankets have been attributed to impacts penetrating a subsurface ice layer and ejecting material with a high volatile content which flowed across the surface (Carr et al., 1977). Other differences include a much smaller diameter at which double ring basins occur on Mars compared to the Moon and Mercury (Wood, 1980), and a greater abundance of central peaks on Mars (Wood et al., 1978). These contrasts are probably due to differences in the physical properties of the target material including volatile content and stratification, although gravity and impact velocity may also have an effect.

Although the depth/diameter relationships and onset diameters of central peaks and terraces appear similar for both lunar and Mercurian craters, the diameter/frequency distribution of central peaks, terraces, and scalloped crater rims (slump features) is different. Smith and Hartnell (1979) found Mercury has a significantly higher percentage of fresh craters with central peaks than the Moon in the 5–75 km

Figure 3.8. Histogram of the central peak (A) and terrace (B) frequency versus crater diameter for the Moon and Mercury. (From Smith and Hartnell, 1979.)

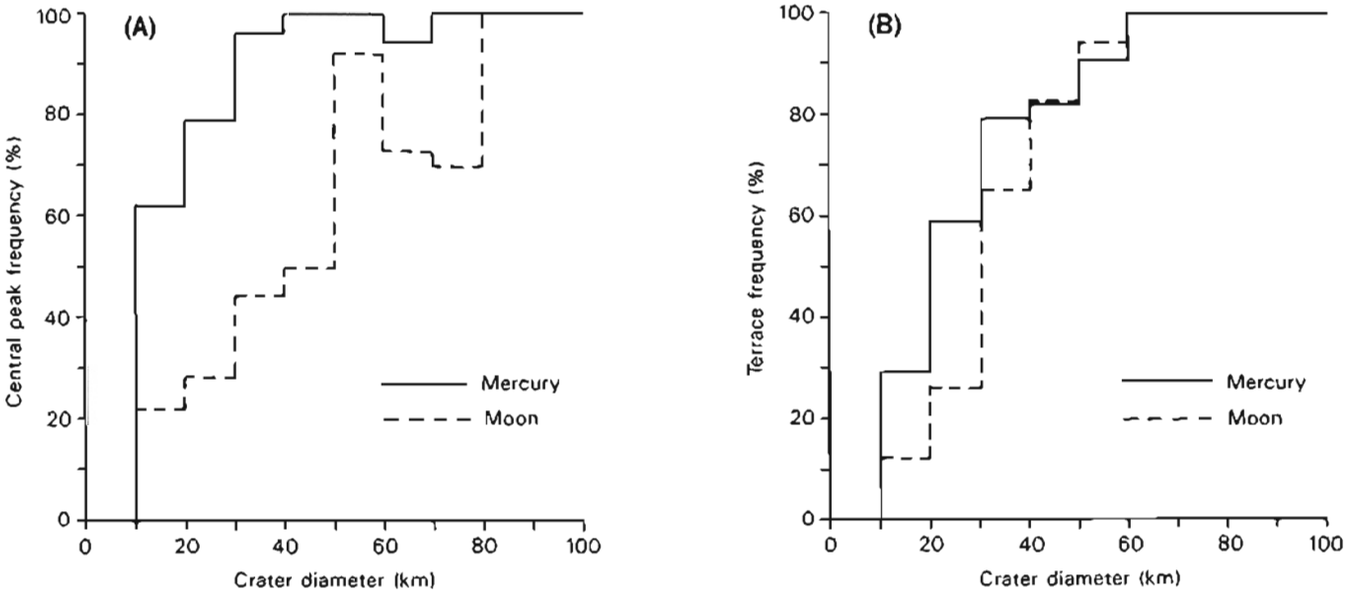

diameter range. Above a diameter of 75 km, all fresh craters on the Moon and Mercury have central peaks. Terraces are more abundant in Mercurian than lunar craters up to a diameter of 45 km (fig. 3.8). They concluded that gravity, terrain type, and impact velocity are important in influencing crater shape. Moreover, that gravity may be a critical factor because of similarities in the terrace and central peak plots that suggest wall failure and hence gravitational potential energy is important. Hale and Head (1980) found that the ratio of central peak diameter to crater diameter is the same for Mercury and the Moon. This, together with a similar peak height to rim height relation (Malin and Dzurisin, 1976, 1978), suggests to them that gravity is not the controlling factor in central peak formation, but rather dynamic rebound plays the major role.

Smith and Hartnell (1979) and Cintala et al. (1977) have found significant differences in the abundances of central peaks, terraces, and scalloped crater rims between fresh craters in the lunar maria and highlands (figs. 3.9 and 3.10). Both studies attribute these contrasts to differences in physical properties of the target materials; the lunar highlands consisting of a thick regolith and breccia (the megaregolith) and the maria consisting of only a thin regolith underlain by unbrecciated volcanic flows.

In a similar comparison of analogous terrain types on the Moon and Mercury, Cintala et al. (1977) found that the morphologies of craters formed in the lunar maria, the Mercurian smooth plains, and the Mercurian cratered terrain are similar. They also found, however, that large differences exist between craters formed in the lunar highlands and the analogous Mercurian cratered terrain (fig. 3.10). This suggests that a difference in the physical properties of the target material, rather than gravity, is a major factor affecting the formation of crater interior morphologic features. Accordingly, they suggested that the similar morphologies of craters formed in Mercurian smooth plains, lunar maria, and Mercurian cratered terrain indicate similar physical properties for all three terrains, but that large differences in Mercurian cratered terrain and the lunar highlands imply dissimilar physical properties. The main difference between the lunar highlands and the Mercurian cratered terrain is the great abundance of intercrater plains on Mercury. Because the lunar maria are volcanic lava flows, they reason that both the young Mercurian smooth plains and the older intercrater plains may also be volcanic deposits.

In summary, the formation of interior and exterior crater morphology is probably a complex interaction of two or more factors such as surface gravity, impact velocity, physical properties of the substrate, and subsurface crustal structure or discontinuities. The differences in the ejecta deposits of Mercurian and lunar craters are almost certainly due to the differences in

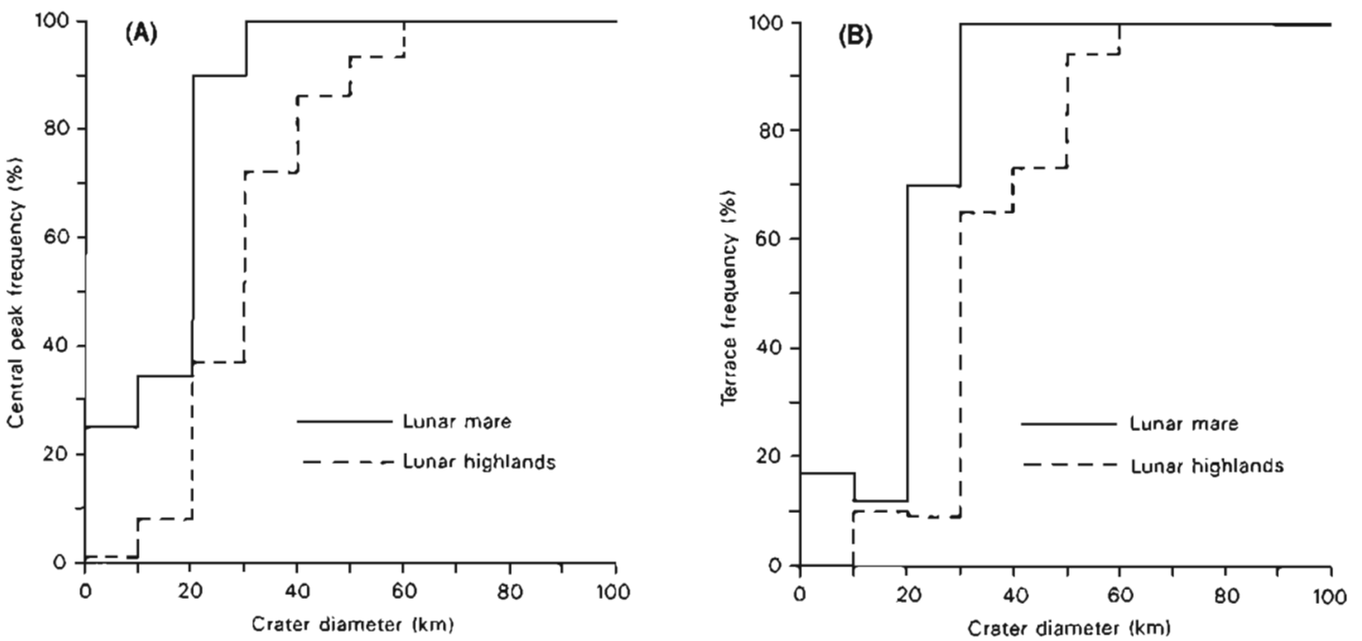

Figure 3.9. Histogram of the central peak (A) and terrace (B) frequency versus crater diameter for the lunar highlands and mare. (From Smith and Hartnell, 1979.)

gravitational acceleration, which reduces the ballistic range and increases the secondary impact velocity for a given range on Mercury compared to the Moon. The frequency of occurrence of interior structures such as slump structures and central peaks in craters appears to be related primarily to differences in the physical properties of the substrate, although gravity and impact velocity may play a role. Similar onset diameters of these features and similar depth/diameter relationships on the Moon and Mercury, together with other observations, suggest that gravitational potential energy and impact velocity are not significant factors affecting these attributes. Comparisons of interior morphologic features between lunar and Mercurian craters suggests that Mercurian smooth and intercrater plains and the lunar maria have similar physical properties that are different from those of the lunar highlands.

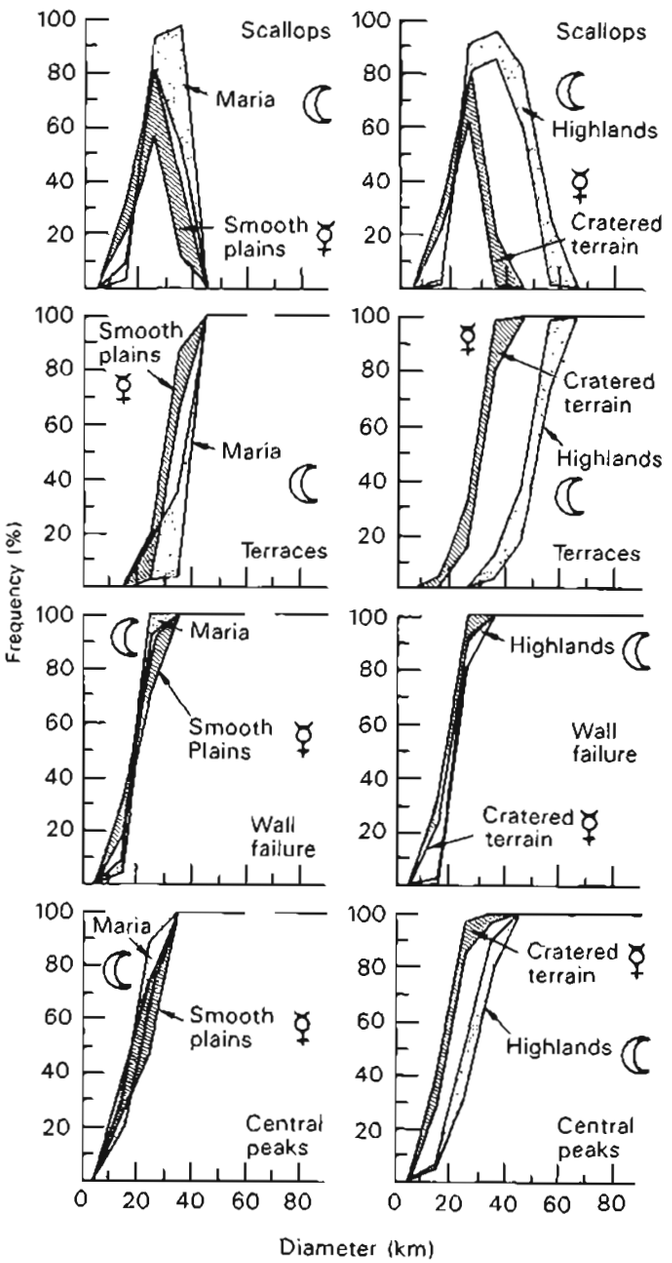

Figure 3.10a. Morphology/frequency distribution comparing craters on the lunar maria to those in the Mercurian smooth plains (left), and craters in the lunar highlands to those in the Mercurian cratered terrain (right). (From Cintala et al., 1977.)

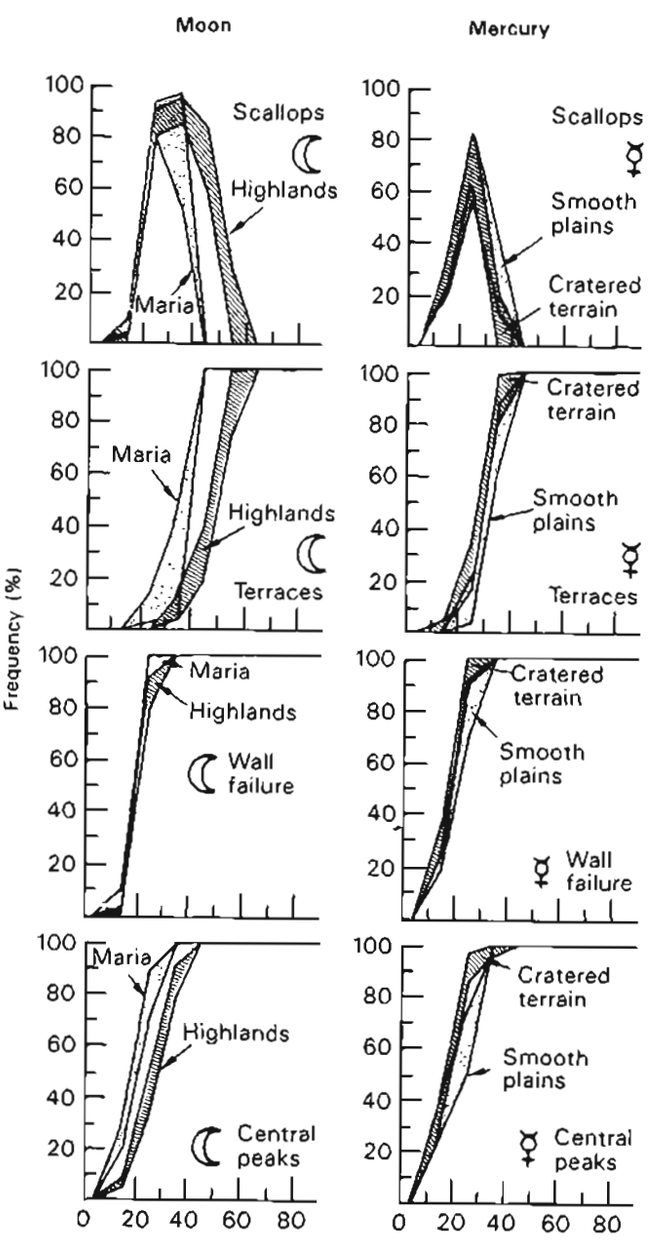

Figure 3.10b. Morphology/frequency distribution, illustrated as ±1σ envelopes around the mean values, for craters on the Moon (left) and Mercury (right). (From Cintala et al., 1977.)

The Caloris and Other Large Basins

Basins are nothing more than very large craters, making the definition of a basin somewhat arbitrary. Hartmann and Kuiper (1962) defined the term as a large circular depression with distinctive concentric rings and radial lineaments. Wood and Head (1976) followed this definition but place special significance on the development of concentric rings. Other investigators (e.g., Murray et al., 1974) considered any crater larger than an arbitrary diameter (in their case 200 km) as a basin.

With increasing size, craters with diameters larger than about 100 km show a gradual transition from a central peak surrounded by an irregular ring of peaks, to single concentric rings of peaks to multiple concentric rings at the largest diameters (fig. 3.11). Wood and Head (1976) termed craters with a central peak surrounded by an irregular ring of peaks as *central peak basins,* and craters with a single concentric ring of peaks as *peak ring basins.* On Mercury, central peak basins first occur at about 90 km diameter, whereas on the Moon they first appear at about 140 km diameter (Wood and Head, 1976; Gault et al., 1975). Multi-ring basins have two or more rings with at least the outer rings being asymmetric in profile (more scarp-like). Only two structures on Mercury have been identified as multi-ring basins: Caloris

Figure 3.11. Comparison of lunar central peak basin Compton (A) and Mercurian central peak basin Hitomaro (B) with lunar peak ring basin Schrödinger (C) and Mercurian peak ring basins Strindberg and Ahmad Baba (D). Compton is 175 km in diameter; Hitomaro is 58 km in diameter; Schrödinger is 320 km in diameter; Strindberg is 165 km in diameter; and Ahmad Baba is 115 km in diameter.

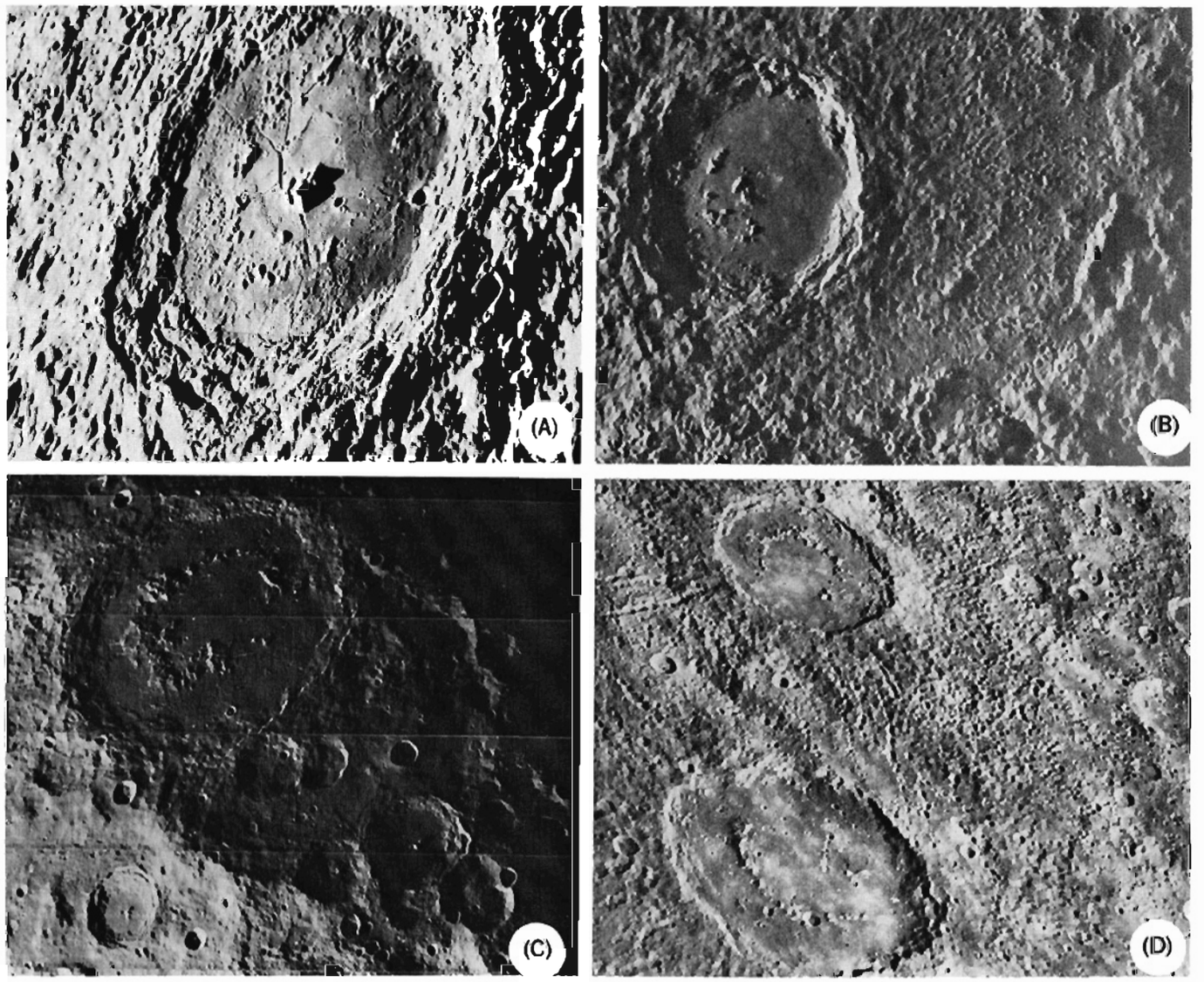

(1300 km diameter) and Tolstoj (400 km diameter). The apparent lack of such structures may be due in part to the poor photographic coverage, adverse lighting conditions, or burial of ring structures by subsequent basin infill. The ring spacing of these basins is significantly less than those on the Moon and Mars. Based on ring tectonic theory, McKinnon (1981) considered this smaller spacing to indicate a relatively thin (< 50–125 km) lithosphere at the time of formation.

The largest structure viewed by Mariner 10 is the Caloris basin (1300 km diameter) (fig. 3.12). This basin has many characteristics in common with the lunar Orientale (fig. 3.13) and Imbrium basins (Strom et al., 1975b; McCauley, 1977). The main ring consists of segmented massifs with rectilinear outlines about 30 × 50 km in size and average about 1–2 km in height above the basin floor. The basin interior is filled with smooth plains that are extensively ridged and fractured. This type of floor structure appears to

Figure 3.12. Photomosaic of the Caloris basin. Unlike other planetary basins, the floor is highly ridged and fractured. Both ridges and fractures display a concentric and radial pattern.

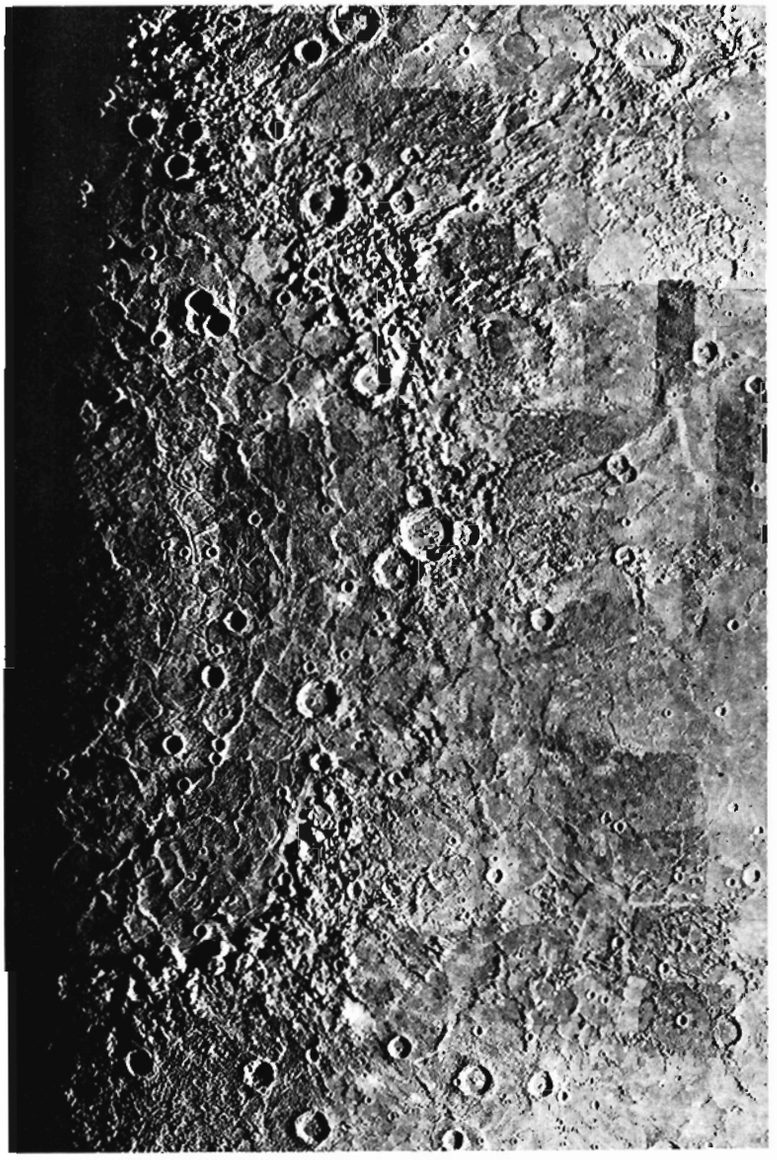

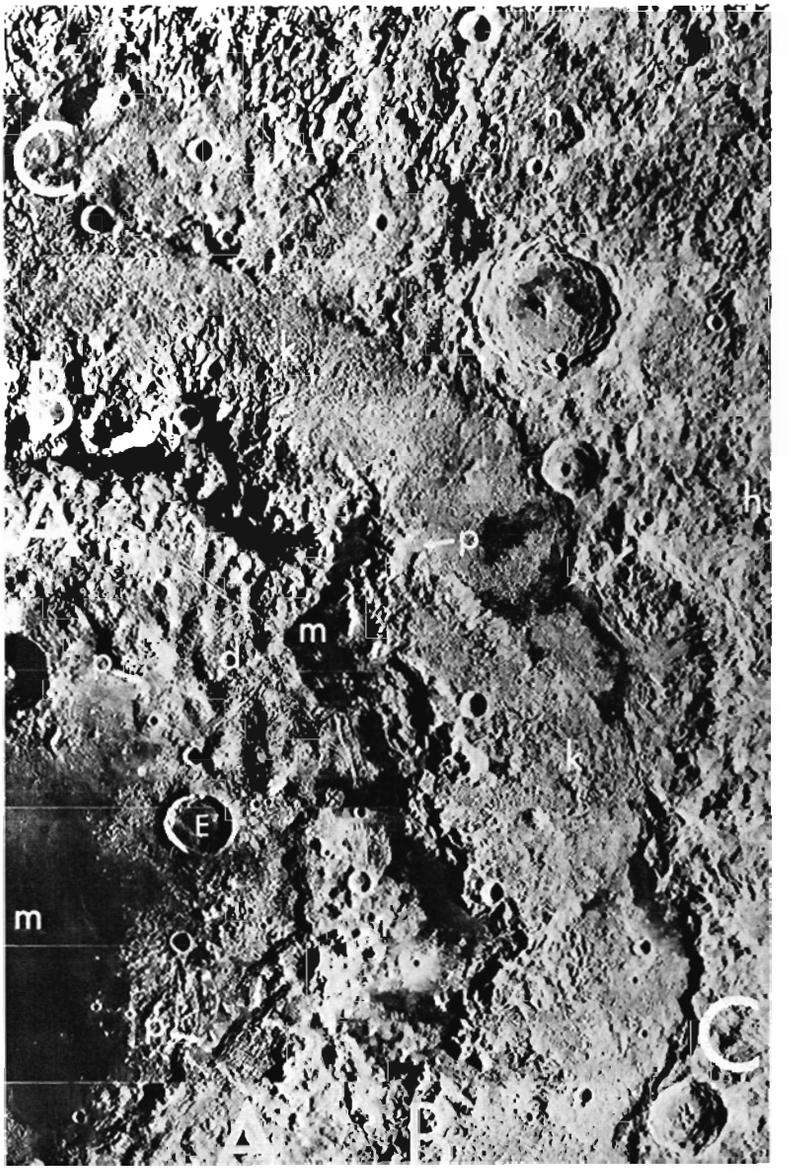

Figure 3.13. Lunar Orbiter 4 photograph (M 181) of a portion of the lunar Orientale basin showing the multi-ring structure and various geologic units associated with the basin. The diameter of the Cordillera ring (C) is about 920 km. The crater Kopff (E) is 40 km in diameter. Geologic units are A, Inner Rook Mountains; B, Outer Rook Mountains; C, Cordillera Mountains; m, mare basalts; d, domical and fractured terrain; k, knobby and hummocky terrain; h, radially lineated and braided continuous ejecta deposits (Hevelius Formation); p, small patches of light smooth plains.

be unique to Caloris; it is not present in any other basin on Mercury, Mars or the Moon. A weakly developed outer scarp occurs at about 100-160 km from the main scarp, and is best seen in the northeastern part of the basin (fig. 3.14). The area between the two scarps consists of a blocky to knobby terrain grading outward beyond the outer scarp into a radially lineated terrain (fig. 3.14). This lineated terrain extends to about one basin diameter from the main Caloris scarp and is embayed by both smooth and hummocky plains (Trask and Guest, 1975). Hummocky plains appear as large lobes around the basin and consist of numerous smooth equidimensional knobs set in a matrix of rolling plains (fig. 3.15). Smooth plains form a broad belt that is circumferential to the basin and extend outward for over one basin diameter (fig. 3.16). Numerous poorly-preserved crater clusters, chains, and irregular troughs lie within the cratered terrain beyond one basin diameter and are probably secondary impact craters from Caloris (McCauley, 1977). With the possible exception of the smooth plains, all these terrains probably represent materials or structures produced by the impact that formed the Caloris basin. The units have been assigned a formal rock-stratigraphic nomenclature (McCauley et al., 1981) patterned after that used in geologic mapping of the Imbrium basin (Wilhelms and McCauley, 1971) and the Orientale basin (Scott et al., 1977).

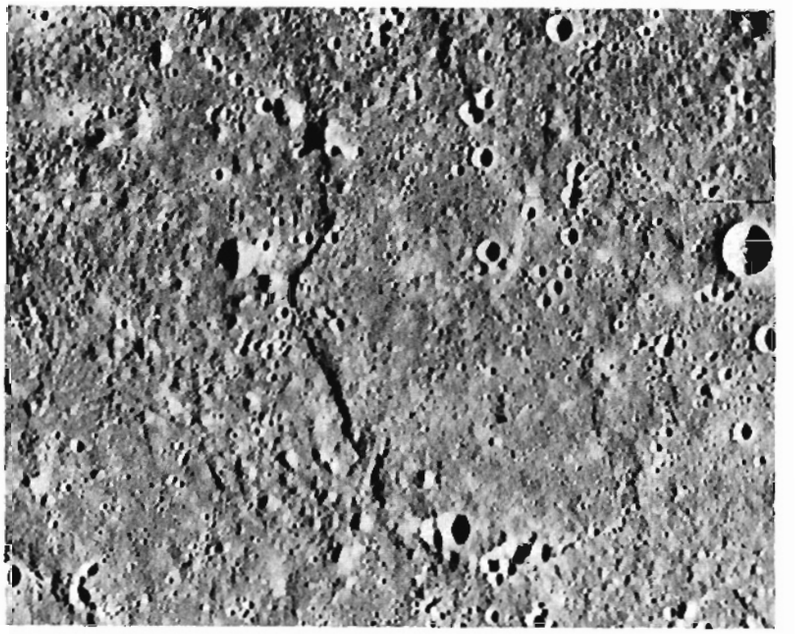

Figure 3.15. The Caloris hummocky plains; a basin ejecta facies. The large hill left of the scarp is about 1.4 km high. The area is located about 200 km east of the rim of the Caloris basin. The area covered by this picture is 153 × 115 km. (FDS 72)

Based on morphologic similarities, McCauley (1977) considered the main Caloris scarp and the weaker outer scarp to be the structural equivalents of the lunar Orientale Montes Rook and Montes Cordillera scarp, respectively (figs. 3.12 and 3.13). The radially lineated terrain extending outward from the outer scarp is thought to be the eroded equivalent of the Orientale radially-braided continuous ejecta deposit termed the Hevelius Formation (fig. 3.13).

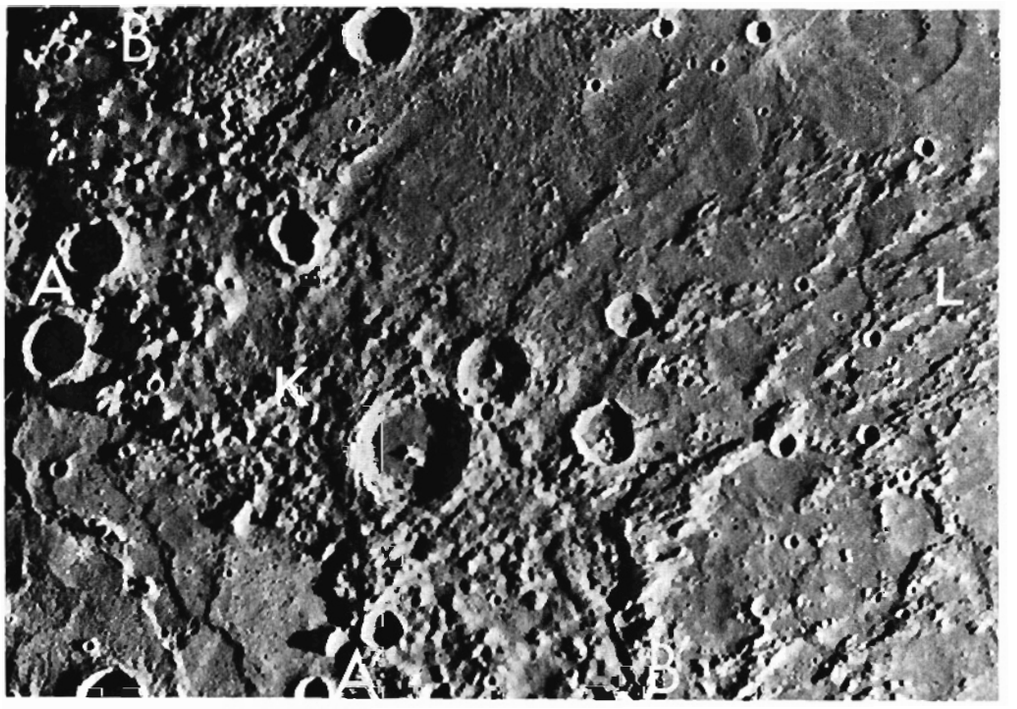

Figure 3.14. The Caloris basin Knobby (K) and Lineated (L) terrain. The inner Caloris ring is denoted by A-A' and the outer ring by B-B'. (FDS 193)

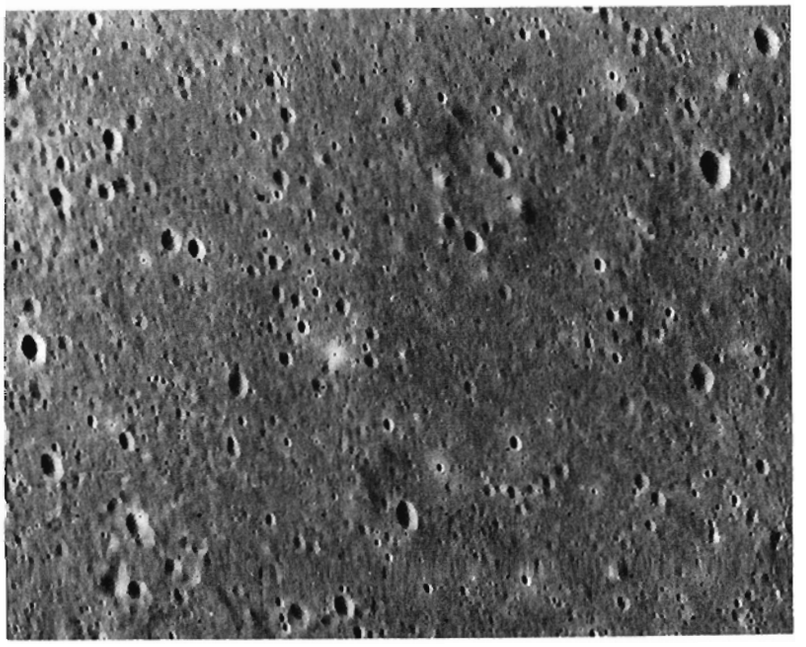

Figure 3.16. Smooth plains located about 700 km east of the Caloris basin. The vertical and horizontal dimensions of this picture are about 50 and 85 km, respectively. (FDS 45)

Its position and extent relative to the outer scarp is essentially the same as that of the Hevelius Formation relative to the Montes Cordillera scarp. The large lobes of hummocky plains have a distribution outside the basin rim similar to that of the Alpes Formation around the lunar Imbrium basin. The Alpes Formation is the textural counterpart of the knobby terrain primarily found between the Outer Rook Mountains and the Cordillera scarp in the Orientale basin (fig. 3.13). However, unlike the Orientale knobby terrain, the Caloris hummocky plains embay and are interspersed with the lineated terrain out to at least one basin radius. McCauley (1977) and McCauley et al. (1981) considered the main Caloris scarp to be the rim of the excavation crater while the hummocky plains and radially lineated terrain are ejecta deposits laid down contemporaneously with the formation of the outer scarp by slumping. McKinnon (1981) pointed out, however, that the basin floor subtends 0.53 radius and the geometry of the shock that would create such a crater is inconsistent with a transient depth less than 90 km (the line of sight depth from the Caloris Montes rim). The volumetric adjustment required to compensate for this transient depth is inconsistent with the weak deformation observed beyond the main scarp. Therefore, the limit of excavation was probably within the main scarp and buried by the smooth plains that fill the basin.

Although it is not possible to date unambiguously the Caloris impact on an absolute time scale, its age relative to the general crater population can be estimated by superposition relationships of ejecta deposits on pre-existing terrain and the degradational state of craters superposed on the ejecta deposits. McCauley et al. (1981) found that numerous craters in the 30 to 100 km size-range are superposed on the Caloris ejecta assemblage and that most of these are Class 1 (USGS C_5 type) and Class 2 (USGS C_4 type). A few smaller craters primarily 30 to 50 km in size are designated upper Class 3 (USGS upper C_3 type) and also are superposed on Caloris ejecta. Therefore, the Caloris impact seems to have occurred near the end of formation of Class 3 craters. Wood et al. (1977), in a study of degradational crater types, found that on both the Moon and Mercury extensive crater degradation occurred during the formation of Class 5 to Class 3 craters, and a lower level of modification has occurred since then. They concluded that the period of intense bombardment ended on both the Moon and Mercury during the transition from Class 3 to Class 2 craters. However, the absolute time represented by this transition is not necessarily the same on both bodies. In any event, the Caloris impact seems to have occurred near the end of intense bombardment on Mercury.

The origin of the smooth plains which fill and surround Caloris is not clear. Both impact (Wilhelms, 1976; Oberbeck et al., 1977) and volcanic (Strom et al., 1975b; Trask and Strom, 1976; Cintala et al., 1977; Hawke and Cintala, 1977) origins have been suggested. However, as mentioned earlier, the structure of the smooth plains that fill Caloris appears to be unique. Although the plains superficially resemble the Orientale Maunder Formation interior to the Outer Rook Mountains and interpreted as impact melt, their overall appearance is dissimilar (Strom et al., 1975b; McCauley, 1977). They have a much more extensive and coarser concentric and radial fracture pattern which transects numerous mare-like ridges not present in the Maunder Formation (fig. 3.17). The fractures become progressively more pronounced (wider and deeper) toward the basin center (Strom et al., 1975b). Mare-like ridges also form concentric and radial patterns. Transection relationships indicate that most of the ridges predate the formation of the fractures. Strom et al. (1975b) suggested that the ridges are compressional features formed by subsidence of the basin floor, and that the fractures represent tensional features produced by subsequent uplift of the central basin. Dzurisin (1976) hypothesized that the subsidence was caused by withdrawal of magma beneath Caloris and subsequently extruded to form

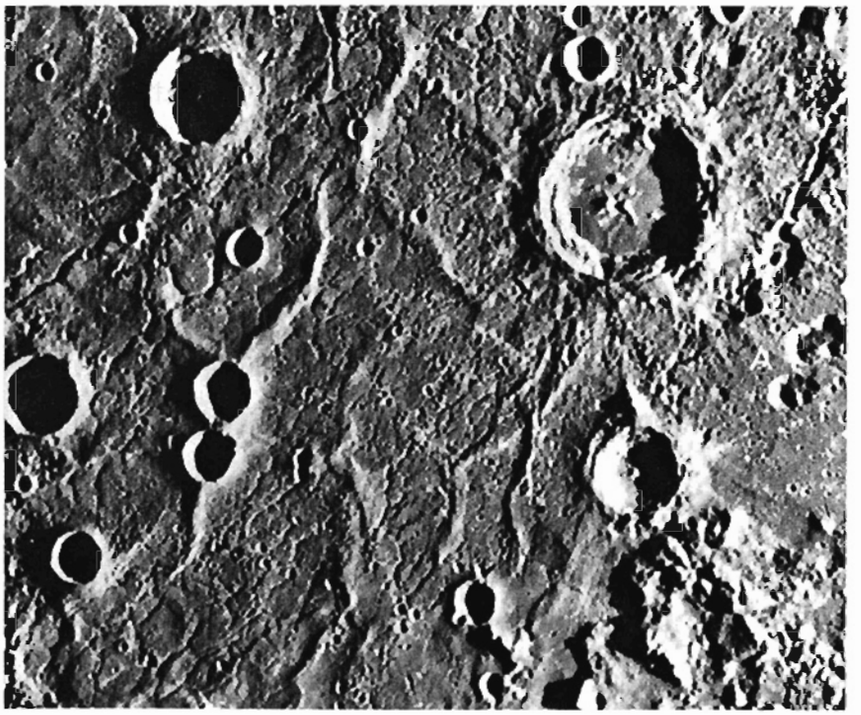

Figure 3.17. Part of the Caloris basin floor showing the ridges and fractures. The length and width of the fractures increase toward the center of the basin (lower right to upper left) and the fractures transect the ridges indicating they are younger. The irregular depressions at A are rimless and probably originated by collapse rather than impact. The largest crater is about 60 km in diameter. (FDS 126)

the smooth plains outside the basin. The central basin uplift is presumed to be caused by relaxation toward isostatic equilibrium following this event. Based on this hypothesis and the fact that Caloris is located near Mercury's axis of minimum moment of inertia, Melosh and Dzurisin (1978a) suggested there may be an annular positive gravity anomaly associated with isostatically uncompensated material constituting the smooth plains surrounding the basin. They hypothesize that it is this positive gravity anomaly, rather than a mascon associated with the basin interior as postulated by Murray et al. (1974), which may account for the coincidence of the Caloris basin with the long axis of the planet's dynamical figure. They assume that the uplift responsible for the fracture pattern is due to isostatic adjustments, but it also may be driven by the annular load itself (McKinnon, 1979). It is also possible that the uplift resulted from an intrusion of basic or ultrabasic magma following the initial subsidence of the floor.

Other large basins on Mercury are more degraded than Caloris, contain a higher density of superposed craters, and so appear to be older. Furthermore, most are filled with unfractured smooth plains that often embay post-basin craters. This, together with the fact that the smooth interior plains often have a much lower crater density than the exterior terrain, indicates the plains are often younger than the basins they occupy (Strom et al., 1975b; Trask and Strom, 1976).

Two very degraded basins about 800 km in diameter have been recognized primarily by circular patches of smooth plains (Schaber et al., 1977; DeHon, 1978). Trask and Strom (1976) suggested that the large area of smooth plains in the north polar region (Borealis Planitia) may occupy an ancient basin about 1000 km in diameter, but identification is uncertain because of incomplete photographic coverage in this region. Figure 3.18 shows another large basin (Beethoven, 630 km diameter) about half the size of Caloris which has been described by Strom et al.

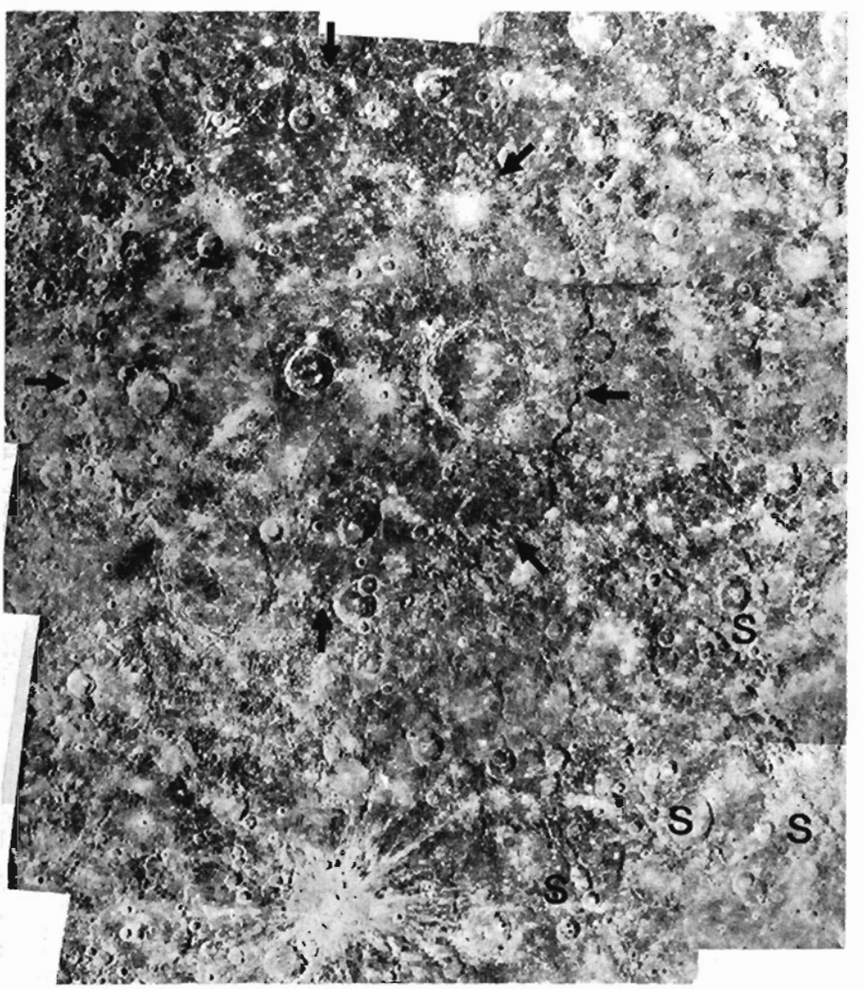

Figure 3.18. Photomosaic of the 625-km-diameter Beethoven basin. The basin is indicated by arrows. Remnants of radial sculpturing (s) occur southeast of the basin and consist primarily of crater chains.

(1975a). Although Mariner 10 photographed this basin under a high illumination (70°), the rim and other basin structure are discernible. The basin is filled with plains that have been moderately cratered by large impacts. No large expanses of exterior plains comparable to those surrounding Caloris are recognized. However, a radial sculpture in the form of crater chains 150–180 km long and about 12 km wide are visible to the southeast of the basin. The chains extend at least one basin diameter from the rim, and are probably secondary impact craters.

Crater Statistics

The crater diameter/frequency distribution of the Mercurian highlands is similar to that of the lunar highlands and the heavily cratered provinces of Mars (fig. 3.19). All show a highly structured curve that cannot be represented by a single distribution function. Recent computer modeling, together with statistical and observational crater investigations, strongly suggest that the lunar highlands are not at saturation density, but instead basically represent a production

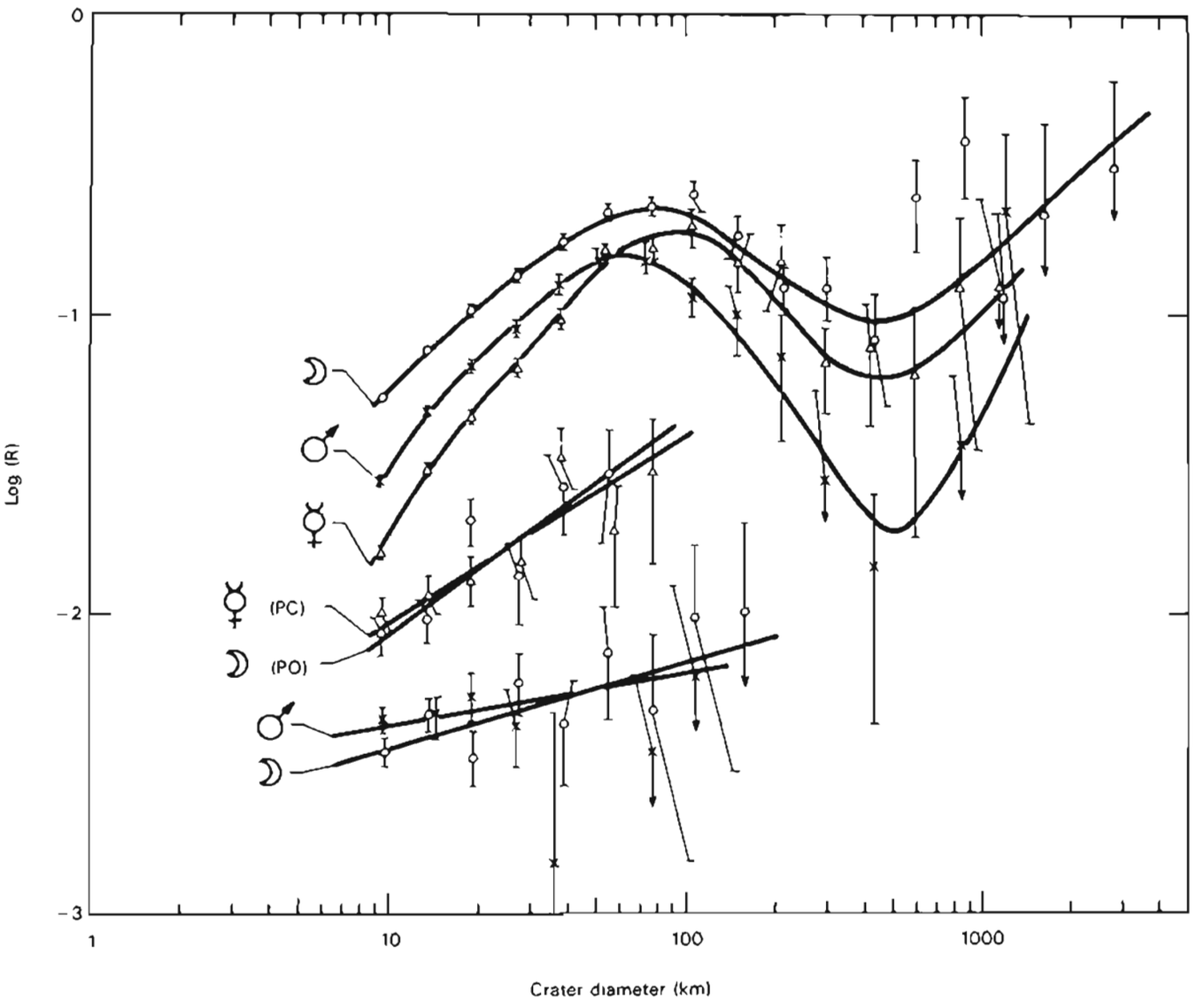

Figure 3.19. Comparison of the crater diameter/density distribution of the lunar, Mercurian, and Martian highlands; the post-Caloris (PC) and post-Orientale (PO) crater populations; and the post-mare and sparsely cratered areas of Mars. The R value is the ratio of the observed distribution function to the function $N = D^{-3}$, where N is the number of craters per unit area and D is the crater diameter.

population (Woronow, 1978; Oberbeck et al., 1977; Strom, 1977; Strom et al., 1981; Woronow et al., 1982). The same conclusion also applies to Mercury and Mars. The similarity in the overall structure of the crater diameter/frequency distribution between the Moon, Mars, and Mercury therefore suggests all three bodies were impacted by the same family of objects. One anomalous feature of the Mercurian highland curve is that at diameters less than about 80 km there is a paucity of craters compared to the Moon and Mars (fig. 3.19). Trask (1975) and Oberbeck et al. (1977) believed that the Mercurian curve more closely represents the true crater production population analogous to a lunar highland curve from which widely distributed basin secondaries have been subtracted.

Alternatively, Strom (1977) considered that the paucity of Mercurian craters relative to the Moon resulted from the obliteration of a fraction of Mercurian craters by emplacement of the intercrater plains. Locally on Mercury a crater excess occurs below a diameter of about 15 km and probably reflects the high density of craters below this diameter, which are superposed on intercrater plains. This excess has been interpreted as predominantly secondaries from craters and basins of the heavily cratered terrain (Trask, 1975; Strom, 1977). Although the overall shape of the Martian curve for the heavily cratered provinces is similar to those of the Mercurian and lunar highlands, the crater density is significantly less at both small and large diameters. It is unlikely that eolian or fluvial erosion and deposition are primarily responsible for this lower density because these processes would not obliterate all crater sizes equally. Three possible explanations are: (1) the total cumulative impact flux was less on Mars than on the Moon and Mercury, (2) an almost complete resurfacing occurred sometime after the onset of the period of heavy bombardment, or (3) surface solidification after accretionary melting occurred later on Mars than on the Moon and Mercury. The latter possibility assumes the period of heavy bombardment was contemporaneous on all three bodies. Both the post-Caloris and the lunar post-Orientale crater populations have a diameter/frequency distribution that is virtually identical in both shape and density (PC and PO in fig. 3.19). Their shapes are very similar (at the 90 percent confidence level) to those of the lunar and Martian highlands over the same diameter range and must represent production populations because of their low crater densities. This lends support to the contention that (1) the lunar and Martian highlands crater population basically represents a production population, and (2) in the case of Mercury, the paucity of craters less than about 80 km diameter resulted from obliteration of a fraction of craters by intercrater plains formation.

For the younger, more sparsely cratered surfaces of the Moon and Mars, the crater populations are quite different from those of the highlands. Both the lunar maria and Martian sparsely-cratered plains display essentially identical diameter/frequency distributions which differ significantly from those of the highlands (fig. 3.19). A Chi-squared test indicates they are different at the 99 percent confidence level. This suggests that at least the Moon and Mars were impacted by two families of objects—one primarily responsible for the period of late heavy bombardment, and the other primarily impacting after mare formation on the Moon and young plains formation on Mars. The flux history of these families on Mercury and Mars is uncertain, because it depends on the origin and source regions of the impacting objects.

In one scenario, the possibility is raised that the period of late heavy bombardment on Mercury may have been longer than that on the Moon and Mars due to an extended period of sweep-up of a family of accretional remnants (Vulcanoids) in the dynamically stable region between Mercury and the Sun (Leake et al., 1981). In spite of attempts to detect objects remaining in the region, none have yet been observed. If the impact flux history of early and late populations on the Moon was broadly similar on the other inner planets, then the earlier population consisted of short-lived objects, which were swept up in about the first billion years of solar system history, while the later population consists of long-lived objects, which have been impacting over about the past four billion years. On Mercury, the signature of this latter population has not yet been identified (Strom, 1979). Perhaps it never reached Mercury in numbers large enough to leave a recognizable signature; or the youngest surfaces on Mercury formed earlier than the lunar maria when the objects responsible for heavy bombardment still dominated. Judging by the cumulative crater density on the lunar maria, the number of objects for post-mare craters was very small compared to the earlier population, and therefore it may be mixed in with the post-Caloris craters.

However, Allen (1977) found that the diameter/frequency distributions of the rayed craters (the freshest craters) on the Moon and Mercury are different. On the Moon the rayed craters have the same distribution function as the post-mare craters; on Mercury

they appear to have a distribution function similar to the post-Caloris craters. Although this tends to support the possibility that the post-mare population never reached Mercury, the statistics these conclusions were based on are poor, and therefore the question should remain open. In any event, the two populations may represent two separate and distinct families of impacting objects or they may represent one family that evolved with time through mutual collision. If the late arriving population is missing from Mercury, it is more likely that they represent two separate and distinct families of objects.

Data on the populations of large craters and basins (>200 km in diameter) suggests that Mercury has a lower basin density than the Moon. Assuming that the unobserved part of Mercury is cratered to the same extent as the observed side, Schaber et al. (1977) found that there are 1.2 times more craters >200 km diameter on Mercury than on the Moon. However, when the difference in surface area between the Moon and Mercury is taken into account, Mercury's crater density is only 0.7 times that of the Moon. Furthermore, the areal density of basins larger than 400 km in diameter on Mercury is only 0.3 times that of the Moon, and for basins between 400 and 700 km the areal density is only 0.2 times that of the Moon. These values are in fair agreement with those of Malin (1976) and Wood and Head (1976) although there are differences among the three data sets. However, the number of basins is small, and the statistical significance questionable.

Malin (1976) observed that the areal densities of the large craters and basins on Mars, Mercury, and the Moon appear to be inversely proportional to the surface areas of the planets. Possible explanations are: (1) each planet swept separate regions of space containing a similar number of objects, (2) there was a resurfacing of the planets which varied proportionally with the area of the planet, or (3) the crusts of each planet solidified at different times during the period of heavy bombardment. Schaber et al. (1977) favored the latter explanation based on large degraded craters and basins which display well-defined secondary crater fields (fig. 3.20). They interpret the

Figure 3.20. The double-ringed basin Ma Chih-Yuan (170 km diameter) has a degraded rim but relatively well-preserved secondary impact craters. This may be the result of isostatic adjustments which have affected the large structure but not the smaller secondaries. (FDS 166665)

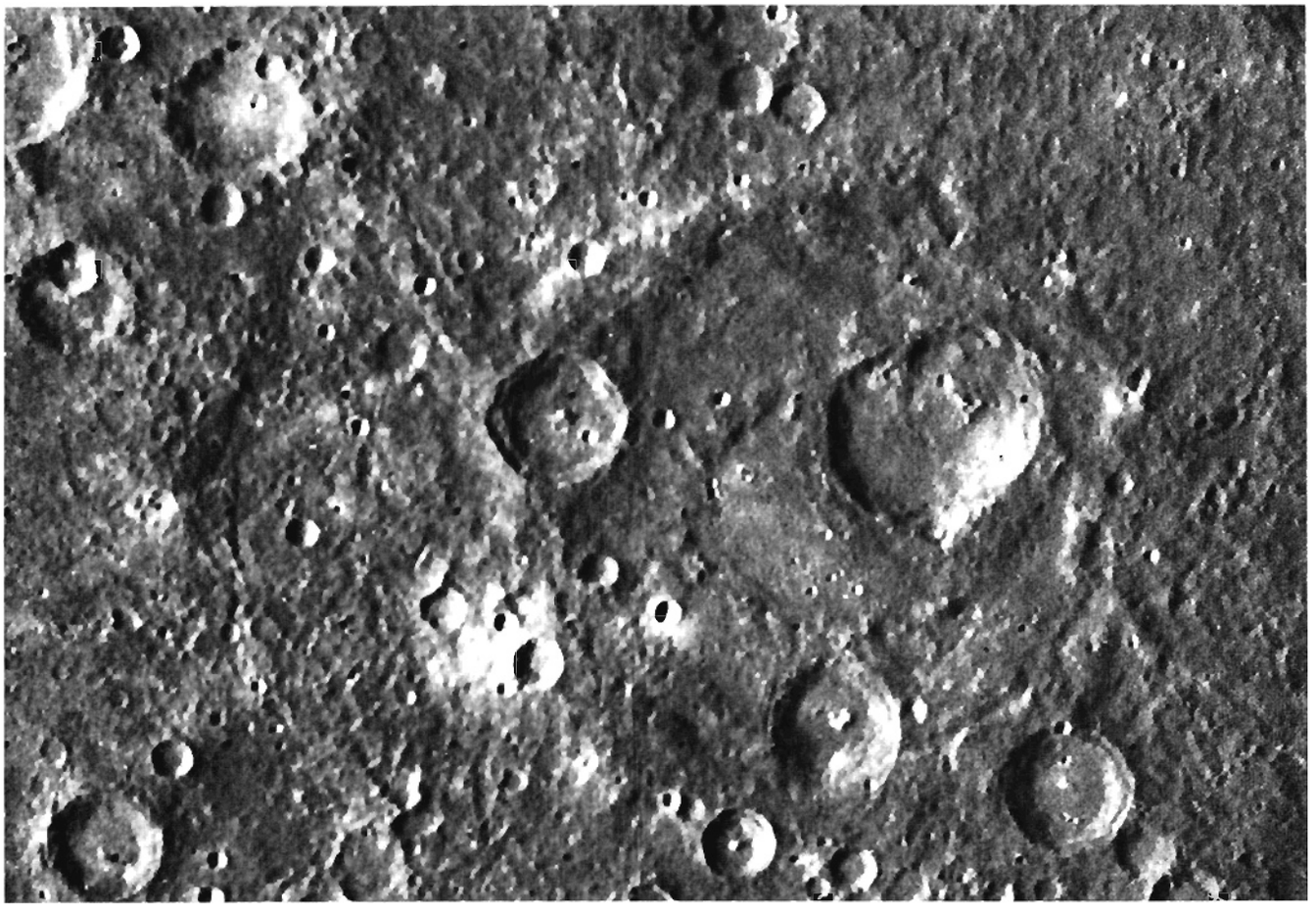

degradation of these craters as resulting from isostatic adjustments in a thermally active crust, which degraded the primary craters but preserved the secondaries. According to this explanation, the paucity of large basins and craters relative to the Moon may have been caused by a very early efficient isostatic adjustment. However, the observation that intercrater plains were, at least in part, emplaced during the period of heavy bombardment and probably obliterated at least a fraction of pre-existing craters suggests that resurfacing played a role in shaping the crater diameter/frequency distribution (Malin, 1976; Strom, 1977). In fact, Schaber et al. (1977) suggested that the viscosities of the lunar and Mercurian crusts were the same over the past 4.4×10^9 years, i.e., during the period of intense bombardment and when at least some of the intercrater plains were deposited.

MAJOR SURFACE UNITS

Four major and several local terrain types have been recognized on Mercury. Local units associated with the Caloris basin were discussed earlier. Although detailed geologic mapping may reveal sub-units of the main terrain types, the major surface units first described by Trask and Guest (1975) adequately represent the general characteristics of Mercury's surface and will be used here.

In general, Mercury's surface can be divided into two plains units, heavily cratered regions, and a peculiar hilly and lineated terrain (fig. 3.21). The plains were divided into two units, termed smooth plains and intercrater plains by Trask and Guest (1975). The smooth plains are sparsely cratered, occur primarily on the side of Mercury viewed by the outgo-

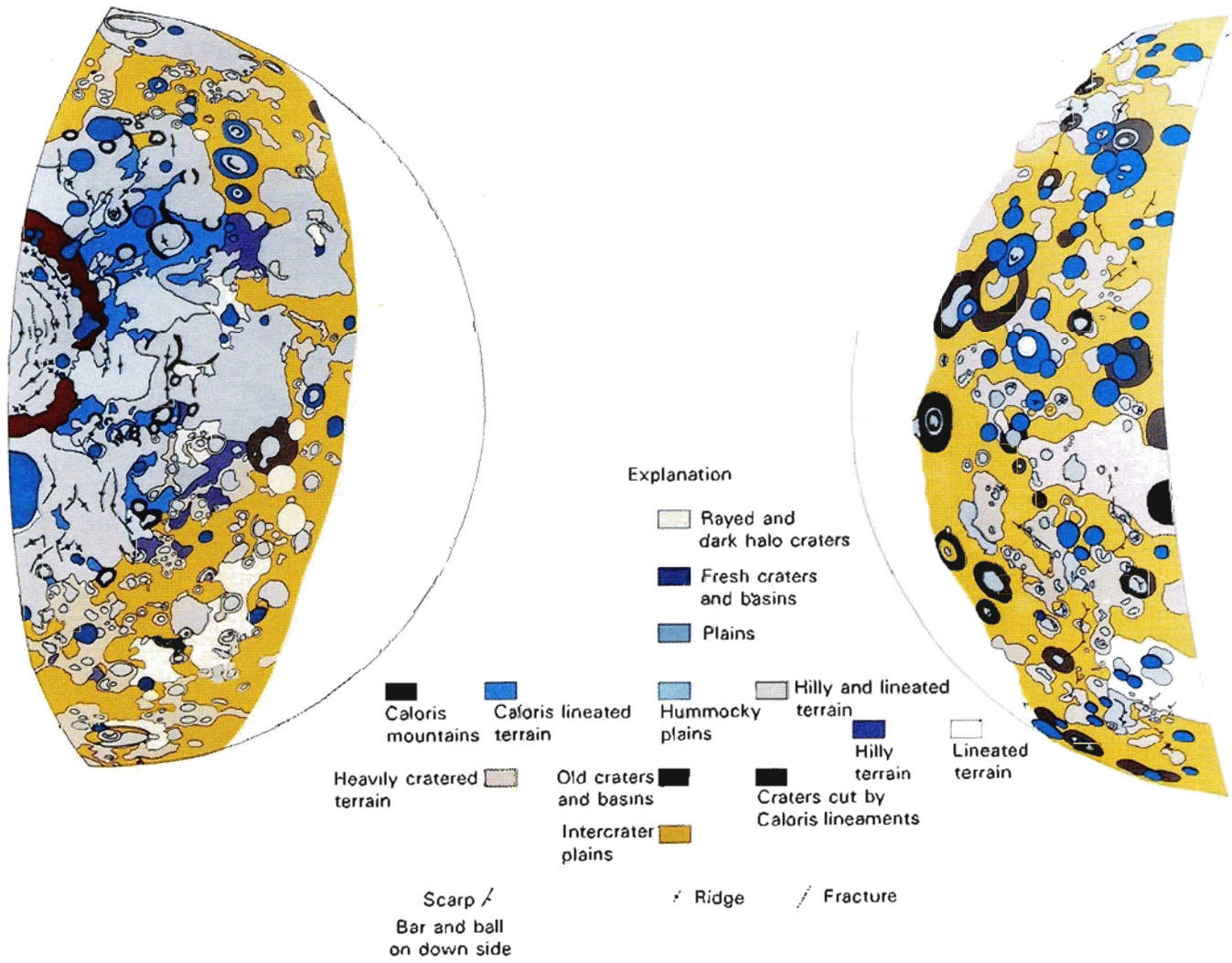

Figure 3.21. Generalized terrain map of outgoing (left) and incoming (right) sides of Mercury. The units shown on these maps are discussed in the text. The intercrater plains are contemporaneous with much of the heavily cratered terrain, not the oldest unit as indicated on the map. (From Trask and Guest, 1975.)

ing Mariner 10 spacecraft, and clearly constitute one of the youngest surface units on the planet. The intercrater plains mingle with heavily cratered regions, have a high density of superposed craters less than about 15 km diameter, and are among the oldest surface units on the planet. Because the heavily cratered terrain and intercrater plains are closely associated, they will be discussed together. The hilly and lineated terrain consists of angular to irregular hills, which disrupt many crater rims. It is locally distributed antipodal to the Caloris basin and is probably related to the impact that formed the basin.

Smooth Plains

In several respects Mercury's smooth plains resemble the lunar maria. They form relatively sparsely cratered, essentially level surfaces, overlapping more densely cratered areas (fig. 3.22). Therefore, they are one of the youngest surface units on the planet. All the larger areas of smooth plains have about the same overall density of superposed craters. They may, however, have been deposited over an extended period of time; the lunar maria, which also have similar crater densities, were deposited over a period of 1 billion years. The smooth plains display numerous ridges that grossly resemble lunar wrinkle ridges (fig. 3.22), except for the general absence of crenulated crests (Strom et al., 1975b). No regions of anomalous polarization or color occur within the smooth plains, such as those occurring in the lunar maria; suggesting a fairly uniform composition probably low in titanium. However, the smooth plains within and surrounding the Caloris basin and in the north polar region are redder than average. However, the color boundary does not always coincide with the boundary between smooth plains and other geologic units (Hapke et al., 1980).

Figure 3.22. Smooth plains southeast of the Caloris basin showing a mare-like wrinkle ridge. The dimensions of the picture are 111 × 148 km. (FDS 70)

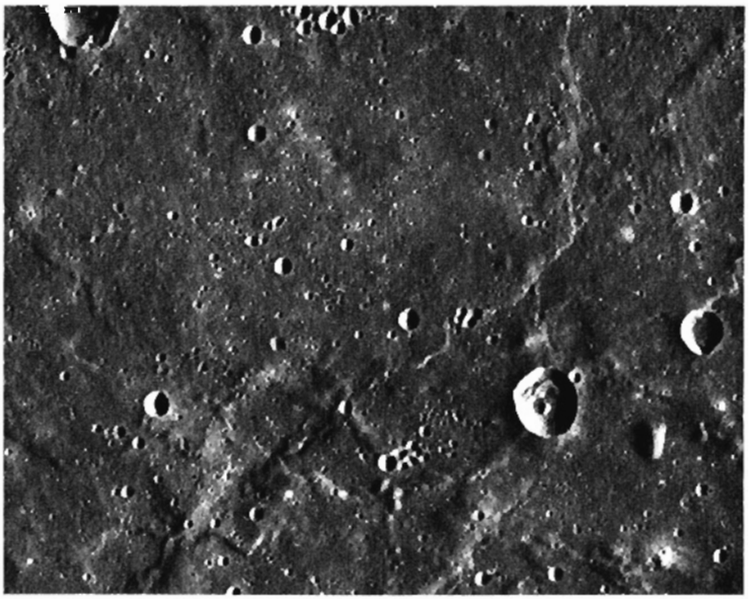

The most extensive tracts of smooth plains occur in and around the Caloris basin and in the north polar region (fig. 3.21). Earth-based radar profiles located about 5° south of the Caloris basin and extending about 60° into the unilluminated region show a relatively smooth surface with height differences less than 1 km (Zohar and Goldstein, 1974). This suggests that plains materials extend over 2000 km beyond the terminator and possibly surround the entire basin. On the portion of Mercury viewed by Mariner 10, the smooth plains are concentrated in the northern hemisphere between 120° and 190°W (Strom et al., 1975a). Mercury, like the Moon and Mars, may therefore have an asymmetric distribution of smooth plains. However, numerous relatively small patches occur over the rest of Mercury viewed by Mariner 10. These occur especially within the heavily cratered terrain and intercrater plains; while many, if not all the interiors of large basins and old circular depressions contain smooth plains.

The origin of Mercurian smooth plains is controversial; both impact and volcanic origins have been suggested. Preliminary analyses of Mariner 10 photography prompted Murray et al. (1974) and Strom et al. (1975b) to propose a volcanic origin based primarily on their widespread distribution, morphological similarities to the lunar maria, and the observation that relatively large areas of smooth plains are younger than the basins they occupy. Wilhelms (1976) and Oberbeck et al. (1977), on the other hand, proposed that the majority of smooth plains are basin ejecta deposits similar to the lunar Cayley Formation and smooth ejecta facies associated with the Orientale basin (fig. 3.23).

The controversy over the origin of the smooth plains centers primarily on the plains within and surrounding the Caloris basin. Wilhelms (1976) correctly pointed out that the morphology of the smooth plains is similar to that of the lunar light plains, which are probably mostly basin ejecta deposits. However, a detailed investigation of thorium abundances from the gamma ray spectrometer experiment indicates that thorium concentrations in lunar light plains in the vicinity of Mare Smythii to be more consistent with volcanic deposits (Haimes et al., 1978). Furthermore,

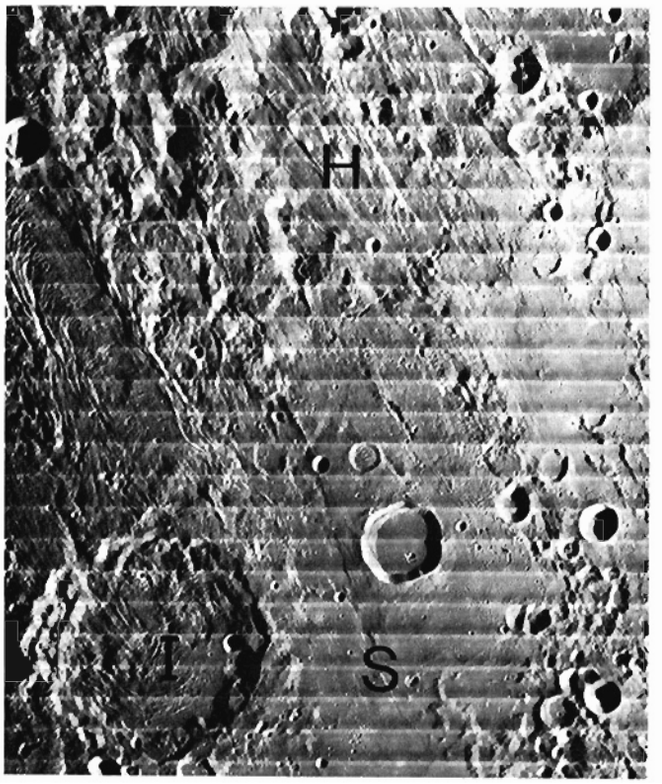

Figure 3.23. The radially braided continuous ejecta blanket (H) grades into a smooth ejecta facies (S) southeast of the lunar Orientale basin. The light smooth ejecta has the same morphology and albedo as the Cayley light plains surrounding the Imbrium basin. The crater Inghirami (I) is 91 km diameter. (LO IV, H 172)

Hawke and Head (1978) and Spudis (1978) presented evidence that the light plains comprising the Apennine Bench Formation are the result of KREEP (K = potassium, REE = rare earth elements, P = phosphorus) volcanism. Wilhelms attributes the Mercurian wrinkle-like ridges to compressive stresses and notes that they are somewhat similar to ridges in some lunar light plains. Furthermore, some Mercurian smooth plains and highlands terrain have similar albedos as have lunar light plains and highlands.

A major difference between the two deposits is that the Mercurian smooth plains cover a proportionately larger area (~15 percent of the surface viewed by Mariner 10) than do the lunar light plains (~4 percent). (See figs. 3.21 and 3.24.) Wilhelms (1976) speculated that this results because Mercurian basin ejecta was more fluid than lunar ejecta, perhaps consisting of mobilized clastic material or partly melted material. According to Wilhelms, this may be the result of large, slow impacts which could produce more partly melted material than on the Moon. However, the similar crater populations on the terrestrial planets indicate the impacting objects had a common origin (see section on crater statistics). If these objects were in heliocentric orbits of large eccentricity (e.g., asteroids or comets), then their impact velocities would have been considerably *greater* on Mercury than the Moon (Wetherill, 1975). If they were in heliocentric orbits of small eccentricity (e.g., accretional remnants), then the impact velocities would have been similar at both the Moon and Mercury. It is therefore unlikely that impact velocity can account for differences between the areal distribution of smooth plains on the Moon and Mercury.

Furthermore, Hawke and Cintala (1977) tentatively identified ponded material exterior to Mercurian craters ranging from 17 to 250 km in diameter. This material is similar to impact melt found in and around lunar craters and appears to be of comparable volume. They concluded that unless the Caloris basin formed under circumstances that did not occur on the Moon, the smooth plains cannot be completely explained by impact melt. Oberbeck et al. (1977) considered the smooth plains surrounding Caloris to have been the result of ballistic erosion and sedimentation by basin ejecta rather than emplacement of impact melt. Under this hypothesis the smooth plains formed by saturated secondary cratering, which eroded the surface and

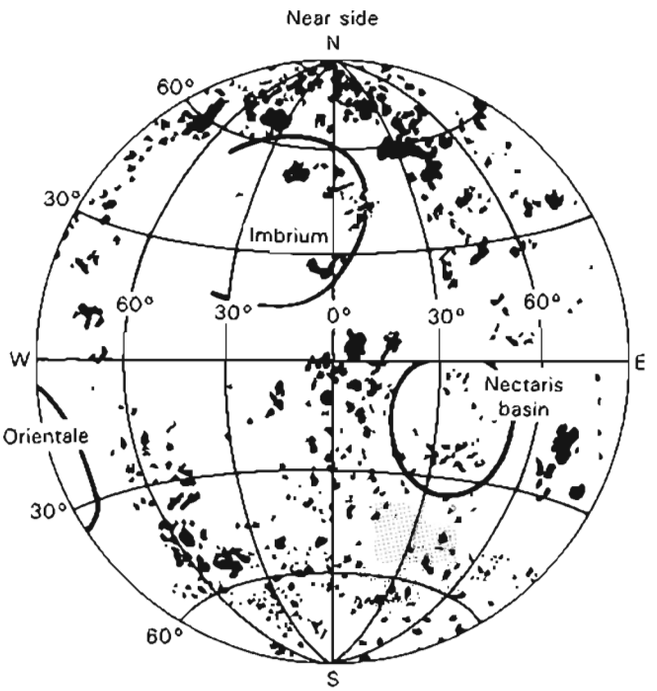

Figure 3.24. Distribution of light plains (black areas) and a region of intercrater plains (stippled area) on the near side of the Moon. (After Howard et al. (1974) with modifications.)

deposited the erosion products in low-lying areas such as craters. The greater surface gravity of Mercury concentrates the ejecta closer to the basin and thus accounts for the greater volume of smooth plains compared to similar deposits on the Moon. However, other large basins do not show a proportionately large volume of smooth plains exterior to their rims (Trask and Strom, 1976; Hawke and Cintala, 1977). One would expect comparable deposits if smooth plains are related to basin ejecta.

The volcanic hypothesis is based primarily on similarities in morphology, distribution, and age relationships between Mercurian smooth plains and the lunar maria. No unambiguous volcanic landforms such as flow fronts or domes have yet been identified in association with smooth plains. However, the apparent lack of these features may be due to the restricted coverage, constant solar elevation angle, and relatively low resolution of the available photography which is similar to Earth-based telescopic observations of the Moon. Under such observing conditions there is little evidence for a volcanic origin of the lunar maria. Several irregular rimless depressions in smooth plains within the Caloris and Tolstoj basins (see figs. 3.12 and 3.25) are probably of internal origin. Similar features on the lunar maria are thought to be caused by volcanic processes. It is possible that internally modified craters, similar to floor-fractured and mare-filled lunar craters, may be present near several plains-filled basins (Schultz, 1977). They often contain bright patches on their floors (normal albedo = 0.36–0.41) which Schultz (1977) and Dzurisin (1977) believed may result from some type of post-impact volcanic activity.

The age relationship of smooth plains relative to basins with which they are associated bears strongly on the origin of the plains. If the plains are of impact origin, then they must be the same age as their associated basin. If they are volcanic, then they must be younger than the associated basin, although the age difference need not be great. The plains interior to the Caloris basin show no flooded craters (Archimedean type craters); all craters display ejecta blankets superposed on the plains and therefore clearly postdate the emplacement of the smooth plains (Strom et al., 1975b). However, only half the basin was photographed by Mariner 10; Archimedean craters may be present on the unphotographed half. Crater statistical studies seem to indicate that the smooth plains in and around Caloris are of different relative ages and younger than the Caloris impact. Wood et al. (1977) found that, like the Moon, the number or density of Class 1 craters (the freshest) on smooth plains around Caloris is about half that in the Mercurian highlands. They concluded that the smooth plains were emplaced after the epoch of Class 1 crater formation had already begun. As previously discussed, McCauley et al. (1978) placed the Caloris impact in late Class 3 time. If these relative age assignments are correct, then the majority of smooth plains were emplaced after the Caloris impact and therefore are probably volcanic. In a recent statistical study of post-Caloris crater densities on the smooth plains and Caloris ejecta facies, Watkins and Strom (1984) found significant age differences. The two Caloris ejecta units (hummocky plains and lineated terrain) apparently have the same crater densities and are therefore the same relative age. However, the smooth plains within and immediately surrounding the Caloris basin have a variety of crater densities, which are less than those on the ejecta units. This suggests not only that the smooth plains were emplaced after the Caloris impact in agreement with the study by Wood et al. (1977), but that they were deposited over a relatively extended period.

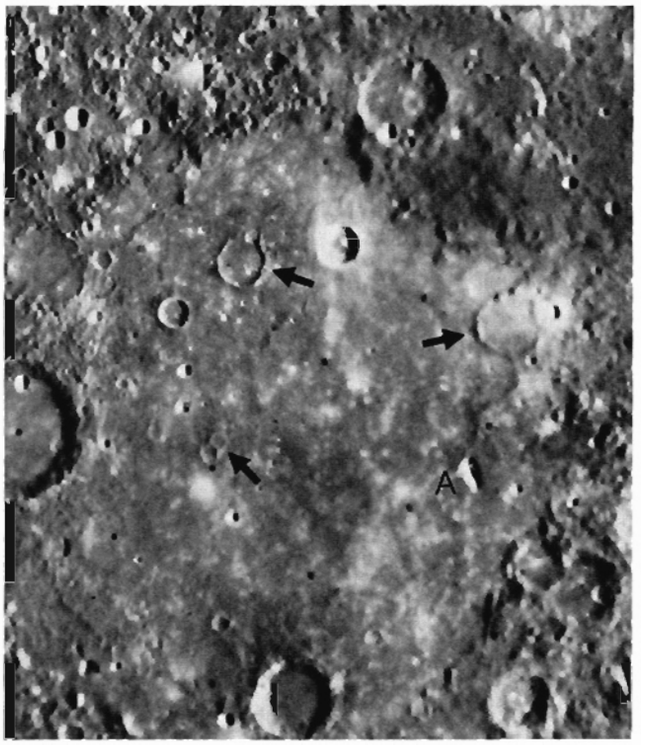

Figure 3.25. Photomosaic of the Mercurian Tolstoj basin (400 km diameter) showing post-basin craters flooded by smooth plains (arrows) and a large elliptical and rimless depression (A) probably caused by collapse.

The normal albedo of the smooth plains within and around the Caloris basin is systematically lower than the Mercurian highlands. Most of the values of the Caloris smooth plains are about 0.12 to 0.13, whereas the Mercurian highlands (intercrater plains) are about 0.16–0.18 (see table 3.2). Also two of the three albedos listed by Hapke et al. (1975) under hummocky plains (a Caloris ejecta facies) are higher (0.14–0.15) than the plains. The anomalously low value (0.10) is found to lie not within the hummocky plains, but in the adjacent smooth plains. Although the number of measured areas is small, the current evidence indicates that the Caloris smooth plains have a different albedo and therefore possibly a somewhat different composition than the highlands and Caloris ejecta, which is consistent with, but does not necessarily prove, a volcanic origin.

Hapke's (1980) color-ratio studies showed that although the area dominated by smooth plains surrounding the Caloris basin and in the north polar region is more reddish than average, the color boundary does not generally correspond to the boundary between smooth plains and other geologic units (fig. 3.4). However, the color boundaries on the Moon derived from photographs taken at similar wavelengths also vary in correspondence to geologic boundaries where known differences in composition occur (fig. 3.26). The abundance of titanium is primarily responsible for the color differences observed on the Moon. High titanium abundances give rise to bluish mare while low titanium abundances produce reddish mare, which is indistinguishable from the color of the highlands. For instance, Sinus Iridum and contiguous portions of Mare Imbrium have the same color as the surrounding highlands as shown in figure 3.26. If the surface of Mercury is depleted in titanium relative to the Moon as Hapke's (1977) study indicated, then one would not expect good correspondence between color and geologic boundaries.

Stratigraphic studies clearly indicate that some large tracts of smooth plains in other basins post-date the basins with which they are associated. Strom et al. (1975b) and Trask and Strom (1976) noted several regions where smooth plains embay craters that post-date the basins in which they occur. Figure 3.27 is a rectified photomosaic of the Borealis Planitia region near the north pole. The smooth plains occupy a circular depression about 1000 km in diameter which contains the 300 km diameter crater Goethe, near the terminator. The plains have flooded craters within the circular depression and the Goethe crater. Furthermore, the crater density is much less on the plains than on the adjacent cratered terrain. Therefore, these smooth plains clearly post-date the formation of the 1000 km circular depression and Goethe. Wilhelms (1976) speculated that these plains were ballistically emplaced by a basin in the terminator. This basin would have to be about the same age and size as Caloris in order to produce these extensive lightly cratered plains. Because the hilly and lineated terrain antipodal to Caloris was probably produced by focused seismic waves from the Caloris impact, one would expect a similar terrain antipodal to this hypothetical basin. This terrain would occur in the sunlit portion of the south polar area, but no such terrain is found there.

The smooth plains within the 350 km Tolstoj basin show relationships similar to those at the Borealis Planitia region; i.e., embayed craters on the floor and a much lower crater density than the adjacent terrain (fig. 3.25). Furthermore, there is a good correspondence between the color boundaries and the interior fill on the north, south, and eastern edges of the basin. Also, the lowest measured albedo (0.08) occurs on the

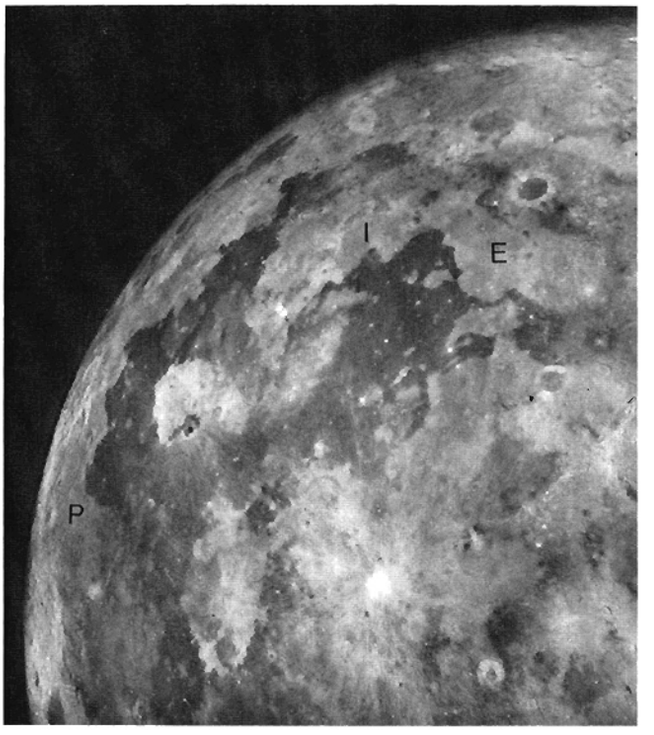

Figure 3.26. Color difference picture of the Moon centered on Mare Imbrium. This photograph is a color ratio image constructed from UV (370 nm) and red (610 nm) negatives. The light regions are reddish and the dark regions are bluish relative to the average of the whole Moon. As on Mercury (fig. 3.4) the color boundaries do not always coincide with geologic boundaries. For example, the color of Sinus Iridum (I), the eastern part of Mare Imbrium (E) and the western portion of Oceanus Procellarum (P) is indistinguishable from that of the adjacent highlands. (From Whitaker, 1972.)

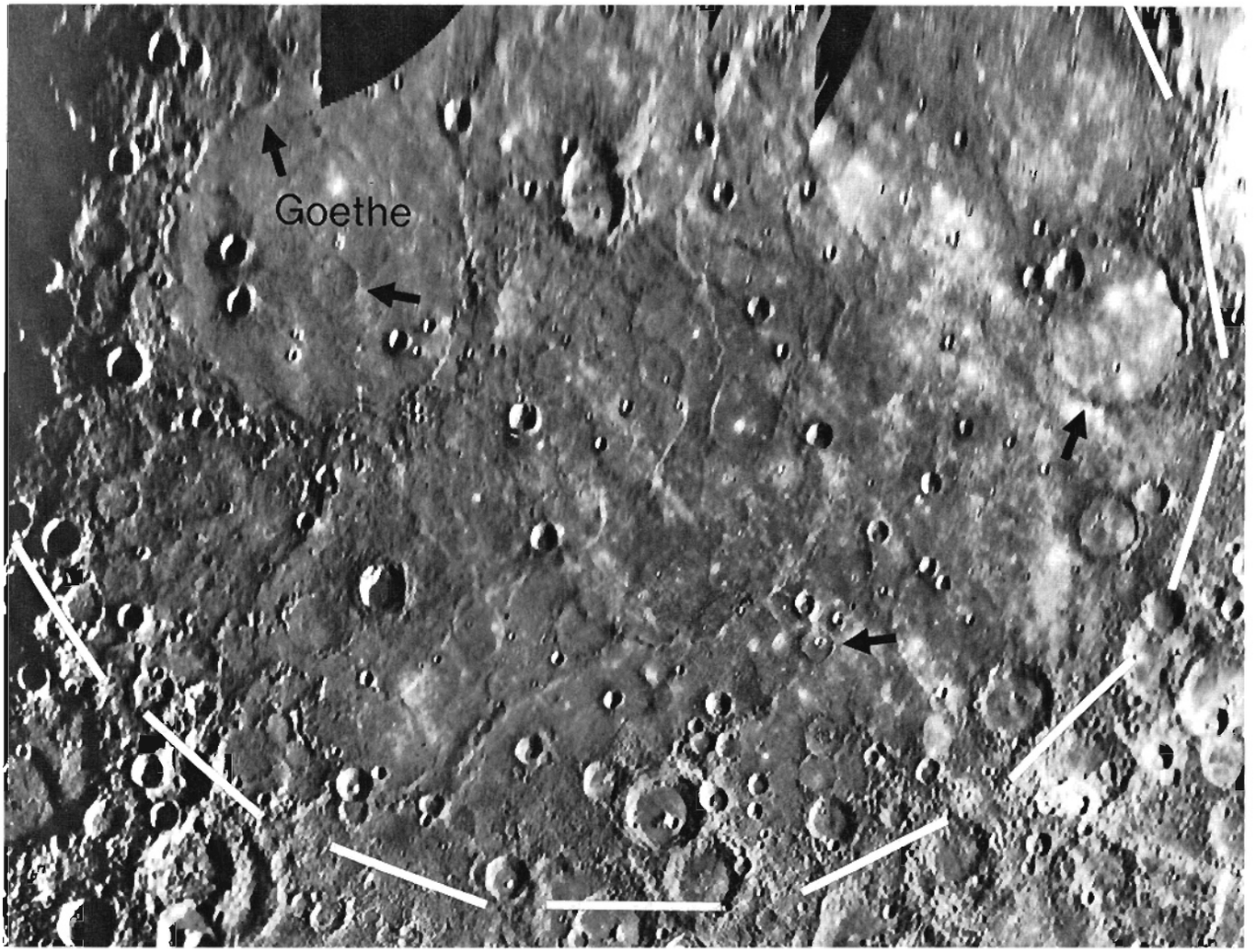

Figure 3.27. Photomosaic of the north polar region of Mercury showing numerous craters flooded by smooth plains. Craters (arrows) on the floor of the Goethe basin (340 km diameter) as well as the basin itself have been flooded by smooth plains. These plains may occupy a large circular depression about 1000 km in diameter (dashed white lines) and obviously post-date this structure and the Goethe basin.

eastern rim of Tolstoj (fig. 3.25) where the topography is very subdued and closely resembles the dark mantling material at similar locations on the Moon (such as Sulpicius Gallus and Taurus Littrow on the rim of the Serenitatis basin and in the vicinity of Rima Bode on the edge of Sinus Aestuum). These lunar materials are probably volcanic pyroclastic deposits (Head, 1976) and it is possible that the Mercurian deposits have a similar origin.

Other areas of smooth plains (i.e., Petrarch crater within the hilly and lineated terrain) show similar stratigraphic relationships and indicate in many instances that smooth plains are younger than their associated basins. Although it has been suggested that in these cases the plains were deposited ballistically from some exterior source, no evident source basins exist nearby. This suggested to Strom et al. (1975b) and Trask and Strom (1976) that at least large areas of smooth plains are volcanic deposits emplaced in a manner similar to the lunar maria.

The current evidence favors a volcanic origin for most smooth plains; a smaller proportion of smooth plains being basin ejecta or impact melt as suggested by Wilhelms (1976) and Oberbeck et al. (1977). The evidence favoring a volcanic origin is summarized as follows: (1) widespread distribution; (2) age differences between smooth plains and the basins they occupy or are adjacent to; (3) age differences between Caloris smooth plains and Caloris ejecta facies; (4) morphological similarity between smooth plains and lunar maria; (5) similarity in the physical properties of mare basalts and smooth plains suggested by comparative crater morphology; (6) apparently similar volumes of impact related deposits around lunar and Mercurian craters of equal size; (7) possible internal modifications of craters near areas of smooth plains; and (8) albedo differences between smooth plains in and around Caloris and other geologic units.

Although no single line of evidence by itself proves a volcanic origin, the combined observations tend to

support this hypothesis. Until more definitive evidence is presented to the contrary, the volcanic origin of much of the smooth plains appears to be a good working hypothesis.

Intercrater Plains and Cratered Terrain

The most widespread terrain type on Mercury is the intercrater plains first described by Trask and Guest (1975). It consists of level to gently rolling plains with a high density of superposed craters less than about 15 km diameter (figs. 3.28 and 3.29). These plains occupy about 45 percent of the highland surface viewed by Mariner 10 and occur between and around clusters of large craters in the more heavily cratered terrain. Many of the superposed small craters form chains or clusters suggestive of secondary impact craters. The high density of superposed craters and stratigraphic relationships clearly indicates that the intercrater plains are older than the smooth plains and that they form some of the oldest terrains on Mercury. Both the Moon and Mars also have intercrater plains. On the Moon, the intercrater plains, termed Pre-Imbrium Pitted Plains, have an extremely limited distribution (see figs. 3.24 and 3.30). Both a volcanic (Scott, 1972; and Strom, 1977) and impact (Howard et al., 1974) process have been suggested for their origin. The intercrater plains on Mars have a somewhat different morphology. They lack the high density of superposed small craters and often contain lunar-like wrinkle ridges (fig. 3.31). Martian inter-

Figure 3.28. Large areas of Mercurian intercrater plains (IP). (FDS 27328)

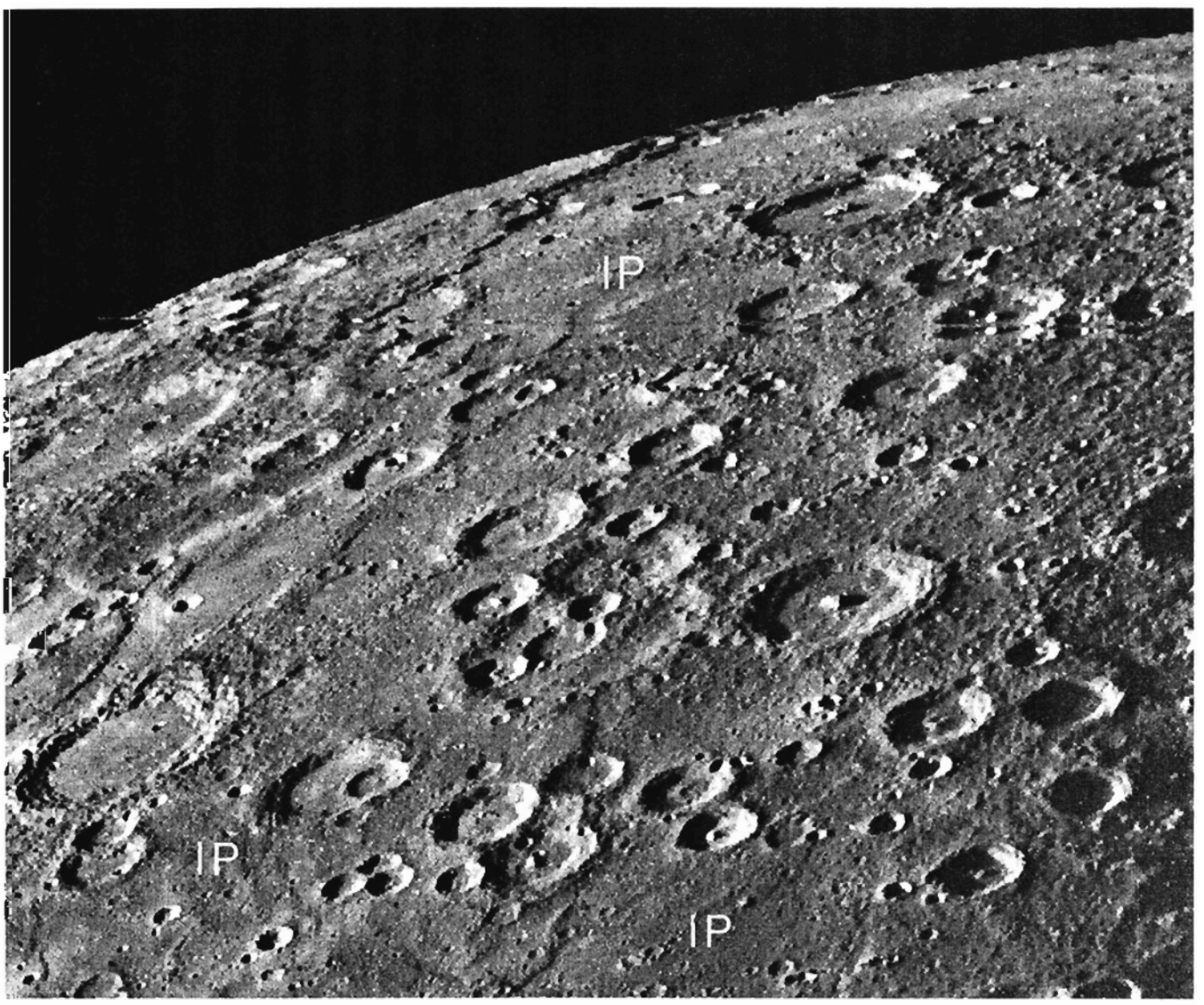

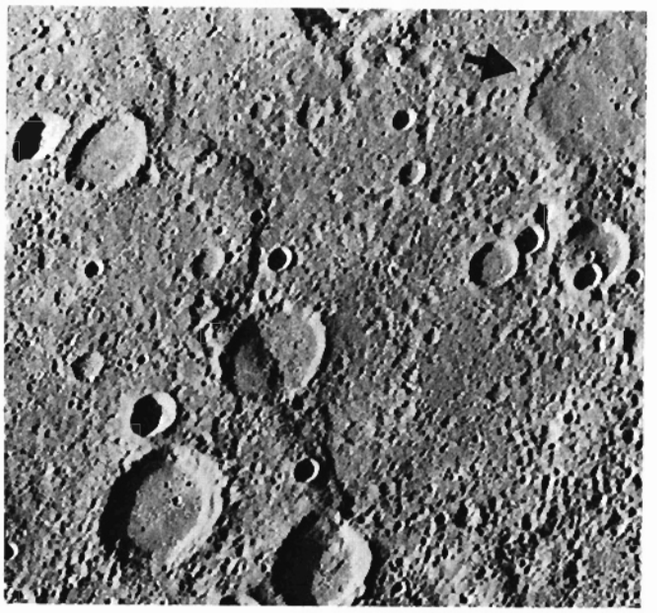

Figure 3.29. High resolution picture of typical intercrater plains. Abundant shallow elongate craters and crater chains are present on the intercrater plains and are probably mostly secondary impact craters from fresher craters and basins of the more heavily cratered terrain. The arrow indicates a 90 km diameter crater which has been embayed by intercrater plains, and therefore, pre-dates the intercrater plains. (The photo is 400 km across.) (FDS 27448)

crater plains have been attributed to early volcanic activity (Wilhelms, 1974).

The age of Mercurian intercrater plains relative to the heavily cratered terrain has important implications for the early history of Mercury. Trask and Guest (1975) and Trask (1976) considered most of the intercrater plains to be older than the craters comprising the heavily cratered terrain because of the abundance of superposed secondaries which they believed were derived from these craters. However, Malin (1976a), Strom (1977), and Leake (1981) noted many old craters which have been embayed by intercrater plains (fig. 3.29). Therefore, some highland craters must predate at least a portion of intercrater plains. In the diameter range of about 20-50 km, the lunar highlands are more heavily cratered than the highlands of Mercury (Murray et al., 1974; Trask, 1976; Oberbeck et al., 1977; and Strom, 1977). Trask (1976) and Oberbeck et al. (1977) considered the Mercurian crater population to more closely represent the original production population in this size range and that the greater crater density in the lunar highlands is due to basin secondaries. However, Strom (1977) showed that the distribution function of the lunar post-Orientale production population is about the same as that of the lunar highlands, suggesting that the crater

Figure 3.30. Region of lunar intercrater plains (IP) southwest of the Nectaris basin in the lunar highlands. (Compare with figs. 3.29 and 3.31.) The crater Nicolai (N) is 42 km diameter. (LO IV, H-88)

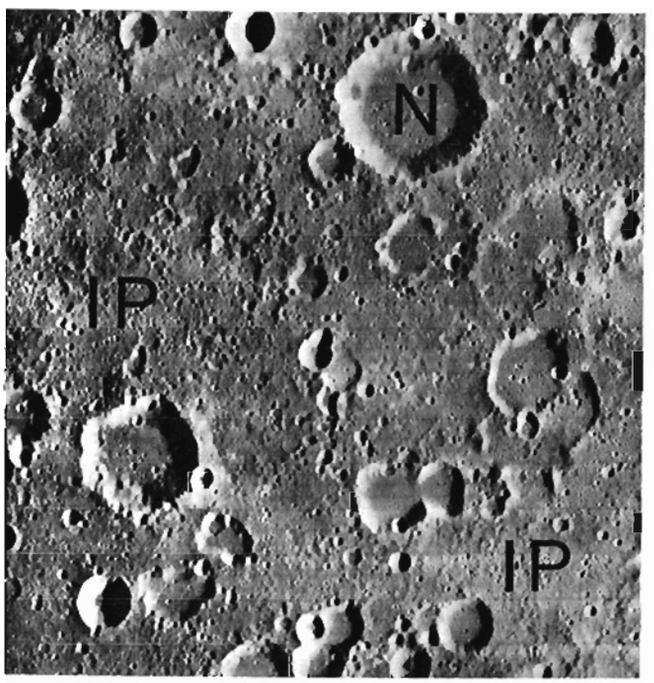

Figure 3.31. Region of Martian intercrater plains in the heavily cratered southern highlands of Mars. (Photo is 260 km across.) (VO97A05).

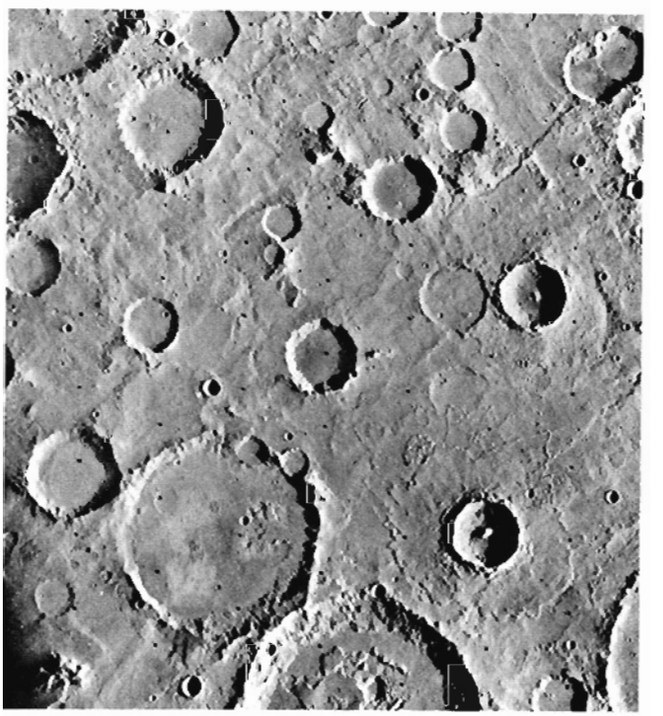

population in the lunar highlands is also basically a production population. Strom suggested that because the Mercurian intercrater plains have embayed some craters, a certain fraction of pre-existing craters must have been obliterated and therefore the paucity of craters relative to the lunar highlands is the result of obliteration by intercrater plains formation. Furthermore, Leake (1981) attempted to date the intercrater plains relative to the various crater degradational classes by superposition of ejecta blankets and embayment relationships. Leake found that intercrater plains were emplaced *during* the formation of Class 5 through Class 3 craters and that the volume of plains generally decreases as age decreases (fig. 3.32). The secondary craters superposed on the intercrater plains appear to be derived mainly from the Class 1-3 craters and Class 4 basins of the heavily cratered terrain. Patches of plains emplaced during the formation of Class 1 and 2 craters are equivalent to the smooth plains discussed earlier. The embayment of certain craters and basins by intercrater plains, their age relative to crater degradational classes, and the paucity of 20–50 km craters relative to the lunar highland crater population strongly suggest that the intercrater plains span a range of ages. They appear to have been emplaced *during* the period of heavy bombardment but the volume apparently decreased with time. The formation of intercrater plains and smooth plains may *not* represent two distinct plains-forming episodes. Instead they may represent a more or less continuous period of plains formation lasting from sometime during the period of heavy bombardment through the emplacement of the youngest smooth plains.

The origin of intercrater plains is less certain than that of the smooth plains. As in the case of smooth plains, both an impact and volcanic origin have been suggested. Wilhelms (1976) and Oberbeck et al. (1977) considered them to be an older basin ejecta facies

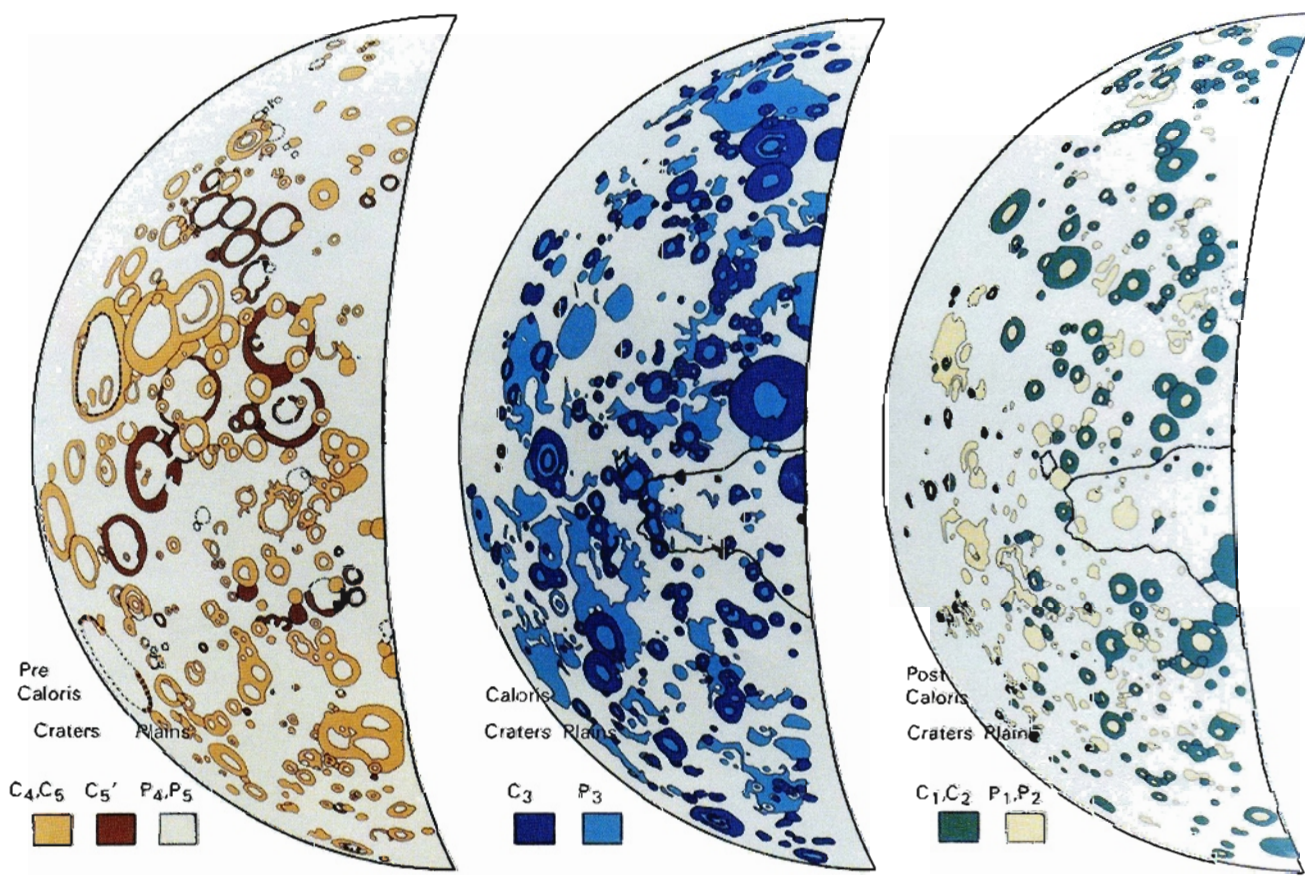

Figure 3.32. Paleogeologic maps of Mercury's incoming side showing the distribution of craters and plains of various relative ages. The oldest craters (C_4–C_5) and plains (P_4–P_5) predate the hilly and lineated terrain outlined by the solid line and are probably pre-Caloris age. C_5 craters predate P_4–P_5 plains. The youngest craters (C_1–C_2) and plains (P_1–P_2) post-date the hilly and lineated terrain and are probably post-Caloris age. The P_3–P_3 plains are equivalent to intercrater plains and P_2–P_1 plains are smooth plains. (From Leake, 1981.)

formed during the period of heavy bombardment. However, a major drawback to this hypothesis is the apparent lack of source basins to account for such a widespread distribution of these plains. Schaber et al. (1977) found that the density of basins <400 km diameter on Mercury is only 30 percent of that on the Moon, and for basins between 400 and 700 km in diameter the density on Mercury is only 21 percent of the lunar basin density. Although the lunar highlands contain small areas of intercrater plains (particularly southwest of the Nectaris basin), their distribution is extremely limited compared to that on Mercury (compare figs. 3.21 and 3.24); yet the density of basins is considerably greater on the Moon. Wilhelms (1976) accounted for this difference by speculating that the crust of Mercury was more plastic than that of the Moon, and that impacts in this "softer" and "hotter" material would produce more impact melt than on the Moon. However, based on apparent total isostatic compensation of ancient basins 800 km in diameter, Schaber et al. (1977) calculated that the average viscosity of the Mercurian crust was about the same as that for the Moon. This suggests that during the period of intense bombardment (during intercrater plains formation) the lunar and Mercurian crusts had similar viscosities.

Evidence for a volcanic origin of intercrater plains is based upon the tentative identification of volcanic landforms, the areal coverage of intercrater plains relative to coverage by craters of the same age, and the overall widespread distribution of these deposits. Malin (1978) and Leake (1981) identified several features in the Mercurian highlands which may be volcanic. These are primarily domical structures, one of which is 30 km in diameter, 2 km high, and has concave lower slopes and convex upper slopes. Malin and Leake considered these features to be volcanic constructs. Dzurisin (1976) also identified linear ridges associated with intercrater plains which he considered to be the sites of extrusive activity. However, the evidence for volcanism associated with these features is not as compelling as that for Martian constructs and the question of their origin should remain open. The main argument for a volcanic origin of intercrater plains is their very widespread distribution compared to lunar deposits considered to be basin ejecta. Leake's (1981) paleogeologic maps of intercrater plains and craters on Mercury show their distribution at various times (fig. 3.32). The areal extent of intercrater plains appears to decrease as age decreases, but there is little relationship between their distributions and craters of similar age. The proportion of intercrater plains to craters of the same age varies greatly from region to region and does not correlate with crater size. This suggests the emplacement of intercrater plains was unrelated to the formation of craters, which implies an internal origin for intercrater plains. Similar relations (fig. 3.32) suggest at least some of the smooth plains may be volcanic. Furthermore, from crater morphological studies (Cintala et al., 1977), the physical properties of intercrater plains appears to be more similar to those of the lunar maria and Mercurian smooth plains than the megaregolith of the lunar highlands. However, impact melt may have properties similar to volcanic flows. In short, the geological evidence is not sufficient to decide between the basin ejecta or volcanic origin of intercrater plains, although a volcanic origin is favored based on the evidence presented above. Thermal history models suggest a magma source and tectonic setting which could produce volcanic activity on a global scale early in Mercurian history.

Hilly and Lineated Terrain

The most peculiar terrain viewed by Mariner 10 consists of hills and depressions which disrupt preexisting landforms, particularly crater rims (Trask and Guest, 1975). This terrain forms a slightly elongated area which is directly antipodal to the Caloris basin (figs. 3.21 and 3.33). The hills are 5–10 km wide and 0.1–1.8 km high (fig. 3.34). Linear depressions with scalloped rims display a rough orthogonal pattern trending northeast and northwest. Several large craters, whose rims have been severely broken up into hills and depressions, contain smooth plains which have not been disrupted (fig. 3.33). Clearly these smooth plains post-date the formation of hilly and lineated terrain.

Schultz and Gault (1975) identified similar terrain antipodal to the lunar Imbrium and Orientale basins. However, the Mercurian hilly and lineated terrain covers a larger area and is more pronounced than its lunar counterpart. They suggest that the terrain is the result of focused seismic waves caused by large basin-forming impacts. Lagrangian computer simulations of shock wave propagation indicate that antipodal seismic effects are significantly enhanced by focusing and are of a magnitude sufficient to cause vertical ground motion of about a kilometer or more and accelerations approaching lunar gravity (Hughes et al., 1977). Furthermore, the seismic effects are significantly more pronounced for a molten planet than a

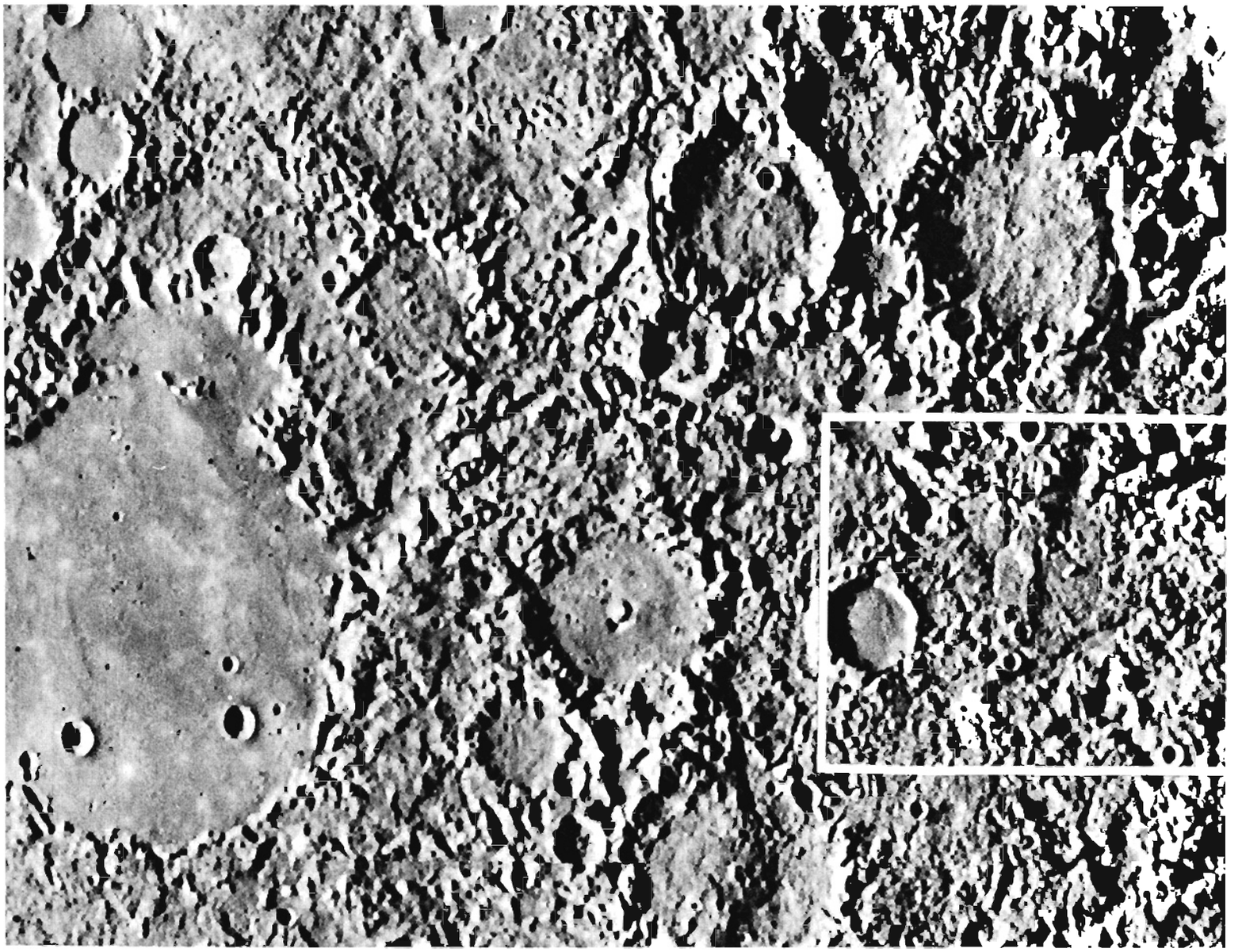

Figure 3.33. Hilly and lineated terrain antipodal to the Caloris basin. Crater rims have been broken up into hills and valleys but in certain cases the smooth plains filling the craters have not been. Therefore these smooth plains post-date the craters in which they lie. (The picture is 543 km across.) (FDS 27370)

solid one, and tensile failure may occur at depths of tens of kilometers below the antipode. Leake (1981) found that Class 1 and 2 craters are superposed on the hilly and lineated terrain, whereas craters of Class 3 and 4 straddling the boundary have had part of their rims disrupted. This places the formation of the hilly and lineated terrain approximately between the production of Class 2 and 3 craters, which is in agreement with the age of the Caloris impact derived by McCauley (1978). Although Wilhelms (1975) suggested that the hilly and lineated terrain is the result of the dissection of the surface by ejecta from basins hidden in the terminator, its Caloris antipodal location, lunar analogs, similar age relative to the Caloris impact, and computer modeling strongly suggest that it was caused by the disruption of the surface induced by focused seismic waves from the Caloris impact. If the smooth plains within several large craters disrupted by this terrain are volcanic deposits, as suggested by Trask and Strom (1976), then it is possible that the tensile fracturing caused by the seismic waves tapped a magma source and provided egress for the eruption of these deposits.

TECTONICS

Of the terrestrial planets explored to date, Mercury displays a unique tectonic framework. This tectonic framework is characterized by the widespread (probably global) distribution of large lobate scarps. These scarps are found on virtually all types of terrain viewed by Mariner 10 and often reach lengths of several hun-

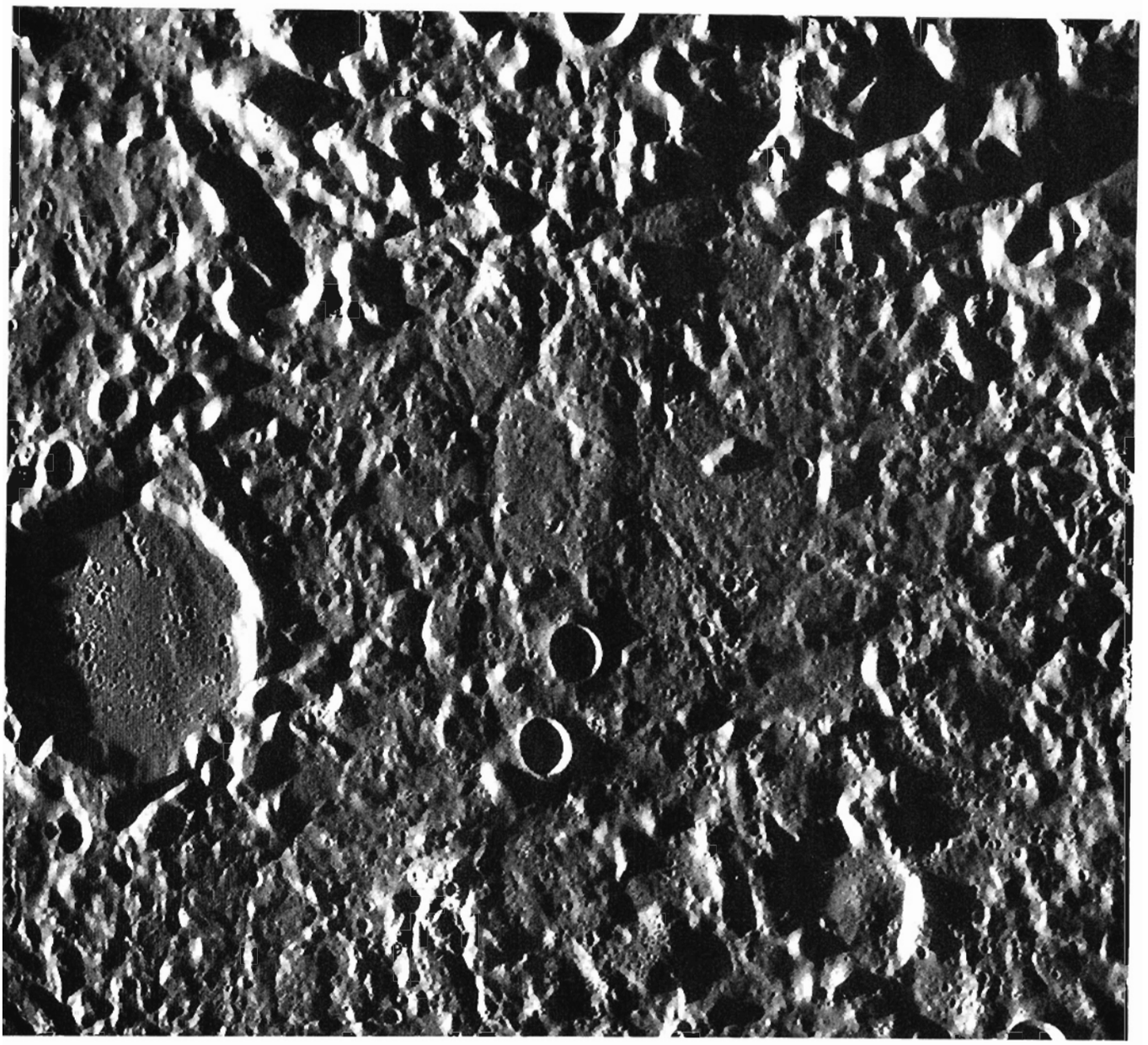

Figure 3.34. High resolution picture of the hilly and lineated terrain. The region has been broken up into hills from about 0.1 to 1.8 km high which are interspersed with smooth material. The largest crater is 31 km in diameter. (FDS 27463)

dred kilometers and heights of about 1 km or more. A system of probably older structural lineaments also has been recognized. These lineaments are primarily represented by linear ridges, valleys, and segments of crater rims showing preferred orientations. To a large extent this tectonic framework is either the direct or indirect result of the formation of Mercury's large iron-rich core and consequent thermal history. However, crustal stresses produced by planetary despinning from an earlier, more rapid rotation rate also may have contributed to Mercury's surface structure.

Lobate Scarps and Lineaments

Lobate scarps are relatively steep escarpments, which generally have a lobate outline on a scale of a few tens of kilometers (Strom et al., 1975b). They vary in length from about 20 km to over 500 km and have heights of a few hundred meters to about 1 or 2 km (figs. 3.29 and 3.35). The crests of the scarps are rounded and the slope of the terrain behind the scarps varies from flat to gently dipping away from the scarp. Often individual scarps transect several terrain types including craters, intercrater plains, and smooth plains. Dzurisin (1976) classified lobate scarps into three types based on large-scale planimetric geometry. However, in detailed morphology they all display the characteristics described above and probably have a common origin. Some scarps are confined to the smooth plains comprising the floors of craters. Although some of these scarps may be flow fronts, a

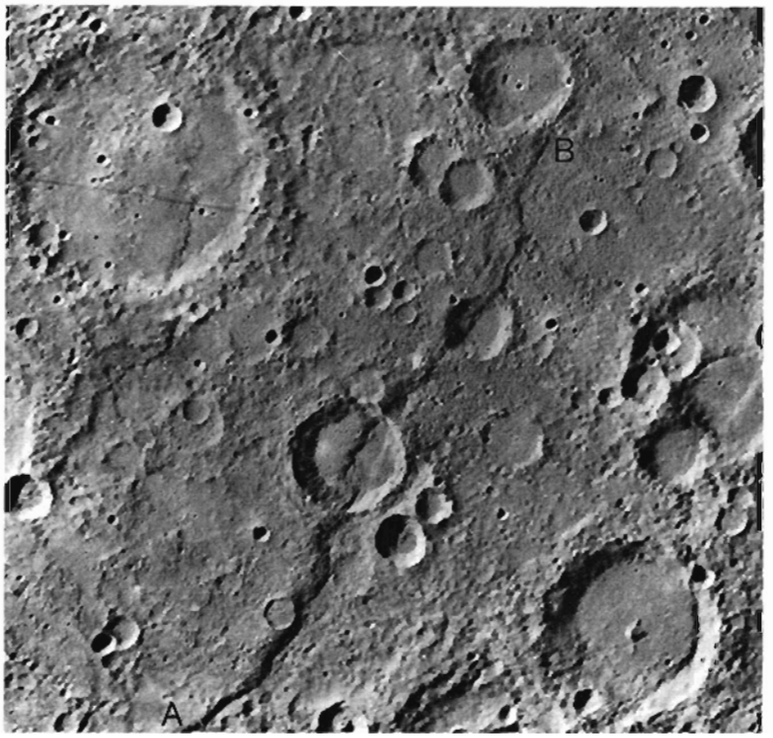

Figure 3.35. Photomosaic of Discovery scarp (A-B). This lobate scarp is one of the largest scarps on Mercury and is probably a thrust fault. It is about 2 km high and over 500 km long, and transects two craters 55 and 35 km in diameter.

tectonic origin is likely for most. The majority of lobate scarps show transection relationships, a general linear trend, large dimensions, and in one case a horizontal offset of a large crater's rim, which indicates a tectonic origin. Strom et al. (1975b) noted that the morphology and overall geometry of these scarps are unlike normal faults seen on the Moon and Mars, and propose that they are thrust or reverse faults caused by compressive stresses. In fact, the southwestern part of the crater wall of Guido d'Arezzo has been horizontally displaced 10 km by Vostok scarp (fig. 3.36). This is consistent with thrusting of the northeastern part of the crater over the southwestern part, causing a shortening of the radius of the crater and the apparent horizontal offset of the wall. By analogy, the vast majority of lobate scarps are probably thrust or reverse faults caused by compressive stresses. Furthermore,

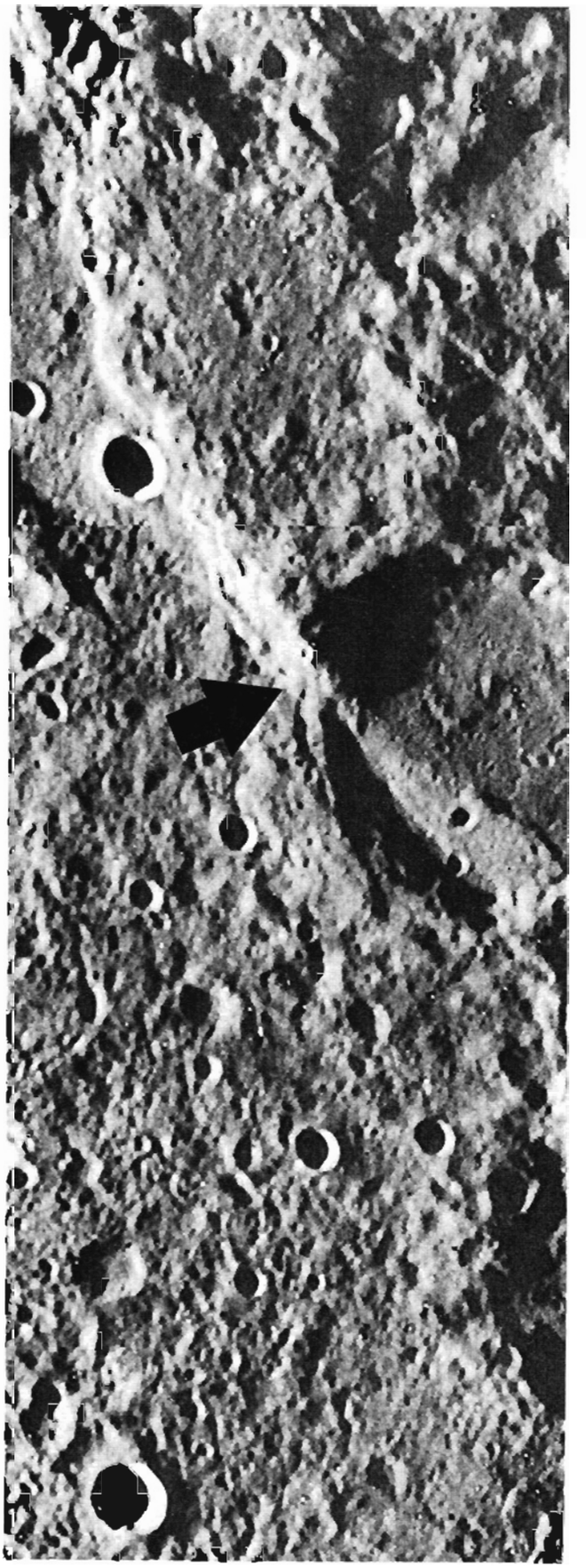

Figure 3.36. The 130 km long Vostok scarp transects two craters (lower crater is Guido d'Arezzo) 80 and 65 km in diameter. The northwestern rim of Guido d'Arezzo has been offset about 10 km by the scarp (arrow). This offset was probably caused by shortening of the crater due to thrusting of the eastern part of the crater over the western part. (FDS 528858)

the lobate scarps are more or less evenly distributed over the surface viewed by Mariner 10 (fig. 3.37), and therefore the entire planet appears to have been subjected to compressive forces which caused a general crustal shortening. From estimates of the fault plane inclination, average height, and measured lengths of lobate scarps, and assuming that the area measured is representative of the planet as a whole, Strom et al. (1975b) estimated that there has been a total decrease in surface area of about 6.3×10^4 to $1.3 \times 10^5 km^2$ (equivalent to a 1–2 km decrease in the radius of Mercury). This value is remarkably close to that calculated for a radius decrease based on thermal history models (Solomon, 1976). In addition to lobate scarps, Dzurisin (1976), and Masson and Thomas (1977) recognized a system of structural lineaments having preferred orientations and closely resembling the lunar lineament system (Strom, 1964). The lineaments consist of ridges, troughs, and linear segments of crater rims. They have at least three, possibly five, preferred orientations trending northeast, northwest, and north-south. The lunar lineament system also shows the same three orientations (Strom, 1964). Dzurisin (1976) considered the Mercurian lineaments to represent modifications of linear crustal joints formed in response to stresses induced by tidal spindown.

The lobate scarps transect intercrater plains, craters, and smooth plains, but in several instances they also have been disrupted by moderate-sized impact craters. However, the craters which disrupt scarps are primarily of Class 1 and 2 degradational types. No intercrater plains have been observed to embay the scarps. This suggests that scarp formation began after inter-

Figure 3.37. Map of the lobate scarps, ridges, plains, and the hilly and lineated terrain on the outgoing (A) and incoming (B) sides of Mercury. (After Strom et al., 1975.)

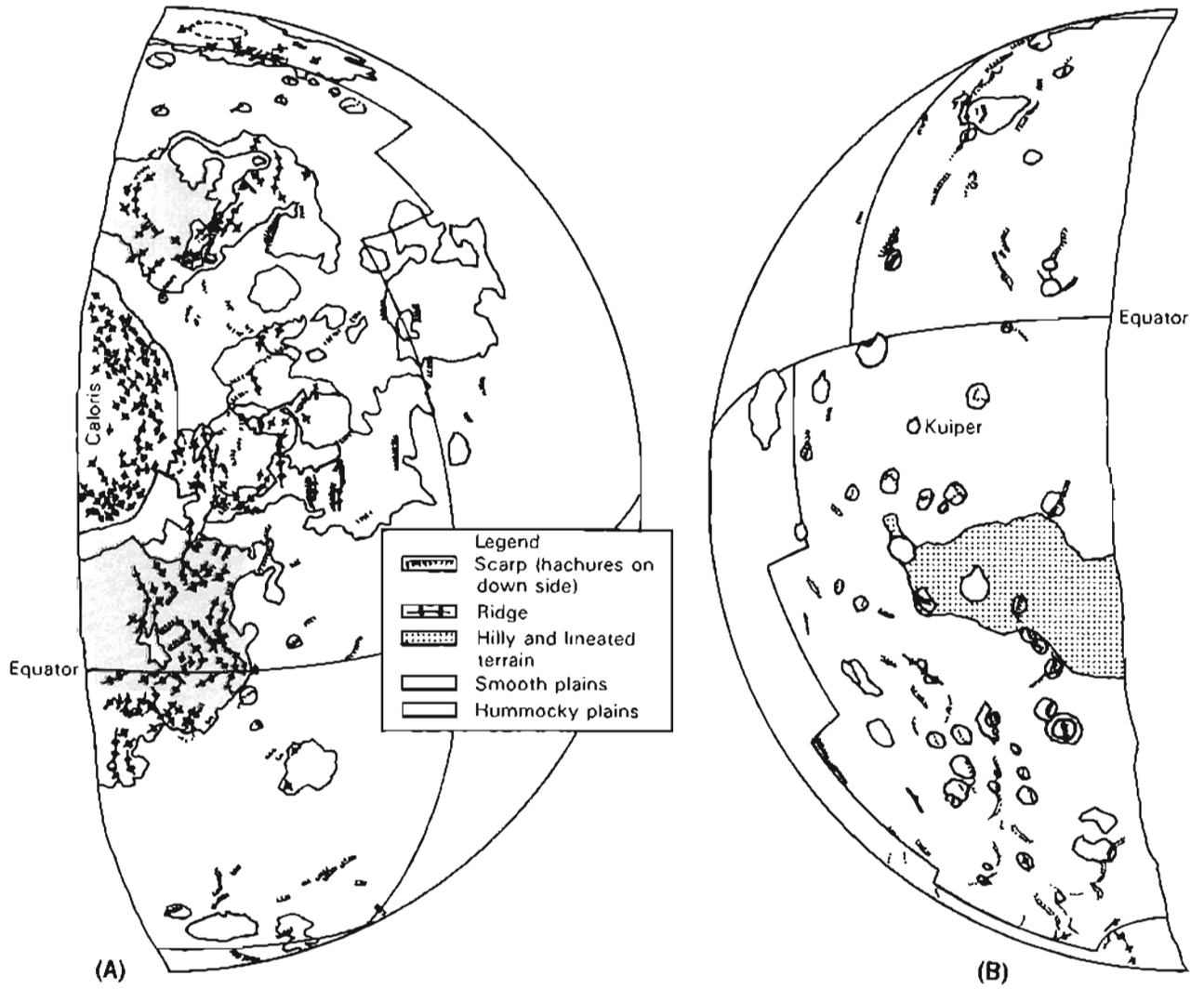

crater plains emplacement, sometime near the end of heavy bombardment, and extended some undetermined time beyond smooth plains emplacement. Lobate scarps transect the smooth plains around the Caloris basin but they are apparently smaller and fewer than those found in the Mercurian highlands. In general, the lineament system is probably older and pre-dates most of the lobate scarps. Dzurisin (1976) pointed out that many large degraded craters and basins show polygonal outlines, suggesting that the joint pattern was established well before the end of heavy bombardment. Furthermore, several lobate scarps have linear segments with trends similar to nearby lineaments, suggesting that some scarps formed along pre-existing joints. Also linear troughs in the hilly and lineated terrain are aligned along trends defined by lineaments elsewhere, and may have formed along pre-existing joints during seismic jostling from the Caloris impact.

The surface of Mercury viewed by Mariner 10 is remarkably free of structures resulting from tensile stresses. Only two areas contain structures which were probably produced by tension and both are associated with Caloris (figs. 3.17 and 3.33). The fractures on the floor of the Caloris basin are probably graben, resulting from an uplift of the floor; troughs in the hilly and lineated terrain antipodal to Caloris may be graben which formed along pre-existing joints during vertical ground motions induced by focused seismic waves from the Caloris impact. No circumferential graben or normal faults are found exterior to basins, as often occurs on the Moon, nor are there systems of radial graben, as occur on Mars. The present surface of Mercury appears to have been dominated by compressive stresses.

Causes of Crustal Deformation

Two main hypotheses have been proposed to account for the tectonic framework of Mercury: (1) a change in the shape of the planet due to despinning from an initially higher rate, and (2) global contraction due to cooling from an initially higher temperature. According to the first hypothesis, tidal slowing of the rotation from an initially higher rate (20 hrs) results in a decrease in polar flattening, producing crustal stresses well above the fracture limit (Burns, 1976; Melosh, 1977; Melosh and Dzurisin, 1978b). Depending on the value of the planetary dissipation constant (Q) the time required to despin Mercury from a rotation period of 20 hours to the present period of 58.6 days is 0.2 to 2.0 billion years (Goldreich and Soter, 1966). The stress regime resulting from despinning produces three zones of faulting: (1) an equatorial zone of compression containing north-south trending thrust faults, (2) a mid-latitude zone of shearing stress containing an orthogonal set of NW and NE trending wrench faults, and (3) polar zones of tensile stress containing east-west trending normal faults (Melosh, 1977; Melosh and Dzurisin, 1978b). However, the south polar region of Mercury displays numerous lobate scarps (thrust faults) but no evidence of normal faulting, although structural lineaments are present here as well as in other areas of the planet. As a result it has been necessary to invoke a combination of despinning and global contraction to account for compressive stresses in the polar regions (Pechmann and Melosh, 1979). The relative importance of despinning and contraction to the development of Mercury's tectonic framework depends on various parameters such as the ratio of the time constant for despinning to that for contraction.

The hypothesis of global contraction to explain the tectonic framework initially invoked a partial solidification of the large iron core (Murray et al., 1979; Strom et al., 1975b). However, Solomon (1976) found that cooling of the lithosphere following core formation alone can account for the radius decrease estimated by Strom et al. (1975b). A solidification of an inner core up to 60 percent of the radius of the outer core, or more likely a combination of lithospheric and inner core cooling (1050 km radius) would satisfy the estimated limits on global contraction (Solomon, 1977). Complete or even extensive solidification of a once molten core is excluded by the limitation on total radius change. This is consistent with a convective dynamo mechanism for the generation of Mercury's magnetic field (Ness, 1978). Global contraction should lead to a more or less random distribution of compressive stresses to produce an azimuthally random distribution of thrust faults on a global scale. Contrary to measurements of Melosh and Dzurisin (1978b), Cordell and Strom (1977) found that the azimuthal distribution of lobate scarps is more or less random (fig. 3.38). Furthermore, the lineament system is an apparently ancient fracture system and predates the formation of lobate scarps (Dzurisin, 1976), whereas they should be more or less contemporaneous under the spindown hypothesis. Although despinning may have influenced the tectonics of Mercury, the azimuthal and areal distribution of lobate scarps, together with their age relationships, suggests that contraction

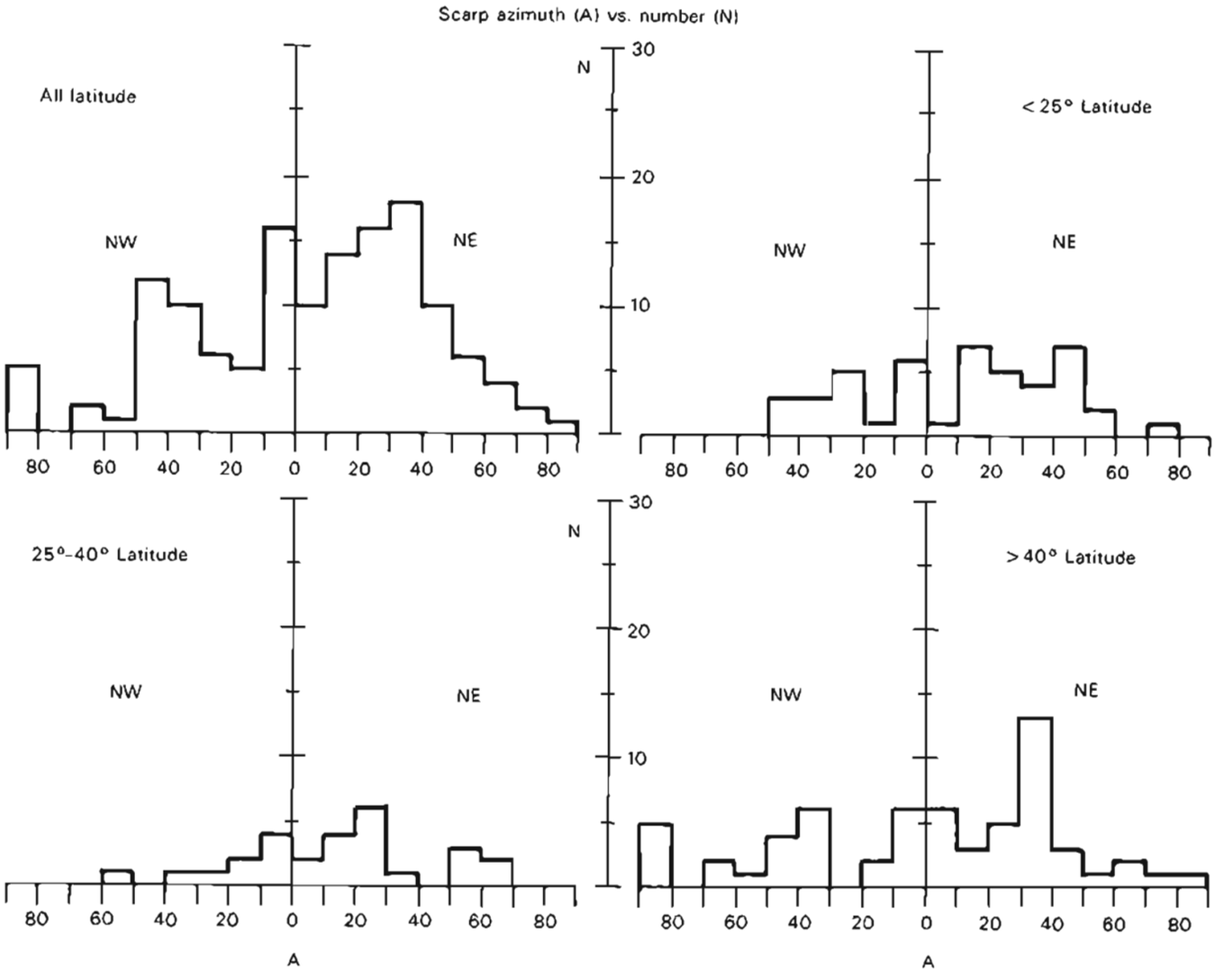

Figure 3.38. Azimuth-frequency histograms of lobate scarps for all latitudes (− 90° to ± 60°), latitudes between ± 25° (< 25° plot), latitudes between + 25 to + 48° and − 25 to − 40° (the 25-40° plot), and latitudes between − 40 to − 90° and + 40 to + 60° (> 40° plot) on the incoming side of Mercury. (After Cordell and Strom, 1977.)

due to cooling of the lithosphere and/or core following core formation was the dominant mechanism responsible for the presently observed tectonic framework.

SURFACE HISTORY AND THERMAL EVOLUTION

The surface history of Mercury is a reflection of its thermal history. If both the smooth and intercrater plains originated by impact basin ejecta processes, then it is likely that little or no volcanic activity occurred on Mercury, at least during the history recorded on its surface. This would imply that either the thermal regime throughout most of its history has led to little melting or there were no means by which magmas could reach the surface in any large quantity. Mercury would then be unique among the terrestrial planets because all others have experienced thermal histories which resulted in extensive volcanic activity over large areas of their surfaces. Indirect evidence suggests, however, that Mercury has experienced considerable melting comparable to, if not more than, the other terrestrial planets. Melting models for the terrestrial planets based on a comparison of various heating mechanisms relative to the Moon indicate that Mercury would be more likely to have experienced global melting than the Moon or other terrestrial planets (Hostetler and Drake, 1980). Compositional information, although meager, indicates that Mercury's surface is composed of silicates low in FeO and titanium, compared to the Moon, suggesting that Mercury is a differentiated planet with a silicate crust

and iron-rich core. The widespread distribution of lobate scarps indicates Mercury was subjected to a period of global contraction. The contraction was probably due, at least in part, to cooling of the interior. These two pieces of evidence together suggest Mercury experienced widespread melting and differentiation followed by cooling.

The discovery of Mercury's dipolar magnetic field also provides strong evidence that Mercury is differentiated into an iron-rich core and a silicate mantle. As discussed earlier, the two most reasonable explanations for its origin are: (1) the field is the result of remanent magnetization due to an ancient dynamo, or (2) it is a presently active magnetohydrodynamic dynamo. Both explanations for Mercury's magnetic field require that the interior is differentiated into a core and mantle and that the core was at least molten in the past and quite probably the outer portion is still molten.

The thermal history of Mercury is highly dependent on the abundance of radioactive isotopes. Thermal models suggest that a core will not form with a uranium abundance of only 30.4 ppb, whereas a core always forms with an abundance of 44 ppb, regardless of values of thermal conductivity and initial temperature (Siegfried and Solomon, 1974). If Mercury retained the uranium and thorium (Th/U$\sim$4) predicted by current cosmochemical models of solar nebula condensation and planetary accretion (Lewis, 1972, 1973; Grossman, 1972; Grossman and Larimer, 1974), then differentiation and core formation are probable for all likely initial temperature distributions and thermal conductivity values (Siegfried and Solomon, 1974). The consequences of core formation on the thermal history of Mercury are dramatic. In a model where the parameters were chosen to favor early differentiation Solomon (1976) found that core formation begins 1.2 billion years after planetary origin and is complete by 1.8 billion years. Most of the differentiation occurs within 200 million years and a temperature rise of about 700° C results from the release of gravitational potential energy. Most of the mantle is melted which should lead to substantial surface modification. However, if the surface of Mercury is as old as the period of heavy bombardment on the Moon (4.0 billion years ago), then core formation would have to have been complete at least 1 billion years earlier than indicated by this model. As a result, extensive early heating is required, which must have involved a much larger fraction of the planetary volume than for the Moon. Core infall would be accompanied by substantial melting of the mantle, and an increase in the planet radius by as much as 17 km (Solomon, 1976). Subsequent to core formation, cooling of the lithosphere or a combination of lithospheric and core cooling leads to a decrease in radius of perhaps 2 km or more (Solomon, 1976, 1977). A somewhat similar thermal model by Toksöz et al. (1978) reached similar conclusions. In any event, thermal history models involving differentiation into a core and mantle predict large scale melting of the mantle, leading to an increase in volume and widespread extensional fracturing of the crust. This provides ideal conditions for extensive volcanic activity; a ready source of lavas and tensional fracturing to provide egress to the surface. Under these conditions it is difficult to understand how Mercury could not have sustained widespread volcanism when the Moon experienced extensive volcanism under a much less severe tectonic and thermal regime.

Figure 3.39 is a schematic representation of the relative age of various events discussed elsewhere in the text. As Chapman (1976) correctly pointed out, absolute chronologies of planets cannot be determined from photogeologic studies alone. Because they depend on a rather accurate knowledge of the impact flux history, which is uncertain, no attempt was made to relate these events to an absolute time scale. However, it is highly likely that the age of Mercury's surface is comparable to that of the Moon's and formed sometime during the first 2–2.5 billion years after planetary formation (Murray et al., 1975). If large tracts of intercrater plains are volcanic then it is possible that this period of volcanism coincided, at least in part, with the period of heavy bombardment. Much of the intercrater plains pre-date or are contemporary with the oldest craters (Classes 4–5) of the heavily cratered terrain, while other large tracts appear to post-date these craters. Perhaps the plains material was extruded along fractures caused by expansion of Mercury during or shortly after core formation. Crustal fracturing during spindown also may have aided the process. The absence of extensional fracturing in the Mercurian highlands may be due to several factors. Crustal expansion and therefore tensional fracturing may have been nearly complete by the time of emplacement of the oldest intercrater plains units. Furthermore, the emplacement of volcanic plains may have covered their source fractures, as have the mare lavas on the Moon. Subsequent cratering (both primary and secondary) also could obliterate fractures.

The Caloris basin and the hilly and lineated terrain appear to have formed near the end of heavy bombardment—when the crust was being subjected

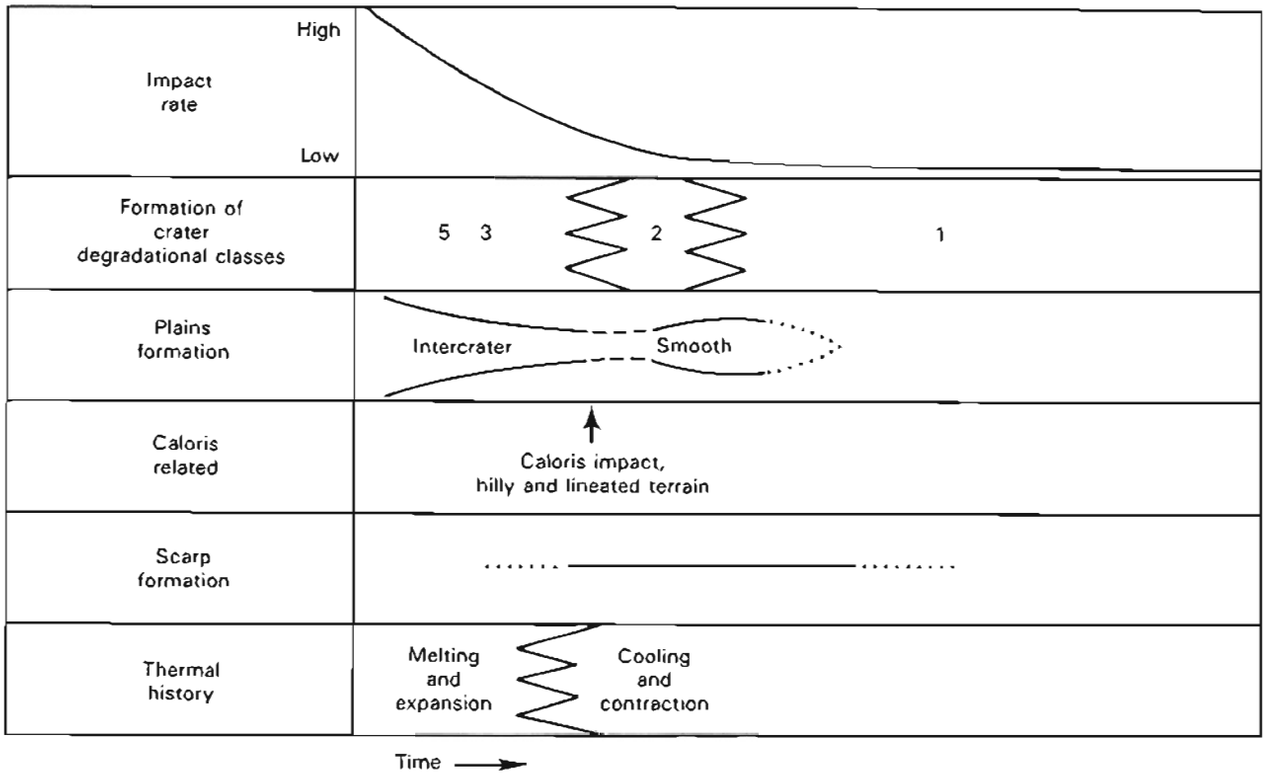

Figure 3.39. Diagram of the relative age of various events in Mercury's history. No attempt has been made to relate these events to an absolute time scale, but they all probably occurred early in the planet's history. The relative ages are interpretations based on investigations by various authors and are independent of the origin of plains units.

to global compression due to cooling of the core and/or lithosphere. Cooling and global compression probably began toward the end of heavy bombardment but before the formation of Caloris and continued past the formation of smooth plains. In general, global compression would tend to close off magma conduits and inhibit surface volcanism except for local areas of tension, e.g. seismic wave focusing at the Caloris antipode (Solomon, 1978). The majority of smooth plains appear to have been emplaced during the period of global compression. However, as Solomon (1977) pointed out, thermal stress will readily allow upward migration of magma to shallow levels where it can move to the surface if the fluid pressure exceeds the lithostatic pressure, or if the crust is weakened by impacts. Since the majority of smooth plains are concentrated in and around large impact basins, they may have been emplaced along fractures produced by the large impacts. Subsequent to smooth plains emplacement, crustal compression waned and died out at some indeterminate time. Since then only occasional impacts have modified Mercury's surface. A diagrammatic representation of this history is shown in figure 3.40.

Although thermal history models predict extensive mantle melting and crustal extensional fracturing, an alternative history can be developed in which little or no volcanism has occurred since the onset of heavy bombardment. In this scenario, the period of planet expansion, mantle melting, and crustal extensional fracturing would have ceased prior to the oldest craters preserved on the surface. This early period of melting may have completely resurfaced the planet. Subsequent cratering would be retained only after the surface was sufficiently solidified. The early, large craters would be more isostatically compensated, which would account for their degraded appearance but well-preserved secondaries. Under this view, the oldest intercrater plains would be the main remnants of the resurfacing, while the later intercrater plains would be ejecta deposits from as yet unidentified basins. Global compression due to cooling would be occurring during this period, and subsequent formation of basins (most of which have not been identified) would produce the smooth plains by impact melt and/or ballistic emplacement. Although this scenario is conceivable, the relatively late onset of compression suggested by crater-lobate scarp transection relationships, the evidence for a volcanic origin of at least large tracts of plains, and the difficulty of accounting for plains formation by impact processes, suggests that the first alternative is a more likely hypothesis.

DISCUSSION

The surface of Mercury closely resembles the Moon in two important respects: (1) the presence of ancient, heavily cratered regions with a lunar-like crater den-

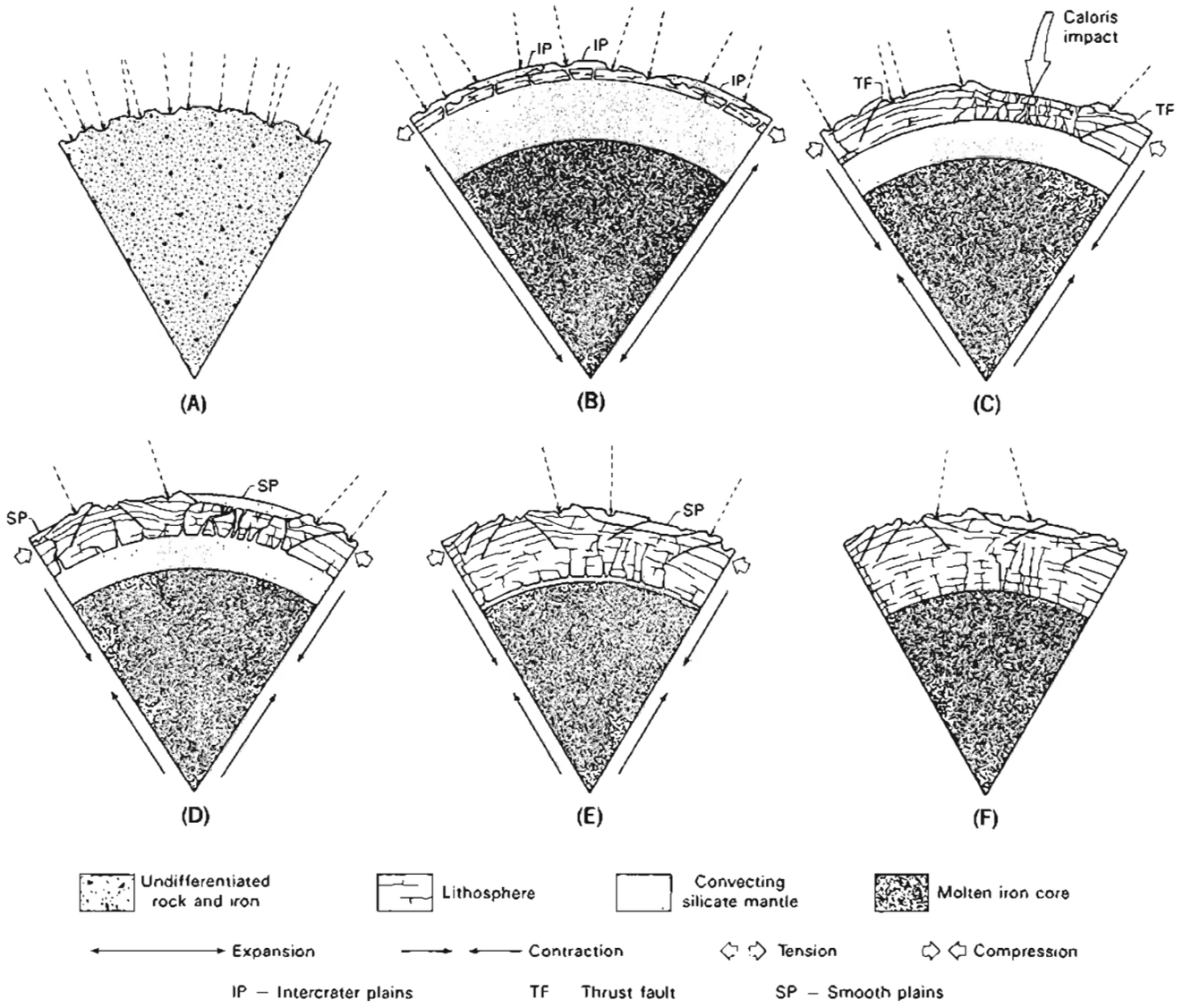

Figure 3.40. Diagram of the possible history of Mercury described in the text. In (A) Mercury has just formed with a large percentage of iron uniformly distributed throughout the planet. In (B) the large iron core has formed and largely melted the silicate mantle causing global expansion and tensional fracturing in a thin solid lithosphere. Volcanic eruptions along these fractures produce the intercrater plains (IP) during the period of heavy bombardment. In (C) the convecting mantle cools sufficiently to cause global contraction which results in compressive stresses and thrust faulting (TF). About this same time the Caloris impact occurs. Soon afterward new eruptions fill the Caloris basin and other areas with smooth plains (SP) near the end of heavy bombardment as shown in diagram D. In (E) further cooling and contraction produce compressive stresses strong enough to close off the volcanic conduits. Finally, cooling and contraction are complete and the planet becomes inactive except for occasional impacts which scar the surface (F).

sity and size distribution, and (2) large areas of younger, smooth plains resembling the lunar maria in both morphology and mode of occurrence. This superficial resemblance can lead to an overemphasis, and possibly an overinterpretation, of the similarities at the expense of the great differences which make Mercury unique in the solar system. Among these differences is Mercury's high mean density, which implies an iron content per unit volume greater than any other planet or satellite in the solar system. This large concentration of iron is probably a consequence of equilibrium condensation processes in the early solar nebula at Mercury's distance from the Sun. Furthermore, the presence of a relatively strong dipole magnetic field implies that the iron is concentrated into an enormous core some 75 percent of the total radius. The early formation of such a large core leads to thermal histories which predict large-scale melting consuming a much larger fraction of Mercury's lithosphere than that of the Moon. As a consequence, Mercury's tectonic regime and internal dynamics must have been very different from the Moon's. This might be expected to produce surface characteristics which differ in important respects from those on the Moon.

The two main differences between the surfaces of Mercury and the Moon are the tectonic framework and the widespread distribution of ancient intercrater plains on Mercury. Both of these characteristics may

be either the direct or indirect result of core formation on Mercury, which leads to extensive lithospheric melting, global expansion, and crustal extension. These conditions might be expected to yield extensive volcanism on a global scale, perhaps producing much of the intercrater plains. The origin of the tectonic structures is more firmly based, and is almost surely the result of compressive stresses due to crustal shortening. Although planetary despinning may have played a role in developing the tectonic framework, global contraction due to cooling of the lithosphere and/or core must have played an important part in order to explain the areal and azimuthal distribution of compressional features. Global contraction is also an indirect consequence of core formation because a significant decrease in radius results from cooling following the extensive melting induced by core formation. Furthermore, the relative age of intercrater plains emplacement and the onset of compression deduced from stratigraphic and transectional relationships is consistent with the stress history predicted by core formation in Mercury.

As Solomon (1978) pointed out, global compression would act to shut off volcanism associated with local stress systems faster than for a planet under global extension; therefore, the time duration of smooth plains emplacement (if volcanic) should be relatively short for Mercury compared to that for volcanic plains on the Moon and Mars. Both the post-Orientale and the post-Caloris surfaces record the same crater population with the same crater density and were imprinted near the end of late heavy bombardment on both bodies (see fig. 3.19). If the flux and decay rate of late, heavy bombardment were the same at Mercury and the Moon (a circumstance which is still uncertain), then both surfaces are about the same age (3.8 billion years). Crater densities on these surfaces are about a factor of three greater than that of the lunar maria (fig. 3.19), and the post-Caloris population is primarily superposed on the smooth plains. Therefore, the Caloris smooth plains may have been emplaced earlier than most of the lunar maria.

The paucity of iron and titanium on Mercury's surface relative to the Moon (Hapke, 1977) is consistent with the higher albedo of Mercury's surface units. Minerals containing these elements contribute to darkening the surface, and the titanium abundance is primarily responsible for the color differences observed on the Moon (see fig. 3.26). A low titanium abundance on Mercury could well account for the much smaller color differences and the poor correspondence between color and geologic boundaries. The depletion of these elements in crustal rocks relative to the Moon may have been the result of greater lithospheric melting leading to more efficient differentiation, particularly by gravity settling under Mercury's greater gravitational acceleration. This process could result in a stratified mantle with the heavier elements concentrated at greater depths (Herbert, 1980). Intercrater and smooth plains emplacement may represent one continuous epoch of volcanism, which tapped source regions depleted in iron and titanium relative to the Moon, and terminated when compressive stresses became strong enough to close off the conduits. In this case, Mercury, unlike the Moon, did not experience a period of late stage iron- and titanium-rich mare-like volcanism. Instead the source region for the older intercrater plains volcanism may have been at a shallower more differentiated level; while at least the younger Caloris smooth plains may have originated from a deeper level where slightly more iron and titanium were concentrated. Although the major differences between the surfaces of Mercury and the Moon can be readily explained in terms of the formation of a large Mercurian core, our current state of knowledge does not preclude other interpretations discussed earlier.

The flight of Mariner 10 has advanced our knowledge of Mercury a thousand fold and provides new insight into terrestrial planet evolution. However, the answers to major questions regarding the origin and composition of some of its surface features must await further investigation. Only an orbital mission with a diverse complement of scientific instruments is capable of providing the information to help answer these questions. Until then we must rely on existing data to sharpen our interpretations and improve theoretical models.

ACKNOWLEDGMENTS

The author thanks Charles Wood, Donald Gault, Mark Cintala, Bruce Hapke, Eugene Smith, Ewen Whitaker, Martha Leake and Newell Trask for providing several illustrations used in the text. Discussions with Ewen Whitaker, Bruce Hapke and Faith Villas on the photometry and spectroscopy of Mercury were very useful. Reviews of the text by Sean Solomon, Charles Wood, William McKinnon, Michael Carr, Donald Wilhelms and Ewen Whitaker are greatly appreciated. Portions of the research were conducted under NASA Grant NSG-7146.